ZEOLITIC IMIDAZOLATE FRAMEWORKS/ POLYBENZIMIDAZOLE NANOCOMPOSITE MEMBRANES FOR HYDROGEN PURIFICATION

YANG TINGXU

NATIONAL UNIVERSITY OF SINGAPORE

2012

ZEOLITIC IMIDAZOLATE FRAMEWORKS/ POLYBENZIMIDAZOLE NANOCOMPOSITE MEMBRANES FOR HYDROGEN PURIFICATION

YANG TINGXU

(B. Eng., Shanghai Jiao Tong University, P. R. China)

A THESIS SUBMITTED

FOR THE DEGREE OF DOCTOR OF PHILOSOPHY

NUS GRADUATE SCHOOL FOR INTEGRATIVE SCIENCES AND ENGINEERING

NATIONAL UNIVERSITY OF SINGAPORE

2012

Declaration

I hereby declare that the thesis is my original work and it has been written by me in its entirety. I have duly acknowledged all the sources of information which have been used in the thesis.

This thesis has also not been submitted for any degree in any university previously.

Yang Tingxu 杨婷旭

Yang Tingxu
11 March 2013

ACKNOWLEDGEMENTS

I wish to take this opportunity to express my sincere appreciation to all the contributors during my years in the National University of Singapore. First of all, I am especially grateful to my supervisor, Professor Chung Tai-Shung, Neal, for his generously guidance and support without hesitation. Over the past three years, he has added value to me with numerous opportunities and well-equipped research facilities. He has trained me as an independent researcher and enlighten me to achieve more than what I ever expect.

I wish to express my gratefully thanks to my mentor, Dr. Xiao Youchang, who has provided invaluable advice, inspiration and encouragement to me during my starting period of PhD candidate. Without him, I may undergo a harder time for the first year, and a significant portion of the work included herein may not have been achieved. I also appreciate the assistance from my TAC members, Professor Zeng Hua Chun and Dr. Pramoda Kumari Pallathadka, for their valuable comments and discussions. I would like to acknowledge the research scholarship by the NUS Graduate School of Integrative Sciences and Engineering (NGS) and thank the Singapore National Research Foundation (NRF) for the financial support that enables this work to be successfully completed. I am also thankful to Ms. Tricia Chong and Ms. Yong Yoke Ping for their kindest advice and help during the patent documentation.

I would like to convey my appreciation to all members of Prof. Chung's group, especially Ms. Wang Huan, Mr. Chen Hangzheng, Mr. Li Fuyun, Miss Chua Mei Ling, Dr. Low Bee Ting, Mr. Ong Yee Kang, Dr. Dave William Mangindaan, Dr. Su

Jincai, Mr. Wang Peng, Miss Xing Dingyu, Dr. Wang Rongyao, and many others for plenty of good times, discussion and sharing of knowledge. Special thanks are due to Mr. Shi Gui Min for all his kind cooperation and help in the laboratory. Finally, I must express my deepest gratefulness to my family for their endless support, especially to my dearest husband Jiye for his unfailing love, patience, and understanding during the three and a half years period of 5450 km long-distance relationship.

TABLE OF CONTENTS

SUMMARY

Hydrogen production is a large and fast expanding industry. In the petroleum and chemical industries, large quantities of H_2 are needed for processing heavy crude oil into useable fuels, producing ammonia for fertilizer and other industrial uses. Due to the growing global awareness of energy security and sustainability, hydrogen has attracted much industrial attention as an effective and green energy carrier. The demand for hydrogen is driven by the need for refiners to expand production and comply with environmental regulations being progressively introduced around the world. In the large scale hydrogen production, carbon dioxide is the main by-product of the water-gas shift reaction. It must be captured to produce high purity H_2 and eliminate environmental concerns.

Comparing with traditional separation methods, membrane based separation technologies show the advantages of environmental friendlier, smaller footprint, and less energy deduction. Among materials for separation membrane fabrication, polymers remain to be the most practical and economical choice. However, the effective separation of H_2 and CO_2 mixtures is challenging because most polymers show undesirable counterbalance characteristics of H_2-selective diffusivity and CO_2-selective solubility. In addition, most of the polymeric membranes cannot survive or keep good H_2/CO_2 separation performance in harsh industrial environments which contain high temperature and pressure, and impurities in the gas streams.

Mixed matrix membranes (MMMs) consisting of polymeric materials and inorganic components have the potential to achieve higher selectivity, permeability, or both relative to the raw polymeric membranes. However, challenges such as pore blockage, chain rigidification and interface voids still exist and restrain the potential separation performance of MMMs materials. In addition, the oversize and agglomeration of nano-particles limit their applications in fabricating practical membrane configurations such as asymmetric hollow fibers.

In this work, a group of ZIFs/PBI nano-composite materials have been developed for high temperature hydrogen purification. Membranes were formed via a novel procedure by incorporating as-synthesized wet-state zeolitic imidazolate frameworks (ZIFs) nano-particles into a polybenzimidazole (PBI) polymer. The resultant ZIFs/PBI nano-composite membranes show very encouraging H_2/CO_2 separation performance and excellent stability under elevated temperatures. Intensive investigations were carried out on (1) conducting fundamental studies for deeply understanding the science and engineering of this material and membrane formation technology, (2) fabricating this material into industrially useful membrane configuration-hollow fiber, by optimizing the nano-particle loadings, spinning conditions, and post treatment methods, and (3) examining the practical applicability by various performance tests under different operating parameters such as high temperatures and impurities commonly contained in the syngas streams. Based on our observation, this newly developed H_2-selective membrane material may have bright prospects for hydrogen purification and CO_2 capture in realistic industrial applications such as syngas processing, integrated gasification combined cycle (IGCC) power plant and hydrogen recovery.

NOMENCLATURE

A	Effective area of the membrane available for gas transport
b	Langmuir affinity constant
C	Local penetrant concentration in the membrane
C_D	Penetrant concentration in Henry's sites
C_H	Penetrant concentration in Langmuir sites
C_H'	Langmuir capacity constant
D	Outer diameter of the testing fibers
D	Diffusion coefficient
dp/dt	Change of pressure with time in the downstream chamber of the permeation cell
d	Average d-space
d_k	Kinetic diameter of the gas molecule
E_D	Activation energy for diffusion
E_P	Activation energy of permeation
ΔH_S	Enthalpy of sorption
I_3	Intensity
k_D	Henry's law constant
L	Membrane thickness
L	Effective length of the modules
l	Thickness of a membrane selective layer
M	Molecular weight
M_W	Molecular weight of the gas component

M_{WA}	Molecular weight of gas A
M_{WB}	Molecular weight of gas B
N	Steady state flux of the permeating gas at standard temperature and pressure
n	Number of fibers in one testing module
P	Permeability coefficient of a membrane to gas
P	Atmospheric pressure
P_0	Pre-exponential factor for the activation energies of permeation
P_{eff}	Effective permeability of a gas penetrant in a mixed matrix membrane
P_C	Gas penetrant permeabilities in continuous phase in mixed matrix membrane
P_D	Gas penetrant permeabilities in dispersed (sieve) phases in mixed matrix membrane
p	Feed gas pressure in contact with the polymer
p_1	Downstream pressure
p_2	Upstream pressure
Δp	Pressure different between the upstream and the downstream of a membrane
P/L	Permeance of a membrane to gas
Q	Volumetric flow rate of pure gas
R	Universal gas constant
R	Hole radius
ΔR	A fitted empirical electron layer thickness of 1.66Å
S	Solubility coefficient

r	Effective pore radius
T	Absolute temperature
T_b	Boiling point
T_g	Glass transition temperature
t	Permeation time
V	Downstream reservoir volume
V_h	Cavity volume
w_0	The weight of the sample in air
w_1	The weight of the sample in hexane
x	Gas molar fraction in the feed
y	Gas molar fraction in the permeate
$\alpha_{A/B}$	Ideal selectivity of component A over B
δ_D	Solubility parameter from dispersion interactions
δ_H	Solubility parameter from hydrogen bonding
δ_P	Solubility parameter from polar attraction
δ_T	Total solubility parameter
η	Gas viscosity
θ	X-ray diffraction angle of the peak
λ	Mean free path of the gas penetrant
λ	Wavelength of X-ray source
ρ_{hexane}	Density of hexane
$\rho_{membrane}$	Density of the membrane
τ_3	o-Ps lifetime
φ	Volume fraction
φ_D	Volume fraction of dispersed (sieve) phase

LIST OF TABLES

LIST OF FIGURES

CHAPTER 1

INTRODUCTION

1.1 Hydrogen for industrial feed and sustainable development

Energy and environmental sustainability are major long-term problems facing our global economy. According to the anticipation in the latest International Energy Outlook 2011 [1] by the U.S. Energy Information Administration, the world marketed energy consumption will increase by 53 percent from 505 quadrillion British thermal units (Btu) in 2008 to 770 quadrillion Btu in 2035. As shown in Figure 1.1(a) [1], fossil fuels (liquids, coal and natural gas) will continue to dominate the energy consumption in this prediction period. As more and more fossil fuels are consumed, the fossil fuels would be depleted in a foreseeable future. Furthermore, the extensive usage of fossil fuels, especially oil and coal with high carbon values, generates greenhouse gases and toxic emissions which cause a series of detrimentally environmental impacts including global climate disruption, sea level rise, and life extinctions. As indicated in Figure 1.1(b) [1], the predicted world energy-related CO_2 emission will increase by 43 percent, from 30.2 billion metric tons in 2008 to 43.2 billion metric tons in 2035. There is an urgent demand to reduce the world's reliance on fossil fuels and increase the sectors of alternative energy sources that are much more environmental friendly.

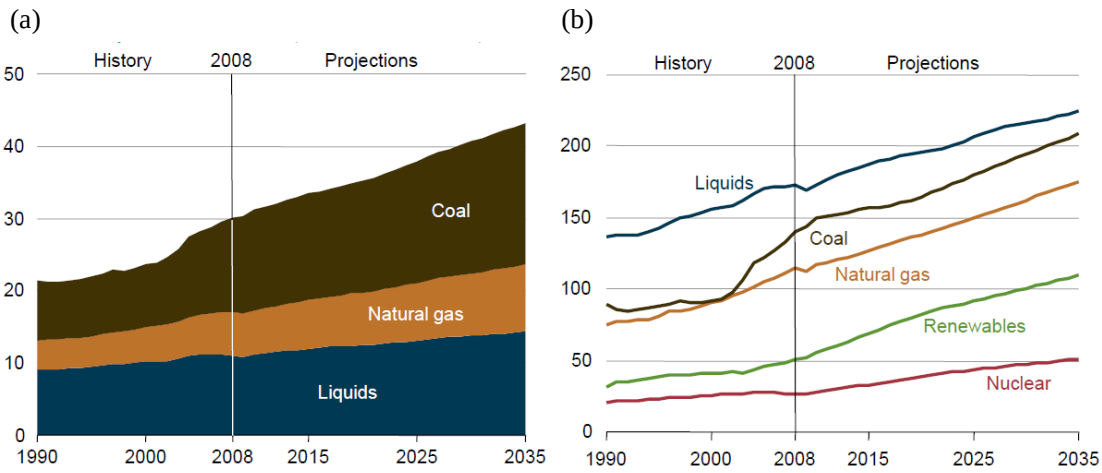

Figure 1.1 World energy consumption by fuel and the related carbon dioxide emissions (1990-2035)
(a) World energy consumption by fuel (quadrillion Btu); (b) World energy-related carbon dioxide emissions by fuel (billion metric tons)

There are plenty of new primary energy sources available, such as nuclear breeders, thermonuclear energy, solar energy, wind energy, geothermal energy, hydropower, ocean currents, tides, and waves. The market share of alternative energy will expand significantly since the related technologies become mature from the intensive research and development over the past decades. Meanwhile, the sustained high oil prices also allow alternative energy resources to become more economically competitive. At the consumer end, about three-quarters of the primary energy is used as fuel and one-quarter is as electricity [2]. Unfortunately, in contrast with the fossil fuels, none of the above mentioned primary energy sources can be directly utilized as a fuel. Therefore, the new primary energy sources must be converted to secondary energy carriers needed by the consumer. The energy carrier of choice must satisfy the following conditions [3]: 1) It must be convenient fuel for transportation; 2) It must be versatile or convert with ease to other energy forms at the user end; 3) It must have high utilization efficiency; 4) It must be safe to use; and in addition 5) the resulting energy system must be environmentally compatible and economical.

Among all the possible fuels, hydrogen is the most promising candidate which possesses 1) the best motivity factors as liquid fuel and gaseous fuel for transportation [4]; 2) the most versatile [5]; 3) the highest utilization efficiency; 4) the highest safety factor; and 5) the least environmental impacts [2]. Hydrogen element is the lightest and the most abundant element in the universe. The normal molecular form of the element is H_2. The detailed properties of hydrogen are listed in Table 1.1.

Table 1.1 Properties of hydrogen

Atomic number, H	1	
Electron binding (ionisation) energy in *1s* ground state	2.18	aJ
Molar mass, H_2	2.016	10^{-3} kg mol^{-1}
Average distance between nucleons, H_2	0.074	nm
Dissociation energy, H_2 to 2H at infinite separation	0.71	aJ
Density, H_2, at 101.33 kPa and 298 K	0.084	kg m^{-3}
Melting point at 101.33 kPa	13.8	K
Boiling point at 101.33 kPa	20.3	K
Heat capacity at constant pressure and 298 K	14.3	kJ K^{-1} kg^{-1}
Solubility in water at 101.33 kPa and 298 K	0.019	m^3 m^{-3}

Currently, the dominant scheme of industrial hydrogen production starts from methane, CH_4, which is the main component of natural gas. The process from methane to hydrogen can be separated into two stages, namely steam reforming and water gas shift reaction. In the steam reforming, a mixture of methane and water vapor undergoes a strongly endothermic reaction at elevated temperature. The reaction equation is shown as follows.

$$CH_4+H_2O\rightarrow CO+3H_2-\Delta H^0 \quad (1\text{-}1)$$

where ΔH^0 represents the enthalpy change and equals 252.3 kJ/mol (at 0.1 MPa and 298 K), with the input water in liquid form. On the right-hand side of this reaction, the hydrogen and carbon monoxide mixture is called “synthesis gas”. This step is typically carried on at high temperature (850 ℃) and high pressure (2.5×10^6 Pa). The subsequent water gas shift reaction usually takes place in a separate reactor.

$$CO+H_2O \rightarrow CO_2+H_2-\Delta H^0 \quad (1\text{-}2)$$

where ΔH^0 equal to -5.0 kJ/mol when the water is in liquid form, and -41.1 KJ/mol when all reactants are in gas form (at 0.1 MPa and 298 K). The generated heat is recovered and recycled back to the steam reforming reaction. This process normally involves two heat exchangers and is one of the main reasons for the high cost of hydrogen production via steam reforming [6].

After the water gas shift reactor, the output gas stream contains components of H_2, CO_2, CO, water vapor and trace amount of N_2, H_2S, NO, etc. The temperature of this gas stream is normally 200-400 ℃. The gas mixture can be separated directly at this temperature or at lower temperatures after cooling and knocking out excess amount of water vapor.

1.2 Membrane technology for gas separation

One general definition of membrane may be: A membrane is a phase or a group of phases that lies between two different phases, which is physically and/or chemically distinctive from both of them and which, due to its properties and the force field applied, is able to control and mass transport between these phases [7]. Membrane technologies are now utilized for separations of a wide variety of mixtures, from gas

mixtures containing smallest like H_2 and He, to mixtures of particles beyond sizes of large molecules, such is viruses or bacteria cultures. Till now, membranes have wide current and potential applications in diverse fields including water treatment, chemical industry, energy, medicine, agriculture, etc.

Based on porosity, separation membranes are generally classified into several types for varieties of membrane processes and applications. The schematic of the classification is shown in Figure 1.2 [8]. Membranes with average pore diameters of larger than 50 nm are classified as macroporous; those with average pore diameters between 2 and 50 nm are classified as mesoporous; and membranes with average pore diameters between 0.1 and 2 nm are classified as microporous. In dense membranes, which show no individual permanent pores, the separation occurs through the fluctuating free volumes in between polymer chains.

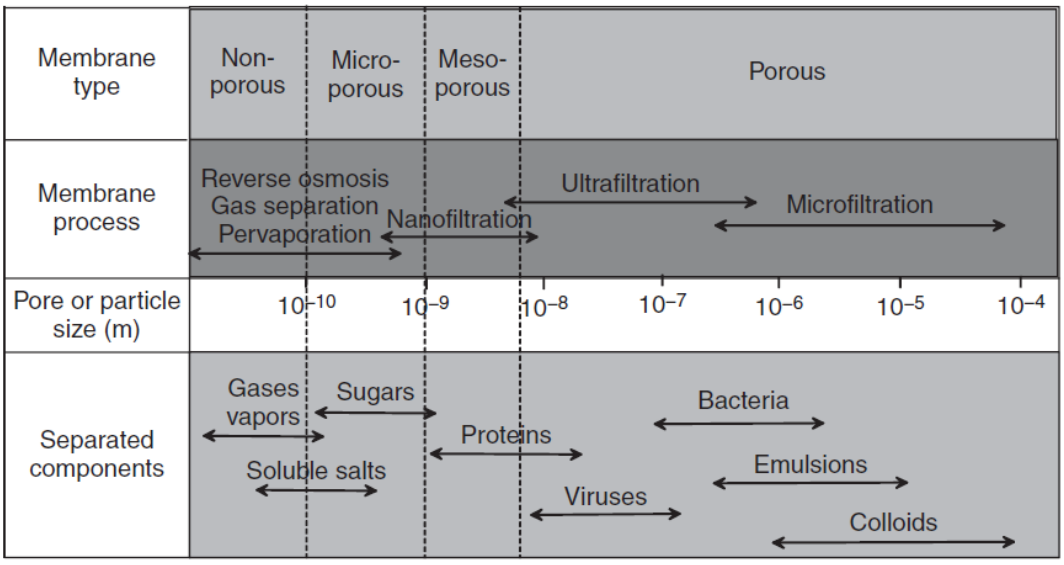

Figure 1.2 Schematic classification of membrane, related processes and separated components

Over the past 30 years, membrane gas separation processes have been gradually adopted by a large number of industries in a variety of sectors, due to continuing improvements in materials science, manufacturing and process engineering. The estimated market scale of polymeric membranes for gas separation has recently reached to the range between 150 and 230 million US dollars per year, with an annual growth of as high as 15% [9] (i.e., the largest among the various membrane processes [10]) By the year of 2000, there are thousands of gas separation modules with dense polymeric membranes operated throughout the world and can be roughly divided into four major application fields (i.e., nitrogen from air, carbon dioxide from natural gas, hydrogen recovery, and vapor recovery) as shown Figure 1.3 [8, 9].

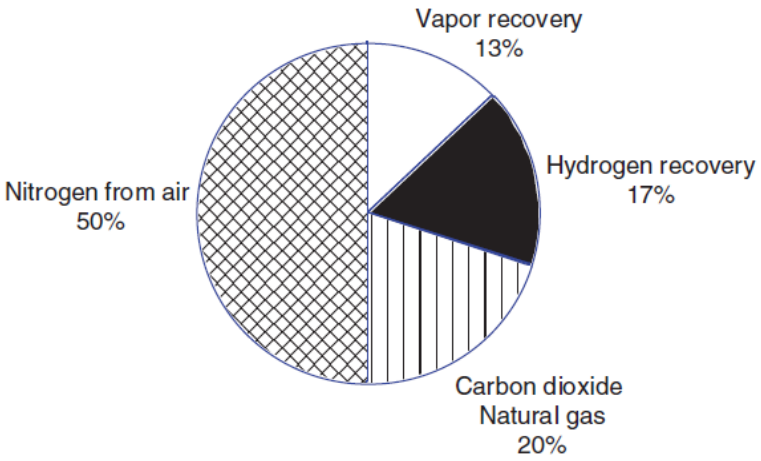

Figure 1.3 Market share in 2000 for membrane gas separations

Membrane gas separation process demands that a prevailing nonequilibrium situation, which is the fundamental difference comparing to conventional processes based on phase equilibrium, such as pressure swing adsorption (PSA) and cryogenic distillation. During practical operation, a difference in partial pressure (or fugacity) of the permeating species between the upstream and downstream sides is applied to generate a chemical potential driving force which will induce the permeation of the species

through the membrane material. The separation is almost systematically operated based on a steady-state regime. The general scheme of membrane gas separation process is shown in Figure 1.4 [8].

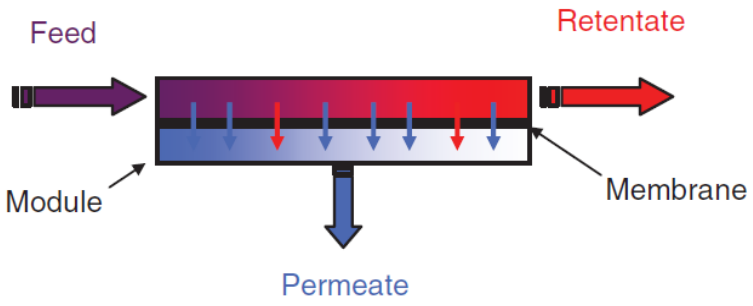

Figure 1.4 Schematic diagram of a basic membrane gas separation process

Conventional gas separation processes such as absorption in basic solvents, PSA and cryogenic distillation have several drawbacks. These drawbacks include the need for solvent regeneration, large footprint for offshore applications, lack of robustness towards different feed compositions, and highly capital and energy intensive. Conversely, membrane for gas separation possesses the advantages of (1) higher energy efficiency, (2) simplicity in operation, (3) compactness and portability and (4) environmentally friendly [11, 12]. Table 1.2 lists the common investigated gases in polymeric gas separation studies and applications [8].

Table 1.2 Physico-chemical properties of a series of gaseous compounds most often investigated in polymeric gas separation studies or industrial applications

	T_b (K)	T_c (K)	Lennard–Jones diameter (Å)	Kinetic diameter (Å)	Lennard–Jones interaction parameter ε (K)
He	4.3	5.3	2.55	2.69	10.2
H_2	20	33	2.89	2.89	60
O_2	90	155	3.46	3.46	107
CO	82	133	3.69	3.76	91.7

CH_4	112	191	3.76	3.87	149
N_2	77	126	3.80	3.64	71
CO_2	195	304	3.94	3.30	195
C_3H_8	231	370	5.12	4.30	237.1
H_2O	373	647	~3.7		809.1

1.3 Diversity of membrane materials

1.3.1 Polymers

In nowadays and foreseeable future, polymers are the majority materials for fabricating large-scale commercializing gas separation membranes due to the advantages of good physicochemical properties, easy processability, and low production costs [13, 14]. Intensive research studies have been conducted to develop new polymers with enhanced gas transport properties. However, to be commercialized for gas separation membranes, a polymer should possess not only good gas separation performance, but also low cost and high stability under certain operating conditions. So far only a small group of polymers have been sold in the market, and less than ten of them are currently in use for industrial gas separation membranes. Table 1.3 provides the gas transport properties of commercial polymers used for fabricating gas separation membranes [8, 15].

Table 1.3 Gas transport properties of commercial polymers used for fabricating gas separation membranes

Commercial polymer	**Permeability at 30 ℃ (Barrer)**				
	H_2	**N_2**	**O_2**	**CH_4**	**CO_2**
Cellulose acetate	2.63	0.21	0.59	0.21	6.3

Ethyl cellulose	87	3.2	11	19	26.5
Polycarbonate, brominated	--	0.18	1.36	0.13	4.23
Polydimethylsiloxane	550	250	500	800	2700
Polyimide (Matrimid®)	28.1	0.32	2.13	0.25	10.7
Polymethylpentene	125	6.7	27	14.9	84.6
Polyphenyleneoxide	113	3.81	16.8	11	75.8
Polysulfone	14	0.25	1.4	0.25	5.6
Polyetherimide	7.8	0.047	0.4	0.035	1.32

There are many considerations in the selection of a polymeric membrane for H_2/CO_2 separation: 1) The membrane should be chosen whether it is H_2-selective or CO_2-selective depending on the application and operating conditions; 2) The membrane should have a good balance of gas permeability and gas pair permselectivity; 3) The membrane should display satisfactory thermal, chemical and mechanical stability toward harsh operating conditions and aggressive feeds; 4) The membrane should maintain acceptable performance with condensable gas species, e.g. CO_2 which results in plasticization and possible deterioration of the separation performance; 5) The membrane should have a good tolerance of trace impurities in the gas stream, such as H_2O, CO, H_2S, N_2 and NO, etc.

1.3.2 Inorganics

There are various types of inorganic membranes that can be utilized for hydrogen purification, including metallic [16-18], silica [19-21], ceramic [22, 23], carbon [24-26], zeolite [27], MOF [28-30] and others (e.g. oxide [31] and glass [32]).

For dense metallic membranes (e.g. Pd and Pt membranes), hydrogen is transported

through a modified solution-diffusion mechanism. Specifically, H_2 molecules are firstly dissociated into protons and electrons and then pass across the membrane. Subsequently at the downstream side, molecular H_2 is formed by the reassociation of the protons and electrons and released. Due to this H_2 specifically transportation mechanism, dense metallic membranes are highly selective for H_2 (can be considered as infinite theoretically) [33]. However, despite their attractive hydrogen purification properties, metallic membranes do not provide an ideal choice for commercialization due to some inevitable drawbacks. The costs of these metals are too high. Moreover, metallic membranes suffer from hydrogen-enbrittlement cracking with increasing time of operation, and are readily sensitive to surface contamination.

Carbon molecular sieve membranes (CMSMs) represent a sub-family of carbon membranes and their H_2/CO_2 separations mainly dependent on pore size. There have been a number of literature reports on CMSMs that are derived from polymeric precursors [24-26]. The gas-separation performance of a CMSM highly depends on precursor selection and treatment, pyrolysis conditions, and post-treatment procedures [24].

Crystalline membranes (e.g. zeolite and MOFs) generally have more uniform pore size (normally 3 to 6 Å) and a narrower pore-size distribution that result in higher gas-separation efficiency. However, till now real crystalline molecular sieve membranes seldom show the expected separation factors because nonstructural pores (pin holes, cracks) destroy the predicted selectivity. Despite increasing publications on the development of zeolite membranes, there is no industrial gas separation using zeolite membranes so far, except for the de-watering of bio-ethanol by vapor permeation

using LTA membranes [34]. Recently, metal–organic framework (MOF) membranes have been fabricated and tested for gas separation. Although MOFs share some common structure-related properties with zeolites, the structural flexibility of MOFs significantly reduces the sharp molecular sieving effect with a pore size assuming from a ‘rigid’ crystallographic frameworks (such as in zeolite) by size exclusion. Specialty, as a group of organic–inorganic material, MOF nanoparticles show better compatibility with organics thus can be easily embedded into organic polymers.

Although several inorganic membranes exhibit excellent gas separation performance, the inherent brittleness of inorganic membranes makes them difficult for large-scale production and handling (such as housing and thermal expansion during heating and cooling). Further technological breakthroughs in the processing and manufacturing of inorganic membranes are necessary before commercialization for large scale industry is feasible.

1.3.3 Organic-inorganic hybrids

To combine the good processability of polymers and the outstanding gas-separation properties of inorganic materials, nano-composite membranes or mixed-matrix membranes (MMMs) are developed. MMMs are comprised of a polymer matrix as the continuous phase, and inorganic particles (e.g. zeolite, carbon, metal, metal oxides and MOFs) as the dispersed phase. Figure 1.5 illustrates the schematic of MMMs [35]. Since it was first invented by Kulprathipanja et al. [36] about 25 years ago, MMMs have been extensively studied. Some of MMMs have shown enhanced separation performance for gas and liquid pairs [35, 37]. There are still many challenges ahead

such as interface voids, pore blockage and chain rigidification [35, 38, 39]. In addition, the oversize of zeolite nano-particles, their mutual agglomeration, and poor interface with the polymer matrix are troublesome issues and must be overcome before considering commercialization. One of the ways to overcome these deadlocks is to identify new selective fillers which have characteristics of inherently nano-size, less aggregation and better interactions with the polymer matrix.

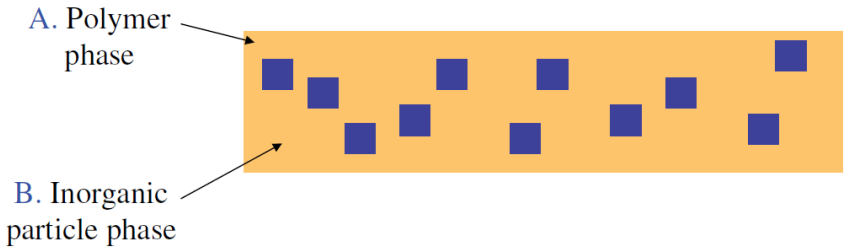

Figure 1.5 Schematic of mixed matrix membranes (MMMs)

Based on the structure and functional role of the inorganic fillers, the filler inside MMMs can be classified as (1) non-porous inert, (2) non-porous activated, (3) high affinity with polymers and (4) porous nanoparticles. Figure 1.6 illustrates the gas transport mechanisms in mixed matrix membranes containing inorganic fillers in different cases [35]. Fumed silica [40] and C60 nanoparticles [41] are examples of non-porous inert, with poor interaction between these particles and polymer chains and thus creating interfacial voids between the two phases. Although the overall gas permeability may increase due to the enhanced surface flow occurring at the interfacial voids [42], this is only resulted from the reduction of the apparent membrane thickness and not indicates the improvement of the real performance. The group of non-porous activated nanoparticles includes activated carbon particles [43], which exhibit favorable interactions toward the gas molecules and thus may improve

the gas sorption. Metal, metal oxides, surface modified zeolites, and MOF particles [44-47] belong to the group of nanoparticles with high affinity to the polymers. These particles possess high affinity with the polymers and hinder the mobility of the polymer chains, which causes polymer chain rigidification and may help to improve the gas pair selectivity of the membrane. Porous nanoparticles including zeolites [36, 48, 49], MOFs [47, 50, 51] and carbon molecular sieves [52], and have the advantages of providing the high diffusivity selectivity of inorganic molecular sieves and high gas permeability due to their high porosity.

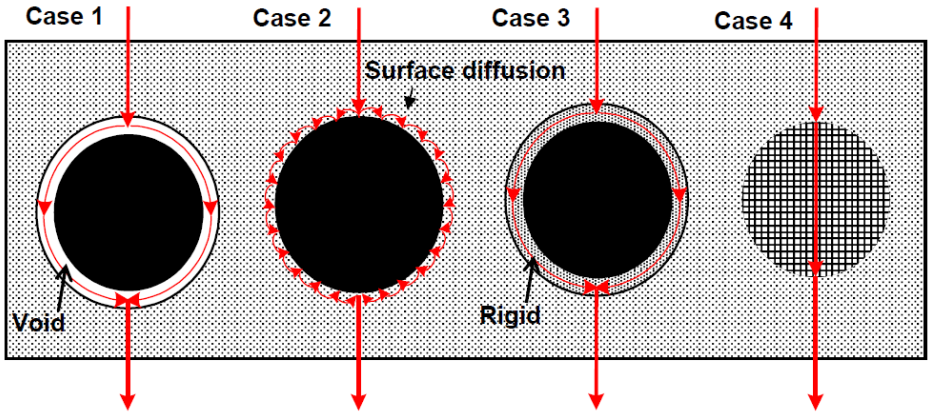

Figure 1.6 Different gas transport routes through mixed matrix membranes (MMMs)

1.4 Gas transport mechanism

The gas permeation in most dense polymeric membranes is controlled by the solution-diffusion mechanism. As indicated in Figure 1.7 [53], the penetrant is sorbed into the upstream membrane face from the external phase, moves by molecular diffusion in the membrane to the downstream face, and leaves through the external phase in contact with the membrane. The pressure of gas at the upstream is higher than the pressure at the downstream, providing the key driving force for the separation process.

The permeability, P of a gas penetrant through a membrane is defined as [7]:

$$P = \frac{Nl}{(p_2 - p_1)} \tag{1-3}$$

where N represents the gas flux through the membrane at steady-state; p_1 and p_2 refers to the downstream and upstream pressures, respectively; and l is the membrane thickness. The permeability of a polymeric membrane is generally indicated in Barrer (1 Barrer $=10^{-10}$ cm^3 (STP) cm /cm^2 sec cmHg). Permeability is independent of the membrane thickness, and is a fundamental property of the polymeric material.

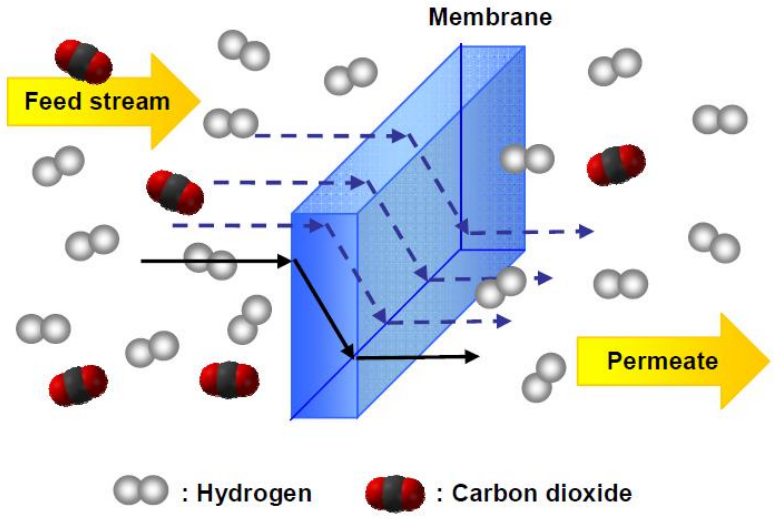

Figure 1.7 Solution-diffusion mechanism for a H_2-selective dense polymeric membrane

Based on the solution-diffusion mechanism, the permeability (P) of a gas across the membrane is a product of the diffusion (D) coefficient and solubility (S) coefficient.

$$P = D \times S \tag{1-4}$$

The diffusion coefficient (D) is a kinetic parameter that measures the overall mobility of the gas penetrant molecules in the membrane, and is influenced by various factors, including (1) the size and shape of the gas penetrant molecules, (2) the cohesive

energy density of the polymer, (3) the mobility of the polymer chains and (4) the free volume size and distribution of the polymer [54]. The solubility coefficient is a thermodynamic parameter and it depends on (1) the condensability of the penetrant gases, (2) the nature of interactions between the penetrants and the polymer and (3) the chain packing density in glassy polymers [54]. The units for the diffusivity and solubility coefficients are 10^{-10} cm^2/s and $cm^3(STP)/cm^3$ cmHg, respectively.

The ideal permselectivity $\alpha_{A/B}$ for component A relative to component B is determined from the ratio of their permeability and expressed by the following equation：

$$\alpha_{A/B} = P_A / P_B \tag{1-5}$$

Based on the solution-diffusion mechanism, the ideal selectivity can also be expressed as follows:

$$\alpha_{A/B} = \left(\frac{D_A}{D_B}\right) \times \left(\frac{S_A}{S_B}\right) \tag{1-6}$$

where (D_A/D_B) and (S_A/S_B) refer to the diffusion selectivity and solubility selectivity, respectively. To obtain a high gas pair permselectivity, both the diffusion selectivity and solubility selectivity should be taken into consideration.

In porous membranes, the gas transport mechanism is classified as Poiseuille flow and/or Knudsen diffusion [53]. As illustrated in Figure 1.8 (a) [13], Poiseuille flow takes place when the pore radius (r) in the membrane is larger than the mean free path (λ) of the gas penetrant. The mean free path (λ) indicates the distance travelled by a gas molecule during collision, and is determined by the following equation [55, 56]:

$$\lambda = \frac{3\eta}{2p}\left(\frac{\pi RT}{2M_w}\right)^{1/2} \quad (1\text{-}7)$$

where η represents the gas viscosity, p refers to the pressure, T is the absolute temperature, M_W is the molecular weight of the gas component and R refers to the universal gas constant.

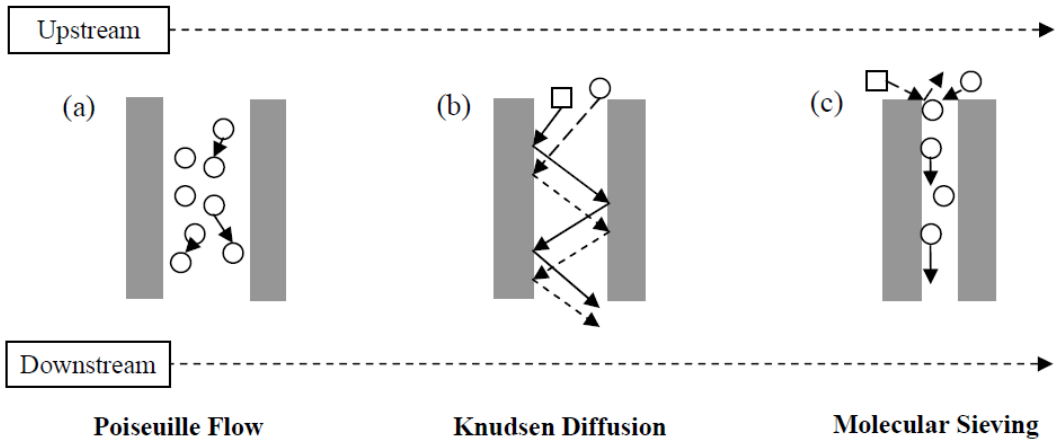

Figure 1.8 Schematics of gas transport mechanisms
(a) Poiseuille flow, (b) Knudsen diffusion and (c) molecular sieving.

As shown in Figure 1.8 (b), Knudsen diffusion occurs when the pore size decreases to around 50-100 Å and the permeation of the gas molecule is independent of neighboring molecules [56]. In Knudsen diffusion, the diffusivity coefficient is inversely proportional to the square root of the gas molecular weight. Therefore, for equimolar binary gas feed across the membrane, the Knudsen selectivity for component A to component B ($\alpha_{K,A/B}$) is expressed by the following equation:

$$\alpha_{K,A/B} = \sqrt{\frac{M_{WB}}{M_{WA}}} \quad (1\text{-}8)$$

where M_{WA} and M_{WB} refers to the molecular weights of gas A and gas B, respectively.

In smaller pores that are generally with diameters less than 7Å, molecular sieving is the dominant gas transport mechanism. As indicated in Figure 1.8 (c), the smaller gas molecules with higher diffusion rates are able to permeate faster through the molecular sieving membranes than the larger molecules with lower diffusion rates [11]. This type of gas transport mechanism is present in common inorganic membranes, such as carbon molecular sieves, zeolites, and some MOFs with small aperture sizes.

1.5 Membrane fabrication and structures

The materials used for the fabrication of membranes include polymers, ceramics, metals, glass, or liquids; the materials may be either neutral or carry electrical charges due to some fixed ions; and the conformations of membranes can be flat, tubular, or a hollow fiber. Figure 1.9 [8] illustrates the schematic drawing of the morphology, materials, and configuration of some technically useful synthetic membranes. For symmetric membranes, there is no difference of the structure and the transport properties over the entire cross section and the membrane flux is determined by the thickness of the entire membrane.

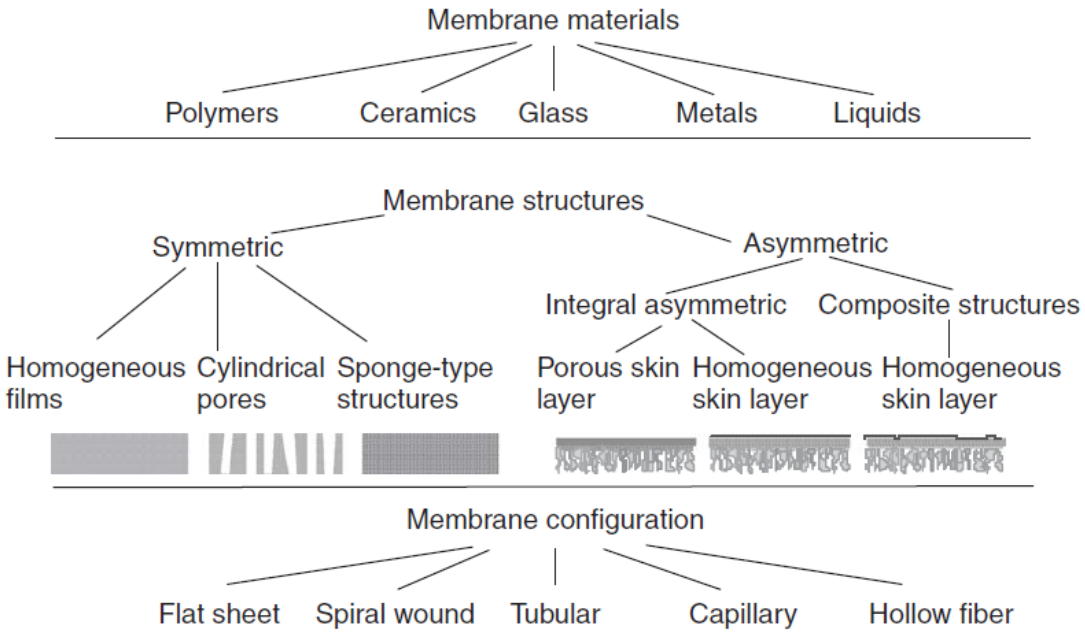

Figure 1.9 Schematic drawing of the morphology, materials, and configuration of technically relevant synthetic membranes

In asymmetric membranes, the structure and the transport properties vary over the cross section of the membranes. Normally, an asymmetric membrane contains a thin skin layer and a thick highly porous supporting layer. The nature of the material or the size of pores in the thin skin layer actually determines the separation characteristics of the asymmetric membrane. The thickness of the skin layer determines the mass flux of the membrane. The porous supporting layer serves only as a mechanical support for the thin and fragile skin and shows little effect on the membrane separation properties. Asymmetric membranes possess the advantages of high fluxes and good mechanical stability, and are mainly applied in pressure-driven membrane processes, including reverse osmosis, ultrafiltration, and gas and vapor separation.

1.6 Types of membrane module configurations

Since most industrial processes require several hundred, sometimes several thousand, square meters of membrane to perform the separation, it is important to develop methods to incorporate large membrane areas into economical membrane packets or modules. As schematically illustrated in Figure 1.10 [57], the three most important membrane configurations are hollow-fine-fiber (with fiber diameters of 100 to 250 μm), capillary-fiber (with fiber diameters of 500–2000 μm) and spiral-wound modules [57]. Plate-and-frame and tubular modules are also used, but their high cost makes them only suitable for small-scale or specialized applications. Table 1.4 [57] summarizes the advantages and disadvantages of the various module types [57].

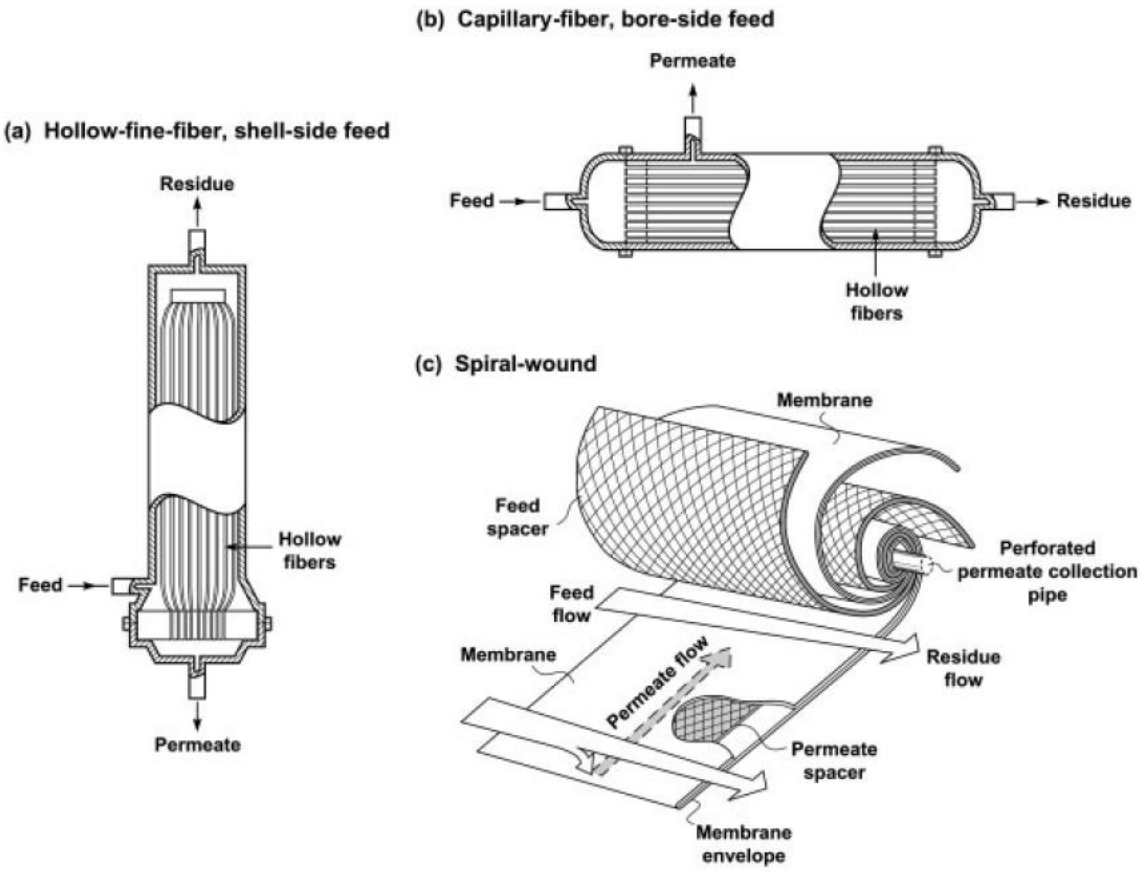

Figure 1.10 Membrane module configurations

Table 1.4 Key characteristics of the three major types of modules used for the industrial applications of gas separation processes with polymeric membranes

	Plate and frame	Spiral wound	Hollow fiber
Packing density (m^2m^{-3})	30-500	200-1000	500-10000
Approximate area per module (m^2)	5–20	20–40	300–600
Pretreatment requirement	Minimal	Fair	High
Resistance to fouling	Good	Fair	Poor
Pressure drop	Low	Fair	High
Flow distribution	Fair	Moderate	Good
Manufacturing cost	High (50–200m^{-2})	Medium (10–50m^{-2})	Low (2–10m^{-2})

Hollow fibers allow a very large membrane area to be contained in a relatively small volume. The production cost of hollow fiber modules is low on a per-square-meter basis (in the range US $2–10/$m^2$), because some high-speed automated spinning and module producing equipment can be used to fabricate the fibers and prepare the membrane modules. A key disadvantage of hollow fiber module is that the polymer membrane must perform the required separation performance as well as withstand certain pressure driving force across the membrane. It is more difficult in hollow-fiber form to produce membrane that has high selectivity, high flux as well as enough mechanically stability than in the flat sheets form that used for spiral-wound modules.

1.7 Process and cost optimization

For hydrogen purification using a one-stage membrane separator, the hydrogen purity of the permeate stream may be less than 95%. To further improve the hydrogen purity in order to meet product requirements in an economical way, using a two-stage membrane separator or coupling with a PSA unit may be applicable. The small footprint of a membrane separator facilitates its integration with other process units.

Recently in early 2012, MTR published a paper on process design using H_2-selective or/and CO_2-selective membranes to separate CO_2 from gasified coal syngas [58]. The best design in this paper using recently developed membranes in MTR shows 40% of the capital cost and 50% of the energy consumption of the conventional Selexol cold absorption process. As shown in Figure 1.11 [58], this optimized membrane process contains two stages of membrane separation and uses both H_2- and CO_2-selective membranes.

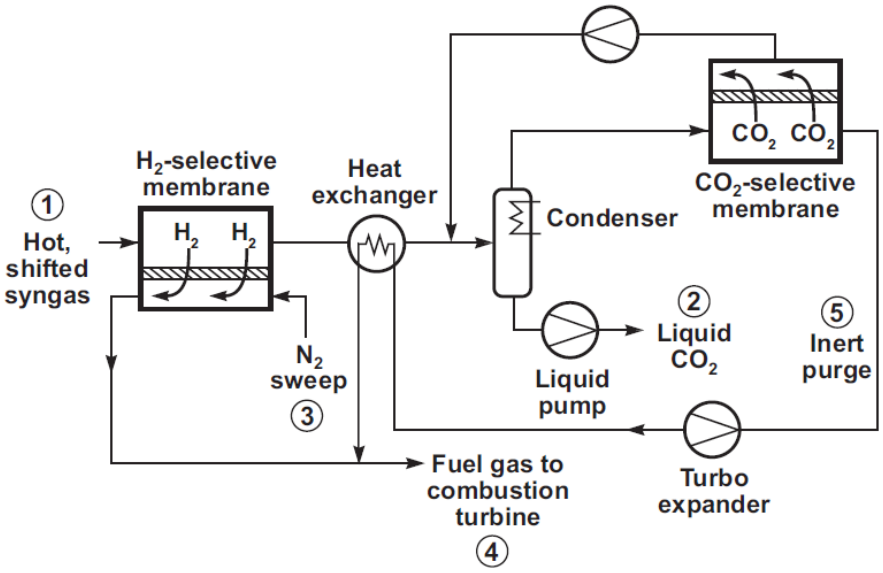

	Stream #				
Stream compositions (mol%)	① Hot, shifted syngas	② Liquid CO_2	③ N_2 sweep	④ Fuel gas	⑤ Inert purge
H_2	50.9	1.1	0	43.7	80.0
CO_2	36.8	96.9	0	3.2	4.0
CO	1.1	0.3	0	0.8	6.5
N_2	0.7	0.3	100	43.8	9.5
H_2S	0.5	1.4	0	0.01	0.02
H_2O	10.0	0	0	8.4	0
Flow rate (tons/h)	622	468	445	595	36.3
Pressure (bar)	50	140	32	32	50
Temperature (°C)	150	10	150	150	25

Figure 1.11 A membrane process designed by MTR consisting both H_2- and CO_2-selective membranes

1.8 Research objectives and organization of dissertation

For syngas separation, an ideal H_2-selective membrane should possess the following features: 1) It can operate continuously at elevated temperatures (around 200 ℃) and directly separate the production stream from the low-temperature water-gas shift reactor, thus eliminating the additional processes and cost to cool the syngas and remove a large amount of water; 2) It can also effectively remove impurities such as CO, N_2 and CH_4 from the feed stream; and 3) It is able to withstand high pressures from the feed gas stream [58]. Compared to other polymers, polybenzimidazole (PBI) is a promising material to meet the aforementioned requirements because it possesses remarkable thermal stability, good chemical resistance, impressive compression strength, and high intrinsic H_2/CO_2 selectivity. However, the major drawbacks of PBI are (1) low H_2 permeability and (2) brittleness [59]. To overcome these bottlenecks, increasing PBI gas permeability by incorporating high porosity nano-particles with high stability and good compatibility with PBI (i.e. ZIFs in this study) is one of the most promising approaches.

The objectives of this research study are (1) to conduct fundamental research on the synthesis and characterization of novel zeolitic imidazolate frameworks (ZIFs)/polybenzimidazole (PBI) mixed matrix membranes (MMMs) and (2) to explore the feasibility of spinning this type of materials into defect-free asymmetric hollow fiber membranes. In other words, the aims are to considerably improve the intrinsic H_2 permeability of the dense ZIFs/PBI membrane and fabricate it into a useful form for H_2/CO_2 separation. For performance evaluation, the temperature-

dependent separation performance evolutions, as well as the effects of impurities such as CO and H_2O vapor on the newly developed membranes are examined.

This dissertation is organized and structured into eight chapters and brief descriptions of the coverage in these chapters are as follows.

Chapter 1: A general review on the importance of utilizing hydrogen as an important chemical and petrochemical industry feed and an alternative clean fuel and energy carrier is presented. This chapter highlights the significance and relevance of membrane technology in hydrogen purification and CO_2 capture specifically for syngas processing. The key consideration factors (i.e. membrane material, structure and configuration, module design and process optimization) for the effective commercial implementation of membrane technology are interpreted. The objectives of this research study are emphasized.

Chapter 2: The current state of the art on polymeric membranes for hydrogen purification is reviewed. The development status about the base materials (i.e. PBI and ZIFs) and membrane fabrication methods in this study are also introduced. Finally, the current challenges encountered and the future prospects in using polymeric membranes for high temperature hydrogen purification are discussed.

Chapter 3: The materials used and the membrane fabrication protocols for both symmetric dense film and asymmetric dual-layer hollow fiber membrane are provided. This chapter documented detailed descriptions of the characterization techniques used to determine the physicochemical and gas transport properties of the membranes.

Chapter 4: The new scheme to prepare ZIF-7/PBI nano-composite membranes with well dispersed nano-size particles is described. The thermal stability, particle dispersion as well as gas transport properties are examined. The gas permeation data points are compared with the prediction from the Maxwell model. Mixed gas testing from ambient to high tempratures are also performed.

Chapter 5: The separation performances of ZIF-8/PBI nano-composite membranes for hydrogen purification from 35 to 230 ℃ are evaluated. Detailed investigations were carried out in the aspects of material characterizations, gas permeation mechanism, as well as performance evolution using feed streams containing CO or water impurities.

Chapter 6: A novel room-temperature synthesis method of nano-scale ZIF-90 particles is described. The physical and chemical structures of the ZIF-90 nanoparticles are examined via multiple advanced instrumental analyses. The applicability of ZIF-90 nanocrystals is demonstrated by fabricating ZIF-90/PBI nano-composite membranes for hydrogen purification. The particle dispersion state and gas separation properties of the membranes are characterized.

Chapter 7: The processibility of ZIF-8/PBI nano-composite material is demonstrated via fabricating asymmetric dual-layer hollow fiber membranes. Defect-free ZIF-8-PBI/Matrimid dual-layer hollow fibers have been successfully fabricated without post annealing and coating by optimizing ZIF-8 nano-particle loadings, spinning

conditions and solvent-exchange procedures. The gas separation performances and the morphology of the hollow fibers are examined.

Chapter 8: The key conclusions derived from this work are summarized and some future research directions are highlighted.

1.9 References

[1] J. Conti and P. Holtberg, International Energy Outlook 2011, U.S. Energy Information Administration, Washington, 2011.

[2] J. W. Sheffield, in Assessment of Hydrogen Energy for Sustainable Development, ed. J. W. Sheffield and C. Sheffield, Springer, Dordrecht, 2007, ch.1, pp. 1-8.

[3] T. N. Vezirolu, F. Barbir, Hydrogen: the wonder fuel, International Journal of Hydrogen Energy, 17 (1992) 391-404.

[4] T. N. Veziroglu, F. Barbir, Hydrogen: its comparison with fossil fuels and its potential as a universal fuel, US Geological Survey Professional Paper, 1570 (1993) 715-724.

[5] T. N. Veziroglu, Hydrogen technology for energy needs of human settlements, International Journal of Hydrogen Energy, 12 (1987) 99-129.

[6] B. Sorensen, Hydrogen and Fuel Cells, 2nd edn., Elsevier, Burlington, 2012.

[7] S. Matteucci, Y. Yampolskii, B. D. Freeman and I. Pinnau, in Materials Science of Membranes for Gas and Vapor Separation, ed. Y. Yampolskii, I. Pinnau and B. D. Freeman, John Wiley & Sons, Ltd., Chichester, 2006, ch. 1, pp. 1-47.

[8] E. Drioli, L. Giorno, Comprehensive Membrane Science and Engineering, Elsevier, Amsterdam, 2010.

[9] R. W. Baker, Future directions of membrane gas separation technology, Industrial and Engineering Chemistry Research, 41 (2002) 1393-1411.

[10] H. Strathmann, Membrane separation processes: Current relevance and future opportunities, AIChE Journal, 47 (2001) 1077-1087.

[11] W. J. Koros, G. K. Fleming, Membrane-based gas separation, Journal of Membrane Science, 83 (1993) 1-80.

[12] J. D. Perry, K. Nagai, W. J. Koros, Polymer membranes for hydrogen separations, MRS Bulletin, 31 (2006) 745-749.

[13] L. Shao, B. T. Low, T. S. Chung, A. R. Greenberg, Polymeric membranes for the hydrogen economy: Contemporary approaches and prospects for the future, Journal of Membrane Science, 327 (2009) 18-31.

[14] Y. Xiao, B. T. Low, S. S. Hosseini, T. S. Chung, D. R. Paul, The strategies of molecular architecture and modification of polyimide-based membranes for CO_2 removal from natural gas-A review, Progress in Polymer Science (Oxford), 34 (2009) 561-580.

[15] V. Abetz, T. Brinkmann, M. Dijkstra, K. Ebert, D. Fritsch, K. Ohlrogge, D. R. Paul, K. V. Peinemann, S. P. Nunes, N. Scharnagl, M. Schossig, Developments in membrane research: From material via process design to industrial application, Advanced Engineering Materials, 8 (2006) 328-358.

[16] S. N. Paglieri, J. D. Way, Innovations in palladium membrane research, Separation and Purification Methods, 31 (2002) 1-169.

[17] P. P. Mardilovich, Y. She, Y. H. Ma, M. H. Rei, Defect-Free Palladium Membranes on Porous Stainless-Steel Support, AIChE Journal, 44 (1998) 310-322.

[18] J. Tong, Y. Kashima, R. Shirai, H. Suda, Y. Matsumura, Thin defect-free Pd membrane deposited on asymmetric porous stainless steel substrate, Industrial and Engineering Chemistry Research, 44 (2005) 8025-8032.

[19] K. Kusakabe, F. Shibao, G. Zhao, K. I. Sotowa, K. Watanabe, T. Saito, Surface modification of silica membranes in a tubular-type module, Journal of Membrane Science, 215 (2003) 321-326.

[20] Y. Iwamoto, K. Sato, T. Kato, T. Inada, Y. Kubo, A hydrogen-permselective amorphous silica membrane derived from polysilazane, Journal of the European Ceramic Society, 25 (2005) 257-264.

[21] J. C. Diniz Da Costa, G. Q. Lu, V. Rudolph, Y. S. Lin, Novel molecular sieve silica (MSS) membranes: characterisation and permeation of single-step and two-step sol-gel membranes, Journal of Membrane Science, 198 (2002) 9-21.

[22] U. Balachandran, T. H. Lee, L. Chen, S. J. Song, J. J. Picciolo, S. E. Dorris, Hydrogen separation by dense cermet membranes, Fuel, 85 (2006) 150-155.

[23] Y. Gu, S. T. Oyama, High molecular permeance in a poreless ceramic membrane, Advanced Materials, 19 (2007) 1636-1640.

[24] Y. Xiao, Y. Dai, T. S. Chung, M. D. Guiver, Effects of brominating Matrimid polyimide on the physical and gas transport properties of derived carbon membranes, Macromolecules, 38 (2005) 10042-10049.

[25] L. Shao, T. S. Chung, K. P. Pramoda, The evolution of physicochemical and transport properties of 6FDA-durene toward carbon membranes: from polymer, intermediate to carbon, Microporous and Mesoporous Materials, 84 (2005) 59-68.

[26] Y. K. Kim, H. B. Park, Y. M. Lee, Gas separation properties of carbon molecular sieve membranes derived from polyimide/polyvinylpyrrolidone blends: Effect of the molecular weight of polyvinylpyrrolidone, Journal of Membrane Science, 251 (2005) 159-167.

[27] G. P. Fotou, Y. S. Lin, S. E. Pratsinis, Hydrothermal stability of pure and modified microporous silica membranes, Journal of Materials Science, 30 (1995) 2803-2808.

[28] A. Huang, H. Bux, F. Steinbach, J. Caro, Molecular-sieve membrane with hydrogen permselectivity: ZIF-22 in LTA topology prepared with 3-aminopropyltriethoxysilane as covalent linker, Angewandte Chemie - International Edition, 49 (2010) 4958-4961.

[29] A. Huang, W. Dou, J. Caro, Steam-stable zeolitic imidazolate framework ZIF-90 membrane with hydrogen selectivity through covalent functionalization, Journal of the American Chemical Society, 132 (2010) 15562-15564.

[30] Y. S. Li, F. Y. Liang, H. Bux, A. Feldhoff, W. S. Yang, J. Caro, Molecular sieve membrane: Supported metal-organic framework with high hydrogen selectivity, Angewandte Chemie - International Edition, 49 (2010) 548-551.

[31] A. L. Ahmad, M. R. Othman, H. Mukhtar, H_2 separation from binary gas mixture using coated alumina-titania membrane by sol-gel technique at high-temperature region, International Journal of Hydrogen Energy, 29 (2004) 817-828.

[32] R. P. Singh, J. D. Way, K. C. McCarley, Development of a model surface flow membrane by modification of porous Vycor glass with a fluorosilane, Industrial and Engineering Chemistry Research, 43 (2004) 3033-3040.

[33] N. W. Ockwig, T. M. Nenoff, Membranes for hydrogen separation, Chemical Reviews, 107 (2007) 4078-4110.

[34] J. Caro, Are MOF membranes better in gas separation than those made of zeolites, Current Opinion in Chemical Engineering, 1 (2011) 77-83.

[35] T. S. Chung, L. Y. Jiang, Y. Li, S. Kulprathipanja, Mixed matrix membranes (MMMs) comprising organic polymers with dispersed inorganic fillers for gas separation, Progress in Polymer Science (Oxford), 32 (2007) 483-507.

[36] S. Kulprathipanja, R. W. Neuzil, N. N. Li (Allied-Signal Inc.), US 4740219, 1988.

[37] L. Y. Jiang, Y. Wang, T. S. Chung, X. Y. Qiao, J.-Y. Lai, Polyimides membranes for pervaporation and biofuels separation, Progress in Polymer Science, 34 (2009) 1135-1160.

[38] C. M. Zimmerman, A. Singh, W. J. Koros, Tailoring mixed matrix composite membranes for gas separations, Journal of Membrane Science, 137 (1997) 145-154.

[39] Y. Li, T. S. Chung, C. Cao, S. Kulprathipanja, The effects of polymer chain rigidification, zeolite pore size and pore blockage on polyethersulfone (PES)-zeolite A mixed matrix membranes, Journal of Membrane Science, 260 (2005) 45-55.

[40] M. Moaddeb, W. J. Koros, Gas transport properties of thin polymeric membranes in the presence of silicon dioxide particles, Journal of Membrane Science, 125 (1997) 143-163.

[41] T. S. Chung, S. S. Chan, R. Wang, Z. Lu, C. He, Characterization of permeability and sorption in Matrimid/C60 mixed matrix membranes, Journal of Membrane Science, 211 (2003) 91-99.

[42] T. C. Merkel, B. D. Freeman, R. J. Spontak, Z. He, I. Pinnau, P. Meakin, A. J. Hill, Ultrapermeable, reverse-selective nanocomposite membranes, Science, 296 (2002) 519-522.

[43] M. Anson, J. Marchese, E. Garis, N. Ochoa, C. Pagliero, ABS copolymer-activated carbon mixed matrix membranes for CO_2/CH_4 separation, Journal of Membrane Science, 243 (2004) 19-28.

[44] S. Yoda, A. Hasegawa, H. Suda, Y. Uchimaru, K. Haraya, T. Tsuji, K. Otake, Preparation of a platinum and palladium/polyimide nanocomposite film as a precursor of metal-doped carbon molecular sieve membrane via supercritical impregnation, Chemistry of Materials, 16 (2004) 2363-2368.

[45] Q. Hu, E. Marand, S. Dhingra, D. Fritsch, J. Wen, G. Wilkes, Poly(amide-imide)/TiO_2 nano-composite gas separation membranes: Fabrication and characterization, Journal of Membrane Science, 135 (1997) 65-79.

[46] Y. Li, H. M. Guan, T. S. Chung, S. Kulprathipanja, Effects of novel silane modification of zeolite surface on polymer chain rigidification and partial pore blockage in polyethersulfone (PES)-zeolite A mixed matrix membranes, Journal of Membrane Science, 275 (2006) 17-28.

[47] T. Yang, Y. Xiao, T. S. Chung, Poly-/metal-benzimidazole nano-composite membranes for hydrogen purification, Energy and Environmental Science, 4 (2011) 4171-4180.

[48] R. Mahajan, W. J. Koros, Mixed matrix membrane materials with glassy polymers: Part 1, Polymer Engineering and Science, 42 (2002) 1420-1431.

[49] Y. Li, T. S. Chung, S. Kulprathipanja, Novel Ag^+-zeolite/polymer mixed matrix membranes with a high CO_2/CH_4 selectivity, AIChE Journal, 53 (2007) 610-616.

[50] T. Yang, G. M. Shi, T. S. Chung, Symmetric and asymmetric zeolitic imidazolate frameworks (ZIFs)/polybenzimidazole (PBI) nano-composite membranes for hydrogen purification at high temperatures, Advanced Energy Materials, 2 (2012) 1358-1367.

[51] T. Yang, T. S. Chung, High performance ZIF-8/PBI nano-composite membranes for high temperature hydrogen separation consisting of carbon monoxide and water vapor, International Journal of Hydrogen Energy, (2012) doi: 10.1016/j.ijhydene.2012.10.045.

[52] D. Q. Vu, W. J. Koros, S. J. Miller, Mixed matrix membranes using carbon molecular sieves: I. Preparation and experimental results, Journal of Membrane Science, 211 (2003) 311-334.

[53] B. T. Low, Polymeric-based membranes for hydrogen enrichment and natural gas sweetening, Ph.D. Thesis, National University of Singapore, 2009.

[54] Y. Yampolskii, I. Pinnau, B. D. Freeman, Materials Science of Membranes for Gas and Vapor Separation, John Wiley & Sons, Ltd., Chichester, 2006.

[55] M. Mulder, Basic principles of membrane technology, Kluwer Academic Publishers, Dordrecht, 1996.

[56] P. S. Tin, Membrane materials and fabrication for gas separation, Ph. D. Thesis, National University of Singapore, 2004.

[57] S. P. Nunes, K.-V. Peinemann, Membrane Technology: in the Chemical Industry, Second, Revised and Extended Edition, WILEY-VCH Verlag GmbH & Co. KGaA, Weinheim, 2006.

[58] T. C. Merkel, M. Zhou, R. W. Baker, Carbon dioxide capture with membranes at an IGCC power plant, Journal of Membrane Science, 389 (2012) 441-450.

[59] T. S. Chung, A critical review of polybenzimidazoles: Historical development and future R&D, Journal of Macromolecular Science - Reviews in Macromolecular Chemistry and Physics, 37 (1997) 277-301.

CHAPTER 2

LITERATURE REVIEW

2.1 Membrane material design principles for hydrogen purification

According to the solution-diffusion model, the gas pair selectivity is the product of solubility selectivity and diffusion selectivity. Table 2.1 summarizes relative physical properties of H_2 and CO_2. For the separation of H_2 and CO_2, the solubility selectivity favors CO_2 transportation due to its higher critical temperature (304 K of CO_2 vs. 33 K of H_2) while the diffusion selectivity favors H_2 transportation due to its smaller kinetic diameter (2.89Å of H_2 vs. 3.30 Å of CO_2). Since the diffusion selectivity and solubility selectivity show opposite preference for H_2 and CO_2 transports, the separation of H_2 and CO_2 mixture by polymeric membranes is complicated and challenging as compared with other gas pairs. Generally, glassy polymers are typically used for fabricating H_2-selective membranes and the separation performance can be improved by amplifying D_{H2}/D_{CO2} while reducing S_{CO2}/S_{H2}. On the other hand, rubbery polymers are preferred for fabricating CO_2-selective membranes and the design rule is increasing S_{CO2}/S_{H2} while minimizing D_{H2}/D_{CO2}.

Table 2.1 Selected physical properties of H_2 and CO_2

Gas properties	**H_2**	**CO_2**
Molecular weight	2.02	44.01
Kinetic diameter (Å)	2.89	3.30
Lennard-Jones collision diameter (Å)	2.827	3.941
Critical temperature, T_c (K)	33.2	304.1
Condensability (K)	60	195
Density at 0 ℃ and 1 atm (g/l)	0.0899	1.977

Membrane gas-separation performance is often expressed in terms of a "trade-off" relationship namely "Robeson upper bound". Figure 2.1 shows the latest Robeson upper bound announced in 2008 for H_2-selective polymeric membranes [1]. Most of the existing polymeric membranes exhibit separation performances that fall below the corresponding trade-off line.

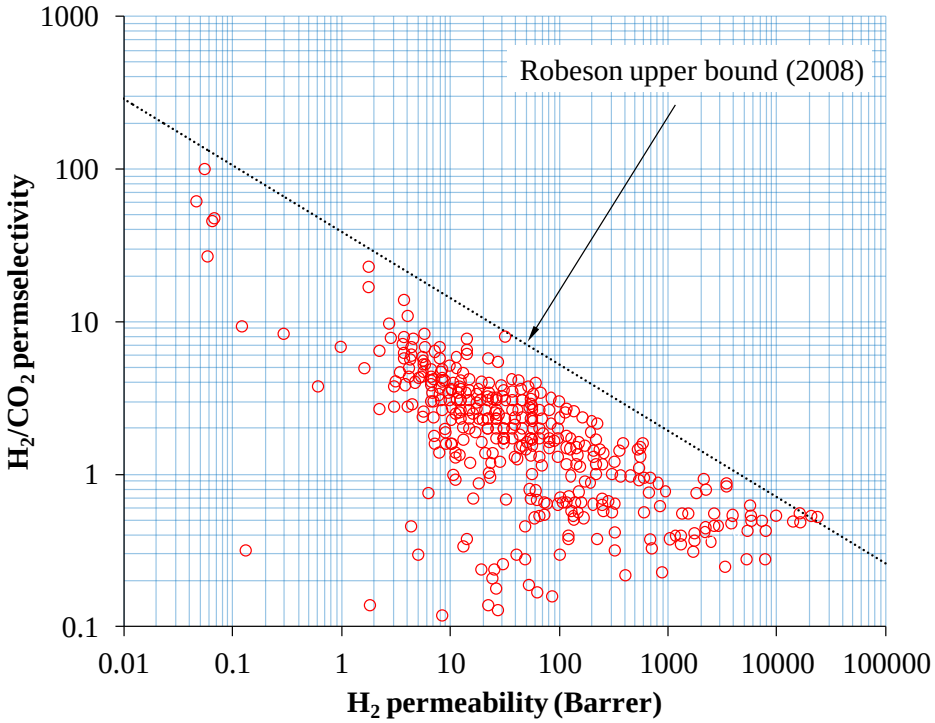

Figure 2.1 Robeson upper bound for H_2-selective polymeric membranes

In the following sections, a literature review of the various methods to design polymeric-based membranes with enhanced H_2/CO_2 separation performance is presented. The materials utilized in this study as well as other important aspects are also described.

2.2 H_2-selective polymeric membranes for hydrogen purification

H_2-selective membranes have the advantages of eliminating the cost on CO_2 recompression for subsequent sequestration. They are often made by glassy polymers since their polymer chains are much more rigid compared with rubbery polymers under the operating conditions. The H_2/CO_2 diffusivity selectivity contributes the main selectivity because H_2 is favored in the transportation. Currently, as shown in Table 2.2, most commercial polymers exhibit undesirable intrinsic H_2/CO_2 selectivity (1.2–5.9) [2-5] except polybenzimidazole (PBI) (~8) [6]. To overcome the low H_2/CO_2 selectivity nature of existing polymeric membranes, researches on H_2-selective polymeric membranes have focused on molecular design of new materials [7-9] and modifications of existing polymers by means of cross-linking (chemical, thermal and UV) [10-13], blending, doping, and mixed-matrix membranes. In this section, progress of molecular design of new materials and chemical cross-linking modification is reviewed in more details.

Table 2.2 Representative H_2 and CO_2 intrinsic transport properties of H_2-selective membranes from commercial polymers

Polymers	***T*** **(°C)**	***P*** **(atm)**	**Permeability (Barrer)**		**H_2/CO_2 selectivity**
			H_2	**CO_2**	
Ethyl cellulose	30	--	87	26.5	3.28
Polyetherimide	30	--	7.8	1.32	5.91
Polyphenyleneoxide	30	--	113	75.8	1.49
Polysulfone (PSF)	30	--	14	5.6	2.50
Polymethylpentene	30	--	125	84.6	1.48
Polyimide (Matrimid®)	30	--	28.1	10.7	2.63
Polyethersulfone	35	3.5	8.96	3.38	2.65
Polystyrene	30	1.36	23.8	10.4	2.3
Poly(vinylidene fluoride) (Kynar)	30	1.36	2.4	1.2	2.0

Poly(methyl methacrylate)	30	1.36	2.4	0.6	4.0
Polybenzimidazole (PBI)	35	3.5	3.7	0.4	8.7

Several H_2-selective polymers with entire new structures have been designed in order to improve H_2/CO_2 separation performance. Xu et al. [7] investigated the gas-transport properties of fluorine containing poly(arylene ether)s (FBP/6FPT and FBP/6FPPr) with large and bulky diphenylfluorene moieties. Impressive H_2/CO_2 diffusivity selectivity (~100) of both polymeric membranes was found. However, the highly unfavorable H_2/CO_2 solubility selectivity (~0.017) greatly diminished the overall H_2/CO_2 permselectivities of these membranes. Wang et al. [8] incorporated cardo and bulky alkyl groups into poly(aryl ether ketone)s, and achieved a maximum increment of 55% in H_2 permeability. These polymers were synthesized for inhibiting the chain packing and optimizing the FFV distribution of the glassy polymers. However, together with increase in H_2 permeability, the H_2/CO_2 permselectivity was reduced. The best performance was measured from the least bulky polymer (PEK-C) in their series of poly(aryl ether ketone) (PEK), with a H_2/CO_2 selectivity of 7.5 and a H_2 permeability of 30 Barrers. Camacho-Zuniga et al. [9] designed and synthesized a series of cardo poly(aryl ether ketone)s with side phthalide groups and varying lengths of aryl ether ketones. H_2/CO_2 selectivity was improved by increasing the length of aryl ether ketone in the polymer backbone. The best separation performance in their work was a H_2/CO_2 selectivity of 5.5, and a H_2 permeability of 5.3 Barrers.

The H_2/CO_2 separation performances in the aforementioned studies are far more from satisfactory, with either low H_2/CO_2 selectivity of low H_2 permeability. This indicates the difficulties faced by researchers in attempting to improve H_2/CO_2 separation

performance through novel polymer designs. Some overall guidelines can be interpreted based on the studies reported in the literatures. Firstly, glassy polymers with high fractional free volume (FFV) are not suitable candidate materials for H_2/CO_2 separation since the presence of more free volume not only improves H_2 diffusivity but also increases CO_2 sorption. Secondly, it is difficult to control the free volume just within a narrow distribution and to tune the *d*-spacing exactly between 2.89Å and 3.30 Å, thus the high value of H_2/CO_2 diffusivity selectivity is hard to be achieved. Comparing with the limited improvement of H_2/CO_2 separation performance via new polymer design, modifications of existing polymers approaches such as cross-linking and mixed matrix membranes have shown more promising.

Chemical cross-linking is a powerful tool to improve H_2/CO_2 selectivity of the membranes. Great improvements have been achieved by diamino cross-linking polyimides, making it one of the most promising ways to improve the intrinsic H_2/CO_2 selectivity. This modification method was first reported by Hayes for increasing O_2/N_2 selectivity [14] and was later introduced by Chung's group for improving the H_2/CO_2 separation performance of polyimide based membranes. Shao et al. firstly performed crosslinking of 6FDA-durene films with diaminobutane dendrimer and found the enhancement in H_2/CO_2 selectivity from 1.3 to 4.7 at 35 ℃ after crosslinking for 60 min [10]. Subsequently, Chung et al. further improved the ideal H_2/CO_2 selectivity of 6FDA-durene membranes from1 to 101 at 35 ℃ via crosslinking with PDA for 10 min [11]. Similarly, an enhancement in H_2/CO_2 selectivity of 6FDA-ODA/NDA copolyimide membranes from 2.6 to 64 was obtained by modifying with PDA [12]. Aberg et al. conducted crosslinking on Matrimid membranes using prolonged PDA and observed a similar enhancement in H_2/CO_2

selectivity from 5.4 to 49 after PDA crosslinking at 50 ℃ for 1 h [13]. Besides the remarkable improvement on H_2/CO_2 selectivity, membranes with chemical cross-linking exhibit better anti-plasticization resistance comparing with their original polymer membranes. However, their hydrothermal stability needs improvement in order to expand their applications in high temperature and humid environments.

2.3 CO_2-selective polymeric membranes for hydrogen purification

CO_2-selective membranes are mostly made from rubbery polymers and commonly known as "reverse selective membranes", such as PEG or PEO-based blended membranes [15-22]. Table 2.3 lists the H_2 and CO_2 separation properties of some representative CO_2-selective membranes. CO_2 selective membranes show the advantages of eliminating the cost on H_2 recompression, no performance reduction and even enhancement under CO_2 induced plasticization, and less requirement of membrane area, except the drawbacks of low thermal stability, weak mechanical strength, and easy crystallization, which are representative problems of rubbery materials for gas separation, limiting the industrial application of this kind of membranes.

Table 2.3 Representative H_2 and CO_2 intrinsic transport properties of CO_2-selective membranes

Polymer	***T*** **(◦C)**	***P*** **(atm)**	**Permeability (Barrer)**		**CO_2/H_2 selectivity**
			CO_2	**H_2**	
Polytrimethylsilylpropyne	25	--	79	36.1	2.19
Poly(4-methyl-2-pentyne)	25	--	10700	5800	1.84
Polyphosphazene	30	2.04	250	25.0	10

Poly(tert-butylacetylene)	25	1	560	300	1.87
Poly(amide-6-b-ethylene oxide)	25	4	132	20	6.6
Poly(ethylene glycol) diacrylate	23	12	--	83	11
Crosslinked PEG copolymer	35	17	--	--	9.4
Crosslinked PEG copolymer	-20	17	410	--	31
polyurethane-ether	--	--	586	76.6	7.7
Poly(styrene-co-butadiene)	30	--	15.3	7.9	1.94
Poly(dimethyl siloxane) (PDMS)	23	1.36	3200	950	3.36

2.4 Polybenzimidazole based membranes for gas separation

To sustain high H_2/CO_2 separation performance in harsh environments of high temperatures and pressures, membranes must possess impressive thermal stability, good chemical resistance and high compression strength. Polybenzimidazole (PBI) is a specialty polymer that has been commercialized for fuel cells [23] and protective fibers [24], and studied for water reuse and desalination [25-27], solvent and protein dehydration [28, 29].

Recently, PBI has been identified as a unique polymeric material for H_2 separation since it exhibits superior thermal stability and good intrinsic H_2/CO_2 selectivity under extreme high temperature environments [30]. However, due to the inherent characteristics of rigid polymeric backbone and high degree of chain packing, PBI shows very low gas permeance even in the hollow fiber configuration [31]. PBI membranes fabricated by means of non-solvent phase inversion processes are also very brittle. Besides engineering methods such as coating PBI on metal tube supports [32, 33], spinning hollow fibers [34, 35] to reduce the thickness of the membranes, various approaches based on material science have been proposed to overcome the

low permeance of PBI membranes, including polymer blending [36], cross-linking blended polymers [37], changing PBI acid moiety [38, 39], N-substitution modification [40-42], thermally rearranging PBI [43], and addition of inorganic particles [44, 45].

Chung et al. [36] studied the hollow fiber spinning of polymer blending of PBI and polyetherimide (PEI). With increasing PBI weight fraction in the spinning dope from 10 wt% to 20 wt%, the fibers showed a nearly doubled O_2/N_2 selectivity from 1.09 to 2.00, but a much reduced O_2 permeance from 4.89 to 0.83 GPU. Hosseini et al. [37] investigated the miscible polymer blends of PBI and polyimide. By blending PBI with a commercialized polyimide-Matrimid, the hydrogen permeability was improved from 0.6 Barrer of pure PBI to 5.47 Barrer of Matrimid/PBI (25/75 wt. %), without reduction of H_2/CO_2 selectivity. The separation performance of the membrane was further improved via chemical crosslinking of blend constituents. The crosslinking of PBI phase with p-xylene dichloride turns out slightly improvement in H_2/CO_2 ideal selectivity, from 9.43 to 13.02. On the other hand, the crosslinking of Matrimid phase with p-xylene diamine results in significantly improvement in H_2/CO_2 ideal selectivity, from 9.43 to 26.09.

Kumbharkar et al. published several works on the gas separation properties of PBI polymers with different chemical structures from lab-scale synthesis. By changing PBI acid moiety [38, 39] during polymer synthesis and *N*-substitution modification [40-42], the polymers show decreased chain packing, improved solvent solubility, but slightly lowered thermal stability. For example, PBI based on 4,4'-(hexafluoroisopropylidene)bis(benzoic acid) (HFA) exhibits about 20 times increment

of H_2 permeability, from 0.6 Barrer of conventional PBI to 12.2 Barrer of PBI-HFA at 35 ℃. However, since the glass transition temperature (T_g) of PBI-HFA drops to 330 ℃ comparing with 416 ℃ of conventional PBI, the H_2/CO_2 selectivity and stability of PBI-HFA at high operating temperatures may not be satisfactory due to the high degree of chain flexibility.

Han et al. [43] reported a new synthesis route to obtain thermally rearranged polybenzimidazole (TR-PBI) membranes via the alkaline hydrolysis of polypyrrolone followed by simple thermal treatment. These TR-PBI membranes have microporous characters (i.e., high fractional free volume) and exhibit exceptionally highly permeable characteristics and good selectivity for gas pairs like CO_2/CH_4 and O_2/N_2. Nevertheless, these membranes show poor H_2/CO_2 selectivity (only 1.1) because it is hard to narrow the free volume size of high free volume polymers to the degree that fulfill the requirement of H_2/CO_2 gas pair separation.

Another method to improve the gas separation performance of PBI based membranes is the addition of inorganic particles [44, 45]. Sadeghi et al. [44] studied the effect of silica nano particles on the permeability of gases in polybenzimidazole (PBI) membranes. The membrane with 20 wt% silica particles shows an encouragingly simultaneously increment of CO_2 permeability and CO_2/N_2 selectivity. However, no data on H_2 permeability was shown in this work. Choi et al. [45] prepared PBI based mixed matrix membranes using nanoporous silicate particles as the dispersion phase. The composite membranes exhibit enhanced H_2/CO_2 selectivity but an extremely low H_2 permeability. Beside the unsatisfactory separation performance, these membranes show large particle sizes and poor particle-polymer interaction, which are the typical

problems of traditional mixed matrix membranes and limit the applicability of them for industrial favored membrane configurations, such as hollow fiber and spiral wound.

2.5 ZIFs based crystalline membranes and mixed matrix membranes

Zeolitic imidazolate frameworks (ZIFs) are a subfamily of metal-organic frameworks (MOFs) which refer to a group of crystalline transition metal complexes with one-, two-, or three-dimensional nano-porous networks. In addition to typical properties of MOFs such as high porosity, tailorable cavity sizes and good affinity with organic polymers, ZIFs also have characteristics of exceptional thermal stability and outstanding chemical resistance. Many studies have reported the encouraging gas separation performance of crystalline ZIF membranes grown on inorganic supports for various gas pairs such as H_2/CO_2 [46-48], CO_2/CH_4 [49], CO_2/CO [50], and C2/C3 hydrocarbons [51].

However, similar to inorganic membranes, disadvantages such as high fabrication cost, mechanical brittleness, and difficulties to prepare robust and large-scale membrane modules have deterred the commercial uses of ZIF membranes. To circumvent these weaknesses, one practical way is to utilize ZIFs by incorporating their nano-particles into organic polymers to make mixed matrix membranes and synergistically combine the merits of both materials.

Ordonez et al. [52] firstly reported mixed matrix membranes with ZIFs particles incorporating into Matrimid polymer matrix. The ZIF-8 particles were synthesized in

DMF solvent with the aid of heating (100 ℃) and triethylamine (TEA), and were dried to powders for later use. The ZIF-8 particles from this method showed small single crystal diameters around 100 nm but strong agglomeration, thus the effective diameters of the particle clusters were around 1 μm. As the ZIF-8 loading increased to 40% (w/w) (28.6 wt %), the gas permeability values increased. At higher loadings of 50% and 60% (w/w) (33.3 wt% and 37.5 wt%), the permeability decreased for all gases, and the selectivities increased consistent with the influence of the ZIF-8 additive. The ideal H_2/CO_2 selectivity at 35 ℃ was enhanced, from 2.96 of pure Matrimid to 4.43 of 60% (w/w) ZIF-8/Matrimid. Comparing with MMMs containing zeolites and silica particles which always show slightly increased selectivity but dropped permeability, the ZIF-8/Matrimid MMMs exhibit increased selectivity without reduction of permeability. This encouraging improvement indicates that ZIFs may be a promising group of materials for using in gas separation MMMs.

Zhang et al. [53] fabricated mixed matrix membranes using 6FDA-DAM polyimide and a 200 nm commercially available ZIF-8 sample produced by BASF and found a significantly enhanced propylene/propane (C_3H_6/C_3H_8) separation performance of the resultant MMMs. The C_3H_6 permeability and C_3H_6/C_3H_8 ideal selectivity in the ZIF-8/6FDA-DAM membrane 48.0 wt% ZIF-8 loading are 56.2 Barrer and 31.0, respectively, which are 258% and 150% higher than the pure 6FDA-DAM membrane, respectively for permeability and ideal selectivity. The selectivity enhancements were also achievable in mixed gas environment as demonstrated via mixed gas permeation tests. This work indicates that ZIF-8 is especially beneficial for improving selectivity for gas pairs with larger kinetic diameters, such as propylene and propane.

Bae et al. [54] (Koros ZIF-90) synthesized submicrometer-sized (>0.8 μm) ZIF-90 crystals by nonsolvent-induced crystallization and incorporated these particle with three kind of polyimide matrices. The ZIF-90 particles showed good adhesion with polymers in the resultant mixed-matrix membranes. The best mixed-matrix membrane made with 6FDA-DAM (a highly permeable polymer) showed a much improved CO_2 permeability (>700 Barrer), combined with a good CO_2/CH_4 mixed-gas selectivity of 37. The membrane also showed an improved ideal CO_2/N_2 selectivity of 22 as compared to 14 for pure 6FDA-DAM.

Following the idea developed by Yang et al. [6] (details are provided in Chapter 4 in this dissertation), Song et al. [55] directly incorporated as synthesised ZIF-8 nanoparticles (size around 60 nm) with Matrimid by solution mixing. This method produces flexible semi-transparent membranes with excellent nanoparticles dispersion (up to loadings of 30 wt%) with good adhesion within the polymer matrix. The membranes showed enhanced permeability with only slightly losses in selectivity for several gas pairs including CO_2/N_2, CO_2/CH_4, O_2/N_2, H_2/N_2 and H_2/CH_4. The mixed matrix membranes were annealed under vacuum and exhibited improvements on their gas permeation properties, which may be due to the residual solvent removal from the polymer matrices and the cavities of ZIF-8 nanocrystals. With increasing ZIF-8 nanoparticles loadings in the membranes, the gas permeability increases significantly, while the selectivity remains almost unchanged comparing with the pure polymer membrane.

2.6 Particle synthesis and dispersion methods for mixed matrix membranes

Since the particle size and surface chemistry apparently influence particle dispersion and interaction with the polymer matrix, the particle synthesis and dispersion methods critically determine the major physical properties of the resultant mixed matrix membranes. These properties include mechanical strength, flexibility, transparency, maximum achievable particle loading, processibility into other membrane configurations with thin selective layers, gas separation performances, and so on.

Existing ZIFs particle synthesis methods include hydrothermal [56, 57], vapor diffusion [57], nonsolvent-induced crystallization [54], TEA facilitated crystallization [52], and room-temperature colloidal chemistry route [46, 58]. Hydrothermal and vapor diffusion typically produce large particle with sizes around 100 μm, which is for fundamental studies and adsorbents. Nonsolvent-induced crystallization generates particle sizes with reduced sizes around 0.8-2 μm, which is still not small enough for MMMs fabrication. TEA facilitated crystallization synthesizes particles with nanoscale sizes around 100 nm. However, this method always generates particles with strong agglomeration and precipitated by-products, which makes the actually sizes of particle clusters as large as 1μm.

Comparing with the aforementioned ZIFs synthesis methods, room-temperature colloidal chemistry route [46, 58] produces ZIFs nanoparticles with much smaller sizes around 30-60 nm, without notable agglomeration formed in the synthesis solution. Cravillon et al. [58] observed that the nano-crystal powder of ZIF-8 became un-dispersible in polar solvents anymore if they were dried directly after synthesis and washing. This was mainly due to that Zn-imidazole (Him) on the particle surface may react among themselves and form strong covalent Zn-im-Zn bonds between the

particles during drying. For this reason, it is important to use the as-synthesized wet-state ZIFs particle during MMMs fabrication in order to prevent particle agglomeration and maintain a good particle-polymer interaction [6, 59, 60].

2.7 Challenges and future prospects

(1) According to the process simulation results [58], membranes with higher H_2/CO_2 selectivity show more potential to reduce energy consumption in the overall operating processes. On the other hand, a high selectivity can make the membranes capable to produce hydrogen with higher purity. To improve the energy efficiency of membrane separation process, and to fulfill the purity requirements of more downstream users, we should develop high H_2/CO_2 selectivity membranes that can be operated in industrial conditions.

(2) Since the pressures of output syngas streams are usually much higher than ambient conditions (>30 atm), a membrane for syngas separation should maintain a good separation performance and stability at high pressures. Unfortunately, the plasticization phenomenon induced by the high condensable gases (such as CO_2) at high partial pressures usually sacrifices H_2/CO_2 selectivity tremendously, and is one of the top challenges faced by membrane technology for gas separation.

(3) The thermal, mechanical and chemical stability of the membranes under high operating temperatures is another challenge faced by membranes for syngas separation. Because most of the current polymeric materials can only be applied

for temperatures below 150 ℃, the choices of materials for high temperature hydrogen purification become very limited. It is needed to design and synthesis more robust polymers, as well as to introduce inorganic components into polymers to improve the overall membranes performance and stability.

(4) Besides the intensive studies on membrane materials with better performances, more efforts should also be put on membrane module fabrication and process design optimization. Nonetheless, data obtained from pilot scale and long term evaluations is still insufficient for engineers to summarize enough experiences and develop mature rules for the industrial operation of this emerging technology.

2.8 References

[1] L. M. Robeson, The upper bound revisited, Journal of Membrane Science, 320 (2008) 390-400.

[2] L. Shao, B. T. Low, T. S. Chung, A. R. Greenberg, Polymeric membranes for the hydrogen economy: Contemporary approaches and prospects for the future, Journal of Membrane Science, 327 (2009) 18-31.

[3] V. Abetz, T. Brinkmann, M. Dijkstra, K. Ebert, D. Fritsch, K. Ohlrogge, D. R. Paul, K. -V. Peinemann, S. P. Nunes, N. Scharnagl, M. Schossig, Developments in membrane research: From material via process design to industrial application, Advanced Engineering Materials, 8 (2006) 328-358.

[4] Y. Li, T. S. Chung, Highly selective sulfonated polyethersulfone (SPES)-based membranes with transition metal counterions for hydrogen recovery and natural gas separation, Journal of Membrane Science, 308 (2008) 128-135.

[5] C. J. Orme, M. L. Stone, M. T. Benson, E. S. Peterson, Testing of polymer membranes for the selective permeability of hydrogen, Separation Science and Technology, 38 (2003) 3225-3238.

[6] T. Yang, Y. Xiao, T. S. Chung, Poly-/metal-benzimidazole nano-composite membranes for hydrogen purification, Energy and Environmental Science, 4 (2011) 4171-4180.

[7] Z. Xu, C. Dannenberg, J. Springer, S. Banerjee, G. Maier, Gas separation properties of polymers containing fluorene moieties, Chemistry of Materials, 14 (2002) 3271-3276.

[8] Z. Wang, T. Chen, J. Xu, Gas transport properties of novel cardo poly(aryl ether ketone)s with pendant alkyl groups, Macromolecules, 33 (2000) 5672-5679.

[9] C. Camacho-Zuñiga, F. A. Ruiz-Treviño, M. G. Zolotukhin, L. F. del Castillo, J. Guzman, J. Chavez, G. Torres, N. G. Gileva, E. A. Sedova, Gas transport properties of new aromatic cardo poly(aryl ether ketone)s, Journal of Membrane Science, 283 (2006) 393-398.

[10] L. Shao, T. S. Chung, S. H. Goh, K. P. Pramoda, Transport properties of cross-linked polyimide membranes induced by different generations of diaminobutane (DAB) dendrimers, Journal of Membrane Science, 238 (2004) 153-163.

[11] T. S. Chung, L. Shao, P. S. Tin, Surface modification of polyimide membranes by diamines for H_2 and CO_2 separation, Macromolecular Rapid Communications, 27 (2006) 998-1003.

[12] B. T. Low, Y. Xiao, T. S. Chung, Y. Liu, Simultaneous occurrence of chemical grafting, cross-linking, and etching on the surface of polyimide membranes and their impact on H_2/CO_2 separation, Macromolecules, 41 (2008) 1297-1309.

[13] C. M. Aberg, A. E. Ozcam, J. M. Majikes, M. A. Seyam, R. J. Spontak, Extended chemical crosslinking of a thermoplastic polyimide: Macroscopic and microscopic property development, Macromolecular Rapid Communications, 29 (2008) 1461-1466.

[14] R. A. Hayes, Amine-modified polyimide membranes, US patent 4,981,497 (1991).

[15] M. Kawakami, H. Iwanaga, Y. Hara, M. Iwamoto, S. Kagawa, Gas permeabilities of cellulose nitrate/poly(ethylene glycol) blend membranes, Journal of Applied Polymer Science, 27 (1982) 2387-2393.

[16] W. Yave, A. Car, S. S. Funari, S. P. Nunes, K. -V. Peinemann, CO_2-Philic polymer membrane with extremely high separation performance, Macromolecules, 43 (2010) 326-333.

[17] S. R. Reijerkerk, M. H. Knoef, K. Nijmeijer, M. Wessling, Poly(ethylene glycol) and poly(dimethyl siloxane): Combining their advantages into efficient CO_2 gas separation membranes, Journal of Membrane Science, 352 (2010) 126-135.

[18] A. Car, C. Stropnik, W. Yave, K. -V. Peinemann, Pebax®/polyethylene glycol blend thin film composite membranes for CO_2 separation: Performance with mixed gases, Separation and Purification Technology, 62 (2008) 110-117.

[19] K. I. Okamoto, M. Fujii, S. Okamyo, H. Suzuki, K. Tanaka, H. Kita, Gas permeation properties of poly(ether imide) segmented copolymers, Macromolecules, 28 (1995) 6950-6956.

[20] H. Chen, Y. Xiao, T. S. Chung, Synthesis and characterization of poly (ethylene oxide) containing copolyimides for hydrogen purification, Polymer, 51 (2010) 4077-4086.

[21] H. Lin, E. Van Wagner, B. D. Freeman, L. G. Toy, R. P. Gupta, Plasticization-enhanced hydrogen purification using polymeric membranes, Science, 311 (2006) 639-642.

[22] L. Shao, T. S. Chung, In situ fabrication of cross-linked PEO/silica reverse-selective membranes for hydrogen purification, International Journal of Hydrogen Energy, 34 (2009) 6492-6504.

[23] Q. Li, J. O. Jensen, R. F. Savinell, N. J. Bjerrum, High temperature proton exchange membranes based on polybenzimidazoles for fuel cells, Progress in Polymer Science, 34 (2009) 449-477.

[24] D. R. Coffin, G. A. Serad, H. L. Hicks, R. T. Montgomery, Properties and applications of celanese PBI-polybenzimidazole fiber, Textile Research Journal, 52 (1982) 466-472.

[25] K. Y. Wang, Q. Yang, T. S. Chung, R. Rajagopalan, Enhanced forward osmosis from chemically modified polybenzimidazole (PBI) nanofiltration hollow fiber membranes with a thin wall, Chemical Engineering Science, 64 (2009) 1577-1584.

[26] L. C. Sawyer, R. S. Jones, Observations on the structure of first generation polybenzimidazole reverse osmosis membranes, Journal of Membrane Science, 20 (1984) 147-166.

[27] D. Y. Xing, S. Y. Chan, T. S. Chung, Fabrication of porous and interconnected PBI/P84 ultrafiltration membranes using [EMIM]OAc as the green solvent, Chemical Engineering Science, 87 (2012) 194-203.

[28] G. M. Shi, Y. Wang, T. S. Chung, Dual-layer PBI/P84 hollow fibers for pervaporation dehydration of acetone, AIChE Journal, 58 (2012) 1133-1145.

[29] K. Y. Wang, M. M. Teoh, A. Nugroho, T. S. Chung, Integrated forward osmosis–membrane distillation (FO–MD) hybrid system for the concentration of protein solutions, Chemical Engineering Science, 66 (2011) 2421-2430.

[30] D. R. Pesiri, B. Jorgensen, R. C. Dye, Thermal optimization of polybenzimidazole meniscus membranes for the separation of hydrogen, methane, and carbon dioxide, Journal of Membrane Science, 218 (2003) 11-18.

[31] S. C. Kumbharkar, Y. Liu, K. Li, High performance polybenzimidazole based asymmetric hollow fibre membranes for H_2/CO_2 separation, Journal of Membrane Science, 375 (2011) 231-240.

[32] J. S. Young, K. A. Berchtold, E. S. Peterson, A. R. Greenberg, J. Acquaviva, F. Onorato, S. Hopkins, Novel polymeric-metallic composite membranes for CO_2 separations at elevated temperatures, in 2005 AIChE Spring National Meeting, Atlanta, GA, (2005) pp. 1489-1494.

[33] K. A. Berchtold, R. P. Singh, J. S. Young, K. W. Dudeck, Polybenzimidazole composite membranes for high temperature synthesis gas separations, Journal of Membrane Science, 415-416 (2012) 265-270.

[34] S. S. Hosseini, N. Peng, T. S. Chung, Gas separation membranes developed through integration of polymer blending and dual-layer hollow fiber spinning process for hydrogen and natural gas enrichments, Journal of Membrane Science, 349 (2010) 156-166.

[35] S. C. Kumbharkar, K. Li, Structurally modified polybenzimidazole hollow fibre membranes with enhanced gas permeation properties, Journal of Membrane Science, 415–416 (2012) 793-800.

[36] T. S. Chung, Z. L. Xu, Asymmetric hollow fiber membranes prepared from miscible polybenzimidazole and polyetherimide blends, Journal of Membrane Science, 147 (1998) 35-47.

[37] S. S. Hosseini, M. M. Teoh, T. S. Chung, Hydrogen separation and purification in membranes of miscible polymer blends with interpenetration networks, Polymer, 49 (2008) 1594-1603.

[38] S. C. Kumbharkar, P. B. Karadkar, U. K. Kharul, Enhancement of gas permeation properties of polybenzimidazoles by systematic structure architecture, Journal of Membrane Science, 286 (2006) 161-169.

[39] S. C. Kumbharkar, M. N. Islam, R. A. Potrekar, U. K. Kharul, Variation in acid moiety of polybenzimidazoles: Investigation of physico-chemical properties towards their applicability as proton exchange and gas separation membrane materials, Polymer, 50 (2009) 1403-1413.

[40] S. C. Kumbharkar, U. K. Kharul, Investigation of gas permeation properties of systematically modified polybenzimidazoles by N-substitution, Journal of Membrane Science, 357 (2010) 134-142.

[41] S. C. Kumbharkar, U. K. Kharul, New N-substituted ABPBI: Synthesis and evaluation of gas permeation properties, Journal of Membrane Science, 360 (2010) 418-425.

[42] S. C. Kumbharkar, U. K. Kharul, N-substitution of polybenzimidazoles: Synthesis and evaluation of physical properties, European Polymer Journal, 45 (2009) 3363-3371.

[43] S. H. Han, J. E. Lee, K. -J. Lee, H. B. Park, Y. M. Lee, Highly gas permeable and microporous polybenzimidazole membrane by thermal rearrangement, Journal of Membrane Science, 357 (2010) 143-151.

[44] M. Sadeghi, M. A. Semsarzadeh, H. Moadel, Enhancement of the gas separation properties of polybenzimidazole (PBI) membrane by incorporation of silica nano particles, Journal of Membrane Science, 331 (2009) 21-30.

[45] S. Choi, J. Coronas, Z. Lai, D. Yust, F. Onorato, M. Tsapatsis, Fabrication and gas separation properties of polybenzimidazole (PBI)/nanoporous silicates hybrid membranes, Journal of Membrane Science, 316 (2008) 145-152.

[46] Y. S. Li, F. Y. Liang, H. Bux, A. Feldhoff, W. S. Yang, J. Caro, Molecular sieve membrane: Supported metal-organic framework with high hydrogen selectivity, Angewandte Chemie - International Edition, 49 (2010) 548-551.

[47] A. Huang, H. Bux, F. Steinbach, J. Caro, Molecular-sieve membrane with hydrogen permselectivity: ZIF-22 in LTA topology prepared with 3-aminopropyltriethoxysilane as covalent linker, Angewandte Chemie - International Edition, 49 (2010) 4958-4961.

[48] A. Huang, W. Dou, J. Caro, Steam-stable zeolitic imidazolate framework ZIF-90 membrane with hydrogen selectivity through covalent functionalization, Journal of the American Chemical Society, 132 (2010) 15562-15564.

[49] S. R. Venna, M. A. Carreon, Highly permeable zeolite imidazolate framework-8 membranes for CO_2/CH_4 separation, Journal of the American Chemical Society, 132 (2010) 76-78.

[50] Y. Liu, E. Hu, E. A. Khan, Z. Lai, Synthesis and characterization of ZIF-69 membranes and separation for CO_2/CO mixture, Journal of Membrane Science, 353 (2010) 36-40.

[51] Y. Pan, Z. Lai, Sharp separation of C2/C3 hydrocarbon mixtures by zeolitic imidazolate framework-8 (ZIF-8) membranes synthesized in aqueous solutions, Chemical Communications, 47 (2011) 10275-10277.

[52] M. J. C. Ordoñez, K. J. Balkus Jr, J. P. Ferraris, I. H. Musselman, Molecular sieving realized with ZIF-8/Matrimid® mixed-matrix membranes, Journal of Membrane Science, 361 (2010) 28-37.

[53] C. Zhang, Y. Dai, J. R. Johnson, O. Karvan, W. J. Koros, High performance ZIF-8/6FDA-DAM mixed matrix membrane for propylene/propane separations, Journal of Membrane Science, 389 (2012) 34-42.

[54] T. H. Bae, J. S. Lee, W. Qiu, W. J. Koros, C. W. Jones, S. Nair, A high-performance gas-separation membrane containing submicrometer-sized metal-organic framework crystals, Angewandte Chemie - International Edition, 49 (2010) 9863-9866.

[55] Q. Song, S. K. Nataraj, M. V. Roussenova, J. C. Tan, D. J. Hughes, W. Li, P. Bourgoin, M. A. Alam, A. K. Cheetham, S. A. Al-Muhtaseb, E. Sivaniah, Zeolitic imidazolate framework (ZIF-8) based polymer nanocomposite

membranes for gas separation, Energy and Environmental Science, 5 (2012) 8359-8369.

[56] K. S. Park, Z. Ni, A. P. Côté, J. Y. Choi, R. Huang, F. J. Uribe-Romo, H. K. Chae, M. O'Keeffe, O. M. Yaghi, Exceptional chemical and thermal stability of zeolitic imidazolate frameworks, Proceedings of the National Academy of Sciences of the United States of America, 103 (2006) 10186-10191.

[57] W. Morris, C. J. Doonan, H. Furukawa, R. Banerjee, O. M. Yaghi, Crystals as molecules: Postsynthesis covalent functionalization of zeolitic imidazolate frameworks, Journal of the American Chemical Society, 130 (2008) 12626-12627.

[58] J. Cravillon, S. Münzer, S. J. Lohmeier, A. Feldhoff, K. Huber, M. Wiebcke, Rapid room-temperature synthesis and characterization of nanocrystals of a prototypical zeolitic imidazolate framework, Chemistry of Materials, 21 (2009) 1410-1412.

[59] T. Yang, G. M. Shi, T. S. Chung, Symmetric and asymmetric zeolitic imidazolate frameworks (ZIFs)/polybenzimidazole (PBI) nano-composite membranes for hydrogen purification at high temperatures, Advanced Energy Materials, 2 (2012) 1358-1367.

[60] T. Yang, T. S. Chung, High performance ZIF-8/PBI nano-composite membranes for high temperature hydrogen separation consisting of carbon monoxide and water vapor, International Journal of Hydrogen Energy, (2012) DOI: 10.1016/j.ijhydene.2012.10.045.

CHAPTER 3

METHODOLOGY

3.1 Materials

3.1.1 Polymers and solvents

In this study, a linear polybenzimidazole with reactive hydrogen atom on each imidazole ring, poly-2, 2'-(m-phenylene)-5, 5'bibenzimidazole, was used as the polymer matrix for nanocomposite membranes fabrication. Both the PBI powder (intrinsic viscosity 1.0 dL/g) for dense membrane fabrication and the PBI dope for hollow fiber spinning were obtained from Hoechst Celanese. The composition of the commercial PBI dope was PBI/DMAc/LiCl (25.6 wt% PBI, 72.4 wt% DMAc and 2.0 wt% LiCl). LiCl was originally added in the commercial PBI dope as a stabilizer to prevent aggregation of PBI molecules in the DMAc solution and to impart a long shelf life. Matrimid® 5218 purchased from Huntsman (USA) was selected as the inner layer material. Matrimid was dried at 120 °C under vacuum overnight and stored in a dry box prior to use. The chemical structures of PBI and Matrimid® 5218 are shown in **Figure 3.1**.The polymer powder was dried overnight at 120 °C under vacuum prior to use. 1-Methyl-2-pyrrolidinone (NMP) (reagent grade), methanol (reagent grade), isopropanol (IPA, industrial grade) and n-hexane (industrial grade) were purchased from Merck. Dimethylacetamide (DMAc, reagent grade) was purchased from VWR International. All the chemicals were used as received without further purification.

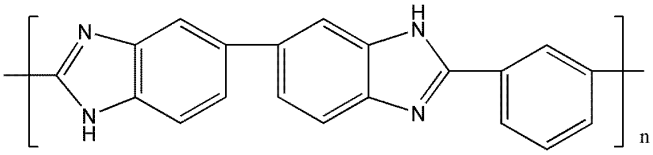

Polybenzimidazole (PBI)

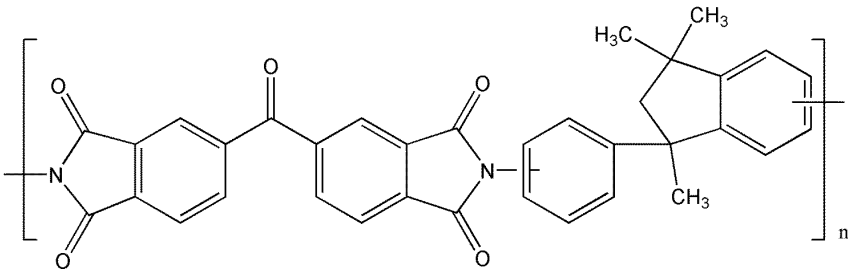

Matrimid® 5218

Figure 3.1 Chemical structures of polymers in this study

3.1.2 ZIFs synthesis agents

Zinc nitrate hexahydrate (Zn $(NO_3)_2$ $6H_2O$) (reagent grade, >98%), benzimidazole (98%), and 2-methylimidazole (reagent grade, 98%) and pyridine (anhydrous, 99.8%) were purchased from Sigma-Aldrich. Imidazole-2-carboxyaldehyde (Ica) (>97%) was obtained from Alfa Aesar. *N, N*-Dimethylformamide (DMF) (reagent grade) was supplied by Fisher. All the chemicals were used as received without further purification. All the reagents and solvents were used as received with no further purification.

3.2 ZIFs nanoparticle synthesis

3.2.1 ZIF-7 nanoparticle synthesis

The dispersed ZIF-7 nano-particles were synthesized at room temperature using the procedure described in a previous report [1]. In summary, DMF (200ml) was added in a solid mixture of Zn $(NO_3)_2$ $6H_2O$ (0.64g) and benzimidazole (Hbim) (1.63g). The resultant solution was stirred at room temperature for 48 hours. After that, the product was collected by centrifugation and then washed with DMF. After washing and 2nd centrifugation, the particles were re-dispersed in fresh DMF before use. Figure 3.2a shows the simulated structure of ZIF-7 based on the crystalline data in the literature [2]. The framework is created by bridging the Zn (II) centers to the N-atoms on the five-membered imidazole ring. The angle made by the Zn-imidazole-Zn bond is 145°, and is similar to the Si-O-Si bond angle in many zeolites. ZIF-7 has narrow and well defined pores useful for gas separation. The diameter of the largest sphere that can pass through the pore is 3.0 Å, while the diameter of the largest sphere that can fit into the cage without contacting the framework atoms is 4.3 Å [3].

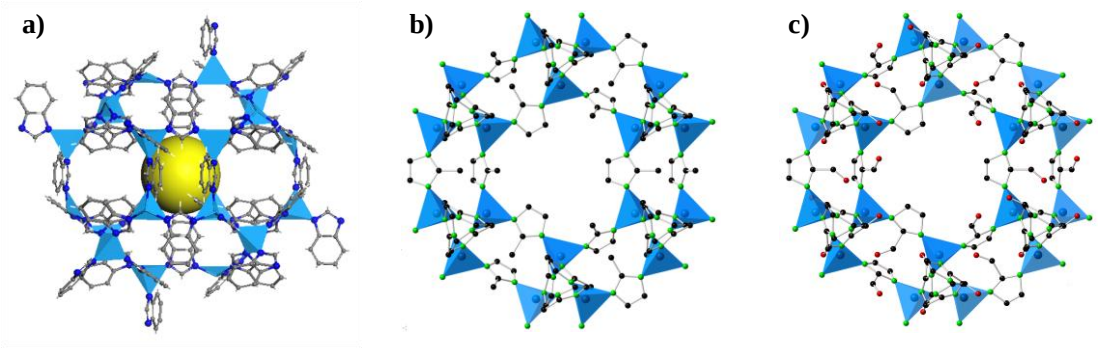

Figure 3.2 Crystalline structures of ZIFs particles in this study
(a) ZIF-7; (b) ZIF-8; (c) ZIF-90.

3.2.2 ZIF-8 nanoparticle synthesis

The dispersed ZIF-8 nano-particles were synthesized at room temperature following the protocol reported in the literature [4]. In a typical synthesis, DMF (200ml) was added in a solid mixture of Zn $(NO_3)_2$ $6H_2O$ (0.66g) and 2-methylimidazole (Hmim) (1.46g). The resultant clear solution was stirred for 18 hours at room temperature to form a light blue colored transparent nano-particle suspension. After the reaction, the product was collected by centrifugation following by washing with fresh DMF. After washing and 2^{nd} centrifugation, the particles were re-suspended in DMF before usage. To maintain the particle size and well dispersion state, the DMF suspension of ZIF-8 nano-particles should be used within one week. The yield of ZIF-8 during synthesis was about 50%, which was determined by the amount of remained zinc oxide in the thermo gravimetric analysis (TGA) of ZIF-8 particle powder under air atmosphere according to the stoichiometry relationship. According to the topology data in the literature [3], ZIF-8 has small windows as well as large interconnected cavities, which is an ideal topology for high performance gas separation. The diameter of the largest sphere that can pass through the pore is 3.4 Å, while the diameter of the largest sphere that can fit into the cage without contacting the framework atoms is 11.6 Å. The structure of ZIF-8 from the [111] direction is shown in Figure 3.2b, with the tetrahedral Zn sites in blue, and the N and C atoms in green and black, respectively. H atoms and bonds have been removed for clarity. This crystalline image was drawn using the Crystal Maker software based on the single crystal data from the literature [3].

3.2.3 ZIF-90 nanoparticle synthesis

The well-dispersed ZIF-90 nanocrystals used in this work were synthesized at room temperature by using an improved method. Pyridine was added into the synthesis system as a moderate deprotonation agent in order to facilitate ZIF-90 nanocrystals formation in the reaction solution. Specifically, imidazole-2-carboxyaldehyde (Ica) (3.379 g, 35.17 mmol) was dissolved in 200 g DMF under heating at 60 ℃ followed by filtering with 1.0 μm PTFE syringe membrane filters. After the Ica solution has been cooled to room temperature, pyridine (2.000 g, 25.28 mmol) was added into it, followed by uniform mixing. Afterwards, the solution of Zn $(NO_3)_2$ $6H_2O$ (1.309 g, 4.40 mmol) in 200 g DMF is quickly poured into mixture of Ica and pyridine under vigorous magnetic stirring. The mixture was slowly turning to be turbid and was kept stirred overnight to ensure complete reaction. The as-synthesized ZIF-90 nanoparticles were collected by means of centrifugation and then were washed by using 50 ml fresh DMF. After being washed with DMF for three times, the particles were re-suspended in about 30 ml NMP prior to use. The yield of ZIF-90 in this enhanced process was approximately 30% based on the amount of zinc element remaining in the nanocomposite membranes, which was determined by using the thermogravimetric analysis (TGA) with air purging. The crystalline structure image of ZIF-90 from the [111] direction is drawn using the Crystal Maker software according to the Crystallographic Information Framework (CIF) data provided by the literature [5]. Figure 3.2c shows the structure of ZIF-90, with tetrahedral Zn sites in blue, N atoms in green, C atoms in black and O atoms in red. H atoms and bonds are omitted for clarity.

3.3 Membrane fabrication and post treatment protocols

3.3.1 ZIFs/PBI dense films

The ZIFs/PBI nano-composite membranes were prepared using a typical ring casting method. To prepare the membrane casting solution, 1.5 wt% dried PBI powder was firstly dissolved in NMP at 120 ℃ with continuous stirring for 48 h. The PBI solution was naturally cooled to room temperature and then filtered by using 1.0 μm PTFE syringe membrane prior to use. The filtered PBI solution was mixed with the as-synthesized wet-state ZIFs nanoparticles dispersed in NMP according to the desired weight ratios. The ZIFs/PBI solution was placed in a sonicator for 15 min and then a rolling mixer for 45 min, with totally three cycles. The casting solution was then poured onto a silicon wafer sealed with a metal ring in a vacuum oven. Subsequently, the solution was degassed under vacuum at 45 ℃ for 1 h, following by slow solvent evaporation at 75 ℃ overnight. After cooling to room temperature, the formed membrane was peeled off from the silicon wafer and then vacuum annealed at 200 ℃ for 24 h. The rates of all aforementioned heating and cooling steps above are fixed as 20 ℃/h. To ensure the fully removal of the solvent trapped inside ZIFs cavities, the dried nano-composite membrane was solvent-exchanged with methanol at room temperature on a rolling mixer for 24 h, and subsequently vacuum dried at 120 ℃ for overnight.

3.3.2 Co-extrusion of ZIF-8-PBI/Matrimid dual-layer hollow fibers

Co-extrusion of dual layer ZIF-8-PBI/Matrimid hollow fibers was employed in this study. For the preparation of the outer-layer spinning dope, the as-synthesized ZIF-8 particles were firstly added into a certain amount of PBI/DMAc/LiCl dope (25.6 wt%

PBI) with continuous stirring, followed by topping up the dope with DMAc to the targeted composition. The solutions were stirred at room temperature for 24 hours to ensure the homogeneous dispersion of nano-particles in the dope. The inner layer spinning dope was a mixture of 21.6 wt% Matrimid and 78.4 wt% DMAc. For the preparation of the inner-layer spinning dope, Matrimid polymer powder was added gradually to DMAc under continuous agitation, and the solution was stirred for 24 hours to ensure complete dissolution of Matrimid. Both the outer layer dope and inner layer dope were left standing for another 24 hours for degassing before loading into the respective syringe pumps (ISCO 1000), followed by another degassing for overnight. During spinning, the inner layer dope and outer layer dope were co-extruded together through a triple-orifice spinneret by a dry-jet/wet spinning process. The air gap for spinning is 5 cm, and tap water is used as the precipitation bath. The detailed description of the set up for dual-layer hollow fiber spinning and process can be found elsewhere [6]. After spinning, the as-spun hollow fibers were immersed in tap water to remove the residual solvent within the membranes. To further remove the residual solvent and study the effect of solvent exchange on hollow fiber morphology and separation performance, two series of solvent exchange protocols were employed. After finishing the solvent exchange process, the fibers were naturally dried at 25 ℃ for 24 hours.

3.4 ZIFs nanoparticles and membranes characterization

3.4.1 Dynamic light scattering (DLS)

In order to examine the particle size distribution of the as-synthesized ZIFs nanoparticles in the NMP liquid suspension, dynamic light scattering (DLS) analyses were conducted using a Brookhaven 90Plus Particle Size Analyzer operated at 20 ℃. The counting rates were around 100-200 kcps and ten measurements were combined as the final result.

3.4.2 Transmission electron microscope (TEM)

The microstructure of ZIFs/PBI mixture was observed under a transmission electron microscope (TEM), JEM 2010. For TEM sample preparation, the solution of 50/50 (w/w) ZIFs/PBI was diluted with methanol and dropped onto a copper grid. The grid was dried under vacuum at room temperature overnight before observation.

3.4.3 Field emission scanning electron microscopy (FESEM)

The morphologies for dried ZIFs nanoparticles and ZIFs/PBI nano-composite membranes were observed using field emission scanning electron microscopy (FESEM), JSM-6700F. The membranes were immersed and fractured in liquid N_2 to obtain the cross-sectional view of the nano-composite membrane. All the samples were coated using a JEOL JFC-1300 Auto Fine Coater (Pt target, 20 mA for 90 s) prior loading into the FESEM chamber. Elemental compositions of the nano-composite membranes were analyzed using an energy-dispersive X-ray spectroscopy (EDX) apparatus along with the FESEM.

3.4.4 Wide-angle X-ray diffraction (XRD)

The crystalline structure of the ZIFs nanocrystals as well as in the ZIFs/PBI nano-composite membranes was characterized by using wide-angle X-ray diffraction (XRD) employing Bruker D8 series, GADDS X-ray diffractor (General Area Detector Diffraction System, with Cu X-ray source, wavelength 1.54Å). For ZIFs nanocrystals, the as-synthesized wet state ZIFs particles were solvent exchanged by using methanol for 12 h and then repeated for twice, followed by drying in vacuum oven at 120 ℃ overnight. For XRD tests, the dried ZIFs powders were separately pressed to be small pellets, while the ZIFs/PBI nanocomposite membranes were cut into small pieces, and were immediately tested. The diameter of both the pellet and the membrane pieces is around 5 mm. The average d-spacing can be calculated from the Bragg's law as expressed in the following equation:

$$n\lambda = 2d\sin\theta \qquad (3\text{-}1)$$

where n represents an integer (1, 2, 3 …), λ refers to the wavelength of X-ray source, d is the intersegmental spacing between the planes in the atomic lattice or two adjacent polymer chains, and θ refers to the diffraction angle.

3.4.5 Nuclear magnetic resonance spectroscopy (NMR)

Solid state ^{13}C cross polarization magic angle spinning (CP/MAS) nuclear magnetic resonance (NMR) spectroscopy was measured at ambient pressure on a Bruker Avance 400 (DRX400) spectrometer using a standard Bruker magic angle-spinning (MAS) probe with 4 mm (outside diameter) zirconia rotors. Cross-polarization with MAS (CP/MAS) was used to acquire ^{13}C data at 100.62 MHz. The MAS sample-

spinning rate was 8 kHz. The ^{13}C chemical shifts are referenced to tetramethylsilane as zero ppm.

3.4.6 Fourier transform infrared spectroscopy (FTIR)

The chemical structure of ZIFs dry powders and ZIFs/PBI nanocomposite membranes were examined by Fourier transform infrared spectroscopy (FTIR) over the wavenumber range of 800-4000cm^{-1} using a Bio-Rad FTIR FTS 135 with 10 ml/min N_2 purging. The ZIFs powders were mixed with KBr and were pressed to be flat pallets and examined under the transmission mode. The membranes were directly measured under attenuated total reflectance (ATR) mode.

3.4.7 Thermo gravimetric analysis (TGA)

The thermal stability of ZIFs nanoparticles and ZIFs/PBI nanocomposite membranes was measured by the thermo gravimetric analysis (TGA) using a TGA 2050 Themogravimetric Analyzer (TA Instruments). The membrane samples were heated from 25 ℃ to 800 ℃ at a heating rate of 20 ℃/min with 100 ml/min air purging. The weight of zinc oxide remained at 800 ℃ was recorded for calculating the weight of ZIF-90 particles in the membranes according to the stoichiometry relationship. The reading of the weight at 200 ℃ was taken as the initial weight, in order to eliminate the effect of absorbed water and residual solvents in the samples.

3.4.8 Positron annihilation lifetime spectroscopy (PALS)

The free volume distribution of composite membranes was studied by positron annihilation lifetime spectroscopy (PALS). All PALS spectra were recorded by using a BaF_2 crystal scintillator detecting the γ photons from the annihilations. In the PALS experiments, incident positron energy of 5KV was performed at a counting rate of 100-150 counts s^{-1}, and a total count of one million was fixed to collect each spectrum. The obtained spectra were analyzed by the PATFIT program using finite-term lifetime methods. The mean free-volume cavity radiuses were calculated from the results of o-Ps lifetime based on the following equation [7, 8]:

$$\tau_3 = \frac{1}{2}\left[1 - \frac{R}{R_0} + \frac{1}{2\pi}\sin\left(\frac{2\pi R}{R_0}\right)\right]^{-1} \quad (3\text{-}2)$$

where τ_3 is the o-Ps lifetime (ns); R refers to the hole radius (Å); R_0 is equal to $R+\Delta R$, where ΔR refers to a fitted empirical electron layer thickness of 1.66Å. The cavity volumes were obtained from $V_h=4\pi R^3/3$.

3.4.9 Positron annihilation spectroscopy (PAS)

The depth profile of porosity in the outer dense-selective layer of hollow fibers was characterized by positron annihilation spectroscopy (PAS) located at our membrane labs. Detailed information about the theory and operation of PAS can be found elsewhere [7, 8]. The hollow fiber samples prepared from each condition were attached and aligned tightly on an aluminum plate along the axis direction. Two layers of hollow fibers were stacked to ensure a seamless surface. The R parameter from Doppler broadened energy spectra (DBES) was measured by an HP Ge detector as a function of positron implantation energy using the slow positron beam with incident energy from 0.1 to 30keV at room temperature. The total number of count for each

DBES measurement was 1.0 millions. The R parameter is defined as the ratio of the total count of the valley region with the energy width between 364.2 and 496.2 keV (from 3γ annihilation) and the total count from the 511 keV peak region with the energy width between 504.35 and 517.65 keV. The R parameter provides information about the porosity of large pores (nm to μm) as a function of the depth from the outer surface.

3.4.10 Differential scanning calorimetry (DSC)

Differential Scanning Calorimetry (DSC) measurements were carried by a PerkineElmer Pyris-1 differential scanning calorimeter from 25 °C to 500 °C with a heating rate of 20 °C min^{-1} in N_2 atmosphere. Two heat cycles of each membrane were preformed to remove the thermal history and the glass transition temperature (T_g) was determined from the second cycle.

3.4.11 Density measurement

The density of each membrane was measured based on Archimedes' principle using an AG204 DeltaRange analytical balance equipped with a density kit with hexane solvent. The weight of the membrane sample in air and in hexane was recorded. All the measurements were conducted at 25 ℃. The density of the membrane $\rho_{membrane}$ can be calculated based on the following equation:

$$\rho_{membrane} = \frac{w_0}{w_0 - w_1} \rho_{hexane} \quad (3\text{-}3)$$

where w_0 and w_1 are the weight of the sample in air and hexane, respectively; and ρ_{hexane} refers to the density of hexane.

3.5 Determination of gas transport properties

3.5.1 Pure gas permeation

The pure gas permeation property of flat sheet membranes was determined using a constant-volume variable-pressure single gas permeation cell. Detailed specification of the configuration and operating procedure for the permeation cell can be found elsewhere [9]. The pure gas tests were conducted at 35 ℃ and a feed pressure of 3.5 atm. At steady state, the increase rate of the pressure (dp/dt) was measured and the permeability of each gas was calculated from the following equation:

$$P = \frac{273\times10^{10}}{760}\frac{VL}{AT(p_2\times76/14.7)}\left(\frac{dp}{dt}\right) \quad (3\text{-}4)$$

where P is the single gas permeability of the membrane in Barrer (1 Barrer = 1×10^{-10} cm^3(STP)cm/(cm^2 s cmHg)), V refers to the downstream reservoir volume (cm^3), L is the membrane thickness (cm), A represents the effective membrane area (cm^2), T is the operating temperature (K) and p_2 indicates the upstream feed pressure (psia). The ideal permselectivity of a membrane for H_2 and CO_2 gas pair ($\alpha_{H2/CO2}$) was determined based on the following equation.

$$\alpha_{H_2/CO_2} = \frac{P_{H_2}}{P_{CO_2}} = \left(\frac{S_{H_2}}{S_{CO_2}}\right)\times\left(\frac{D_{H_2}}{D_{CO_2}}\right) \quad (3\text{-}5)$$

where P_{H2} and P_{CO2} represent the pure gas permeability of H_2 and CO_2, respectively, while S_{H2}/S_{CO2} and D_{H2}/D_{CO2} refer to the selectivity components from solubility and diffusion coefficients of the gas pair, respectively.

The pure gas permeation of hollow fibers was measured by a permeation tube system described in a previous work [10]. Modules were prepared with ten fibers of around 15 cm in length. Three modules were prepared and tested from the same spinning conditions and the average experimental data were reported. A feed pressure was applied to the outer shell side of the fibers, and the permeate side was connected with the atmosphere. The feed pressures for H_2 and CO_2 were both 3.5 atm, and all the modules were tested at room temperature (25 °C). The permeate fluxes were determined using a bubble flow meter. The permeance is defined as the thickness normalized permeability *P/l*, which was calculated according to the following equation:

$$\frac{P}{l} = \frac{Q}{A\Delta p} = \frac{Q}{n\pi DL\Delta p} \tag{3-6}$$

where *P* represents the permeability of the selective layer material (Barrer), *l* is the thickness of the separation layer (cm), *Q* is the flow rate of the permeate side ($cm^3\ s^{-1}$), *n* refers to the number of fibers in the testing module, *D* is the outer diameter of the fibers (cm), *L* is the effective length of the module (cm), and Δp is the pressure difference cross the membrane (cmHg). The permeance is indicated in the unit of GPU (1 GPU = 10^{-6} cm^3 (STP) cm^{-2} s^{-1} $cmHg^{-1}$ =3.35 $\times 10^{-10}$ mol m^{-2} s^{-1} Pa^{-1}). The ideal separation factor, $\alpha_{A/B}$, is calculated from the following equation:

$$\alpha_{A/B} = \frac{(P/l)_A}{(P/l)_B} \tag{3-7}$$

3.5.2 Mixed gas permeation

Mixed gas permeation tests of dense films were performed using a constant-volume variable-pressure mixed gas permeation cell. Detailed description on the setup and operation of the permeation cell can be found elsewhere [11]. The mixed gas tests were conducted from 35 to 180 ℃ at 7 atm using a binary gas mixture of 50 vol% H_2 and 50 vol% CO_2 as the feed. The permeability of each gas was calculated based on the following equations.

$$P_{H_2} = \frac{273\times10^{10}}{760}\frac{y_{H_2}VL}{AT(76/14.7)(x_{H_2}p_2)}\left(\frac{dp}{dt}\right) \tag{3-8}$$

$$P_{CO_2} = \frac{273\times10^{10}}{760}\frac{y_{CO_2}VL}{AT(76/14.7)(x_{CO_2}p_2)}\left(\frac{dp}{dt}\right) \tag{3-9}$$

where P_{H2} and P_{CO2} are H_2 permeability and CO_2 permeability, respectively, p_2 refers to the pressure (psia) of the upstream feed gas, and x and y represent the molar fractions of each gas in the feed and the permeate sides, respectively.

The separation factor of mixed gas tests is expressed as the mole fraction ratio of H_2 to CO_2 in the downstream divided by the mole fraction ratio of H_2 to CO_2 in the upstream, as indicated in the following equation.

$$\alpha_{H_2/CO_2} = \frac{P_{H_2}}{P_{CO_2}} = \frac{y_{H_2}/y_{CO_2}}{x_{H_2}/x_{CO_2}} \tag{3-10}$$

Mixed gas permeation measurements of dense films were also carried out from ambient to high temperatures using a constant-pressure variable-volume apparatus

combined with a gas chromatography (GC) equipped with a thermal conductivity detector (TCD) and pulsed discharge helium ionization detector (PDHID). Detailed descriptions of the apparatus scheme and operating procedure can be found elsewhere [12]. For H_2/CO_2 mixed gas tests, a 50/50 (mol/mol) H_2/CO_2 gas mixture at 2 atm was employed as the upstream feed gas and the permeation measurements were conducted at various temperatures ranging from 35 °C to 230 °C. The effect of CO on H_2/CO_2 separation was investigated using a tertiary gas mixture containing 1.0 mol % CO and an equal molar fraction of H_2 and CO_2, i.e., 49.5 mol % for each gas. To test the effect of water vapor, the feed gas mixture was first saturated with water vapor through a water tank at controlled temperatures before being fed into the permeation cell. In order to prevent the concentration polarization at the upstream side of the membrane, a much higher flow rate comparing with the gas penetrates was maintained at the retentate stream. Helium was used as the sweep gas at the downstream side of the membrane, and a high flow rate of 100 ml/min was applied to ensure the negligible partial pressures of H_2 and CO_2. After passing through the permeation cell, the downstream sweep stream was introduced into a gas chromatography (GC) to detect the concentration of each penetrant. The steady state permeability (P_A) of each gas component was calculated using the following equation [13, 14]:

$$P_A = \frac{Q_A L}{A(p_{A_2} - p_{A_1})} \qquad (3\text{-}11)$$

where Q_A is the steady state gas flow rate through the membrane (cm^3(STP)/s), L represents the membrane thickness (cm), A refers as to the effective membrane area (cm^2), and p_{A1} and p_{A2} indicate the upstream and downstream partial pressures (cmHg) of the gas component A, respectively. The H_2/CO_2 selectivity during mixed gas tests was calculated as the ratio of their gas permeability.

The mixed gas permeances of the hollow fibers were characterized using a modified variable-pressure constant volume gas permeation cell. The detailed description of the modified permeation cell set-up can be found elsewhere [15]. The hollow fibers were made into modules by using 1/4 in. standard steel union tees supplied by Swagelok. Each module consisted of one fiber with an effective length of approximately 12 cm. Two modules were tested for the same condition and the averages were taken for calculation. A 50/50 (mol/mol) H_2/CO_2 mixture with 7 atm pressure was employed as the upstream feed gas and the tests were conducted at temperatures from 25 °C to 180 °C. The permeances (P/l) of H_2 and CO_2 for each fiber were determined using the following equations:

$$\left(\frac{P}{l}\right)_{H_2} = \frac{273\times10^{10}}{760}\frac{y_{H_2}V}{AT\left(x_{H_2}p_0\times76/14.7\right)}\left(\frac{dp}{dt}\right) \tag{3-12}$$

$$\left(\frac{P}{l}\right)_{CO_2} = \frac{273\times10^{10}}{760}\frac{y_{CO_2}V}{AT\left(x_{CO_2}p_0\times76/14.7\right)}\left(\frac{dp}{dt}\right) \tag{3-13}$$

where $(P/l)_{H2}$ and $(P/l)_{CO2}$ are the H_2 and CO_2 permeances, respectively. x and y refer to the gas molar fraction (%) in the feed and the permeate, respectively.

The mixed gas separation factor is determined from the following equation, which represents the ratio of mole fraction ratios of H_2 and CO_2 in the downstream to the upstream.

$$\alpha_{H_2/CO_2} = \frac{(P/l)_{H_2}}{(P/l)_{CO_2}} = \frac{y_{H_2}/y_{CO_2}}{x_{H_2}/x_{CO_2}} \tag{3-14}$$

3.5.3 Measurements of gas sorption

To determine the sorption capacity evolution of ZIF-90/PBI nano-composite membranes, carbon dioxide sorption curves were measured using a Cahn D200 microbalance sorption cell. Detailed specification of the dual volume sorption cell can be found elsewhere [16]. The membrane samples were measured at 35 ℃ over a wide pressure range of 0-30 atm. For each sorption curve measurement, about 80 mg membrane samples were punched into small pieces with a diameter of 1 cm and then loaded into a quartz sample bowl. Subsequently, the whole system was evacuated for 24 h. During the test, the cell chamber was fed with CO_2 at a certain pressure and the increment in the sample mass at equilibrium state was recorded. The equilibrium gas sorption capacities were adjusted by the buoyancy force of the samples and empty bowls. Generally, dual-sorption model was employed to analyze the gas sorption in glassy polymer, as shown in the following equation [17].

$$C = C_D + C_H = k_D p + \frac{C_H' b p}{1 + b p} \tag{3-15}$$

where C refers to the sorbed gas concentration in the polymer expressed by gas volume (cm^3) per polymer volume (cm^3) , C_D and C_H indicate the concentrations of the gas penetrant sorbed in the Henry sites and Langmuir sites, respectively, k_D refers to the Henry's law constant indicating gas dissolution in the equilibrium-defined polymer, p (atm) is the feed gas pressure in contact with the polymer, C'_H represents the Langmuir capacity of the polymer, and b is the Langmuir affinity parameter representing the affinity of the gas to a Langmuir site. The Langmuir capacity can indicate the amount of excess free volume in a polymer matrix.

The solubility coefficient (S) of a single gas in a glassy polymer is expressed as the equilibrium gas concentration divided by the gas pressure, as shown in the following equation.

$$S = \frac{C}{p} = k_D + \frac{C_H' b}{1 + bp} \tag{3-16}$$

The diffusion coefficient (D) of a single gas in the membrane can be subsequently determined based on the solution-diffusion model [18] as shown below.

$$D = \frac{P}{S} \tag{3-17}$$

3.6 References

[1] Y. S. Li, F. Y. Liang, H. Bux, A. Feldhoff, W. S. Yang, J. Caro, Molecular sieve membrane: Supported metal-organic framework with high hydrogen selectivity, Angewandte Chemie - International Edition, 49 (2010) 548-551.

[2] A. Phan, C. J. Doonan, F. J. Uribe-Romo, C. B. Knobler, M. Okeeffe, O. M. Yaghi, Synthesis, structure, and carbon dioxide capture properties of zeolitic imidazolate frameworks, Accounts Chem. Res., 43 (2010) 58-67.

[3] K. S. Park, Z. Ni, A. P. Côté, J. Y. Choi, R. Huang, F. J. Uribe-Romo, H. K. Chae, M. O'Keeffe, O. M. Yaghi, Exceptional chemical and thermal stability of zeolitic imidazolate frameworks, Proceedings of the National Academy of Sciences of the United States of America, 103 (2006) 10186-10191.

[4] J. Cravillon, S. Münzer, S. J. Lohmeier, A. Feldhoff, K. Huber, M. Wiebcke, Rapid room-temperature synthesis and characterization of nanocrystals of a prototypical zeolitic imidazolate framework, Chemistry of Materials, 21 (2009) 1410-1412.

[5] W. Morris, C. J. Doonan, H. Furukawa, R. Banerjee, O. M. Yaghi, Crystals as molecules: Postsynthesis covalent functionalization of zeolitic imidazolate frameworks, Journal of the American Chemical Society, 130 (2008) 12626-12627.

[6] D. F. Li, T. S. Chung, R. Wang, Y. Liu, Fabrication of fluoropolyimide/polyethersulfone (PES) dual-layer asymmetric hollow fiber membranes for gas separation, Journal of Membrane Science, 198 (2002) 211-223.

[7] S. J. Tao, Positronium annihilation in molecular substances, The Journal of Chemical Physics, 56 (1972) 5499-5510.

[8] M. Eldrup, D. Lightbody, J. N. Sherwood, The temperature dependence of positron lifetimes in solid pivalic acid, Chemical Physics, 63 (1981) 51-58.

[9] W. H. Lin, R. H. Vora, T. S. Chung, Gas transport properties of 6FDA-durene/1,4-phenylenediamine (pPDA) copolyimides, Journal of Polymer Science, Part B: Polymer Physics, 38 (2000) 2703-2713.

[10] L. Jiang, T. S. Chung, D. F. Li, C. Cao, S. Kulprathipanja, Fabrication of Matrimid/polyethersulfone dual-layer hollow fiber membranes for gas separation, Journal of Membrane Science, 240 (2004) 91-103.

[11] L. Shao, T. S. Chung, S. H. Goh, K. P. Pramoda, Polyimide modification by a linear aliphatic diamine to enhance transport performance and plasticization resistance, Journal of Membrane Science, 256 (2005) 46-56.

[12] H. Wang, D. R. Paul, T. S. Chung, Surface modification of polyimide membranes by diethylenetriamine (DETA) vapor for H_2 purification and moisture effect on gas permeation. submitted to Journal of Membrane Science (2012).

[13] H. Z. Chen, T. S. Chung, CO_2-selective membranes for hydrogen purification and the effect of carbon monoxide (CO) on its gas separation performance. International Journal of Hydrogen Energy, 37 (2012) 6001-6011.

[14] R. D. Raharjo, B. D. Freeman, D. R. Paul, G. C. Sarti, E. S. Sanders, Pure and mixed gas CH_4 and n-C_4H_{10} permeability and diffusivity in poly(dimethylsiloxane), Journal of Membrane Science, 306 (2007) 75-92.

[15] B. T. Low, N. Widjojo, T. S. Chung, Polyimide/polyethersulfone dual-layer hollow fiber membranes for hydrogen enrichment, Industrial and Engineering Chemistry Research, 49 (2010) 8778-8786.

[16] R. Wang, C. Cao, T. S. Chung, A critical review on diffusivity and the characterization of diffusivity of 6FDA-6FpDA polyimide membranes for gas separation, Journal of Membrane Science, 198 (2002) 259-271.

[17] W. J. Koros, G. K. Fleming, S. M. Jordan, T. H. Kim, H. H. Hoehn, Polymeric membrane materials for solution-diffusion based permeation separations, Progress in Polymer Science, 13 (1988) 339-401.

[18] J. H. Petropoulos, Mechanisms and theories for sorption and diffusion of gases in polymers, in Polymeric gas separation membranes, ed. D. R. Paul and Y. P. Yampol'skii, CRC Press, Boca Raton, (1994) ch. 2, pp. 17-81.

CHAPTER 4

ZIF-7/PBI NANO-COMPOSITE MEMBRANES FOR HYDROGEN PURIFICATION

This chapter is published as a journal paper

Tingxu Yang, Youchang Xiao, Tai Shung Chung, Poly-/metal-benzimidazole nano-composite membranes for hydrogen purification, Energy & Environmental Science, 4 (2011) 4171-4180.

4.1 Introduction

Since the reserve for conventional fossil fuel has depleted, cost of fossil energy is no longer cheap and the greenhouse gas emitted from the end users of fossil fuel has created a variety of environmental problems, global research initiatives from both governments and industries have shifted their foci to alternative and renewable energy sources. As a promising candidate, hydrogen energy offers many unique advantages. For instance, hydrogen is "green" since its only combustion product is water. Meanwhile, the combustion heat of hydrogen is as high as 28,900 kcal kg^{-1}, approximate three times of gasoline with the same mass [1].

Currently, large scale hydrogen production is achieved through the water-gas shift reaction following the stream reforming of methane [2, 3]. Carbon dioxide is the main by-product of this unit operation in the leaving stream. It must be captured for effective H_2 usage and environmental concerns. Therefore, the removal of CO_2 is the primary step in the hydrogen purification. Current CO_2 separation technologies are highly capital and energy intensive. Amine-based methods work only at low temperatures, and consume a bundle of energy in the subsequently CO_2 release and absorbent regeneration. Cryogenic distillation and pressure-swing adsorption are energy intensive processes for CO_2 capture and may cost power plants an energy deduction up to 35% [3]. In contrast, membrane based separation technologies consume less energy because of no phase change during the separation process, and are therefore more economically applicable.

A few of inorganic materials have exhibited exciting selectivity or permeability for hydrogen purification [4-6]. Nonetheless, the considerable cost and mechanical brittleness may make inorganic membranes less commercially attractive. In addition, the preparation of defect-free layers of these inorganic materials on a large scale is extremely challenging [7, 8]. Currently, the dominating materials for H_2 purification are organic polymers. This is because polymers possess the advantages of easy processing, reasonable performance, and economically acceptable [2, 3, 7, 8]. According to the solution-diffusion model, the ideal permselectivity of a membrane for a gas pair is the product of diffusivity selectivity and solubility selectivity [9]. For the pair of H_2 and CO_2, the diffusivity selectivity is generally larger than one since the molecular size of H_2 is smaller. On the other hand, the H_2/CO_2 solubility selectivity is less than one as a result of the higher critical temperature and condensability of CO_2 [3]. Therefore, one can molecularly design H_2-selective or CO_2-selective membranes depending on different selective priority and end use requirements.

CO_2-selective membranes are mostly made from rubbery polymers and commonly known as “reverse selective membranes”, such as PEG or PEO-based blended membranes [10-17]. CO_2 selective membranes show the advantages of eliminating the cost on H_2 recompression, no performance reduction and even enhancement under CO_2 induced plasticization [16], and less requirement of membrane area [3], except the drawbacks of low thermal stability, weak mechanical strength, and easy crystallization, which are representative problems of rubbery materials for gas separation, limiting the industrial application of this kind of membranes.

H_2-selective membranes have the advantages of eliminating the cost on CO_2 recompression for subsequent sequestration. They are often made by glassy polymers since their polymer chains are much more rigid compared with rubbery polymers under the operating conditions. The H_2/CO_2 diffusivity selectivity contributes the main selectivity because H_2 is favored in the transportation. Researches on H_2-selective polymeric membranes have focused on molecular design of new materials and modifications of existing polymers by means of blending, doping, chemical cross-linking and mixed-matrix membranes [3]. Great improvements have been achieved by diamino cross-linking polyimides, making it one of the most promising ways to improve intrinsic H_2/CO_2 selectivity [18-24]. Besides, membranes with better anti-plasticization resistance through chemical cross-linking [24, 25] had also been reported. Nevertheless, the reductions of separation performance under mixed gases tests and higher testing temperatures are relatively common for cross-linked polyimide membranes.

To separate gases from hydrogen and syngas production streams, it is preferable if the membranes show thermally, chemically and mechanically stabilities at high temperatures and high pressures. Unfortunately, most of available polymer materials employed currently can only be used below 150 °C [26] and are not stable in much harsh high-temperature environments. Thus polybenzimidazole (PBI) was specifically chosen in this study because it has remarkable resistance to high temperatures (up to 500 °C) [27] with superior compression strength [28]. However, PBI exhibits low gas permeability due to the relatively high density chain packing [29, 30], and PBI membranes made by non-solvent phase inversion processes are very brittle. This material is not suitable for directly gas separation usages at room temperature.

Although coating PBI on metal tube supports [31] and spinning PBI into dual-layer hollow fibers [32] could introduce a thin selective layer with a large surface area and thus improve its gas separation performance, molecularly modifications of PBI materials with enhanced intrinsic gas separation performance may be a better approach. So far there are six modification methods have been reported to improve PBI gas permeability and selectivity, namely, 1) Blending with other polymers, such as polyetherimide [33], polysulfone [34], and polyimide [32], 2) Varying the acid moiety during the PBI synthesis [30], 3) Cross-linking segments of blended polymers [35], 4) Thermally rearranging the polymer at high temperatures [36], 5) N-substitution modification [37], and 6) Incorporating inorganic silica nano-particles [38].

Mixed matrix membranes (MMMs) consisting of polymeric materials and inorganic components have been extensively studied during the last two decades [39-52] since the basic idea was invented by Kulprathipanja et al. [53] about 25 years ago. A progress review has been conducted by Chung et al. [54]. There are still many challenges ahead such as interface voids, pore blockage and chain rigidification [39, 40, 54]. In addition, the oversize of zeolite nano-particles, their mutual agglomeration, and poor interface with the polymer matrix are troublesome issues and must be overcome before considering commercialization. One of the ways to overcome these deadlocks is to identify new selective fillers which have characteristics of inherently nano-size, less aggregation and better interactions with the polymer matrix.

One candidate might be three-dimensional (3D) or two-dimensional (2D) nanoporous networks of transition metal complexes, named as metal-organic frameworks (MOFs)

[55, 56], which exhibit a high porosity with exactly tailorable cavity sizes. As compared to commercially available inorganic particles like zeolites, MOFs are postulated to be able to better incorporate into organic polymer matrix due to the organic linkers present in the frameworks. Zeolitic imidazolate frameworks (ZIFs) are a subfamily of MOFs with all the above advantages while at the same time exhibit exceptional chemical and thermal stability [57]. Studies of molecular sieve membranes grown from several ZIFs have revealed the potential of this material for gas separation [58-63]. As a member of ZIFs, ZIF-7 with a pore size of 3.0 Å shows thermal stability up to 550 °C and good chemical resistance to water and organic solvents [57]. Since ZIF-7 has a pore size exactly between the molecular kinetic diameters of H_2 and CO_2 (2.9 Å and 3.3 Å, respectively), the supported molecular sieve membrane grown from pure ZIF-7 has shown a high hydrogen flux and a good H_2/CO_2 selectivity [59, 63]. However, most works show difficulties of increasing ZIF loading and preventing ZIF nano-particles from aggregation.

Therefore, the objectives of this work are to combine the superior thermal stability of PBI and remarkable H_2/CO_2 selectivity of ZIF-7 and to examine the fundamental science and engineering of designing H_2-selective mixed matrix membranes made of these two materials with a fully dispersed morphology for the separation of gas streams from steam reforming and syngas at high temperatures.

4.2 Results and discussion

4.2.1 ZIF-7 particle dispersion in the PBI matrix

In addition to aiming at higher separation performance, nano-size particles were chosen in mixed matrix composite membranes to achieve better interactions between polymer matrix and particles and lower non-selective voids. However, particle agglomeration was often observed in previous studies when inorganic nano-particles such as zeolite [39, 40, 45], silica [38], MOF-5 [64], and ZIF-8 [65] were embedded into polymer matrices at high loadings. This phenomenon is due to strong interactions between particles, or poor interactions between particles and polymer matrix. To overcome or minimize particle agglomeration, ZIF-7 was synthesized with an excess amount of benzimidazole in this study and then mixed with PBI containing reactive hydrogen atoms on polymer chains. Without performing standard drying procedure, ZIF-7 particles were avoided to forming strong interactions with each other, and thus can be distributed homogenously in PBI with less agglomeration. The chemical structures of PBI and ZIF-7 are shown in Figure 4.1.

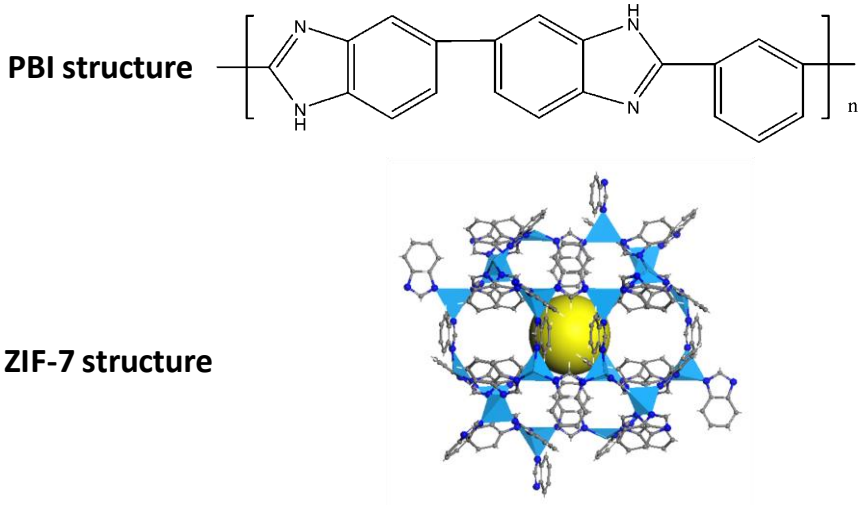

Figure 4.1 Chemical structures of poly-2,2'-(m-phenylene)-5,5' bibenzimidazole and ZIF-7

Since data from dynamic light scattering (DLS) of solutions can be a directly evidence of agglomeration [66], DLS was conducted to study the apparent particle size distribution in ZIF-7 PBI suspensions. Four suspensions were prepared in different conditions and kept still in room temperature for 24hrs before tests. They are 1) As synthesized ZIF-7 particles suspended in DMF, before centrifugation and washing; 2) ZIF-7/DMF suspension after 1st centrifugation, washed by DMF, and re-suspended in fresh DMF; 3) ZIF-7/NMP suspension after 2nd centrifugation, washed by DMF, and then re-suspended in fresh NMP; and 4) (ZIF-7 + PBI)/NMP after 3rd centrifugation, washed by NMP, and re-suspended in the PBI-NMP solution. Figure 4.2 shows the apparent particle size distributions of ZIF-7 in these suspensions. There is no significant change of particle size distribution in suspensions after redistributing ZIF-7 in DMF, NMP and then PBI-NMP solutions. These encouraging results indicate that the effects of centrifugation, solvents and PBI addition on the dispersion of ZIF-7 particles may be negligible. Hence no obvious non-uniformity and agglomeration are observed after solvent evaporation during membrane casting. In contrast, it was observed that the nano-crystal powder became un-dispersible in polar solvents anymore if it was dried directly after synthesis and washing. The similar phenomenon was reported of ZIF-8 by Cravillon et al. [67]. This was mainly due to that Zn-imidazole (Him) on the particle surface may react among themselves and form strong covalent Zn-im-Zn bonds between the particles during drying [67].

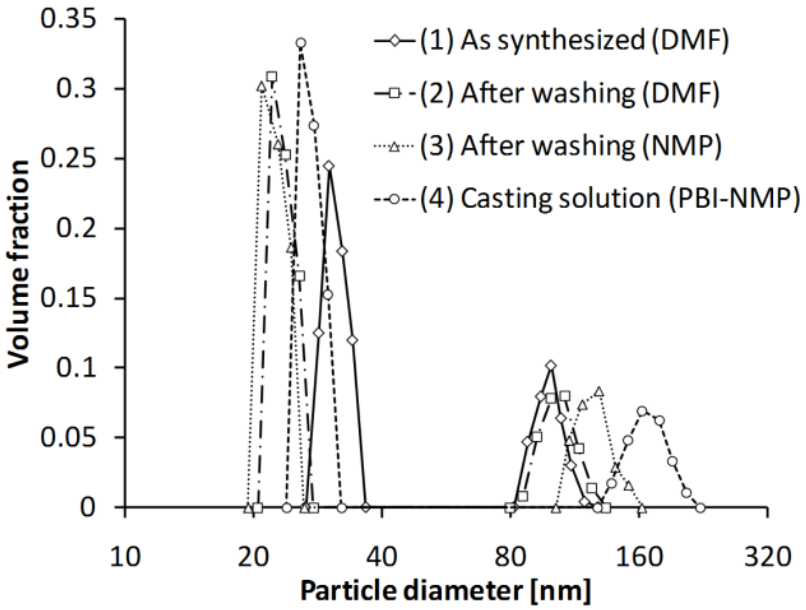

Figure 4.2 Comparison of ZIF-7 particles size distribution under different conditions

The particle dispersion of ZIF-7 in the PBI matrix was investigated using a transmission electron microscope (TEM) and Figure 4.3(1) shows the morphology of a 50/50 (w/w) ZIF-7/PBI mixture precipitated in methanol. Good dispersion of ZIF-7 particles in PBI is present, without observable much particle agglomeration. Meanwhile, nice interphase interaction between ZIF-7 and PBI is achieved. This is because that PBI can act as a coating agent on ZIF-7 surface, thus the addition of PBI prevents ZIF-7 particles from agglomeration and reduces interphase voids in the mixture. This method is similar to a previous study by Li et al. [68] where a SPES primer was used to prevent the agglomeration of zeolite 4A in PES-zeolite 4A MMMs. To further verify the ZIF-7 agglomeration state in the formed membranes, the cross-section of 50/50 (w/w) ZIF-7/PBI membrane was observed by FESEM (Figure 4.3(2)). In this image, the small white spheres reflect to the polymer nodules of PBI, and the ZIF-7 particles are filled into the polymer matrix, as pointed by the white arrows. It is

also worth to be noted that no agglomeration and void between particles and polymer is observable in this membrane.

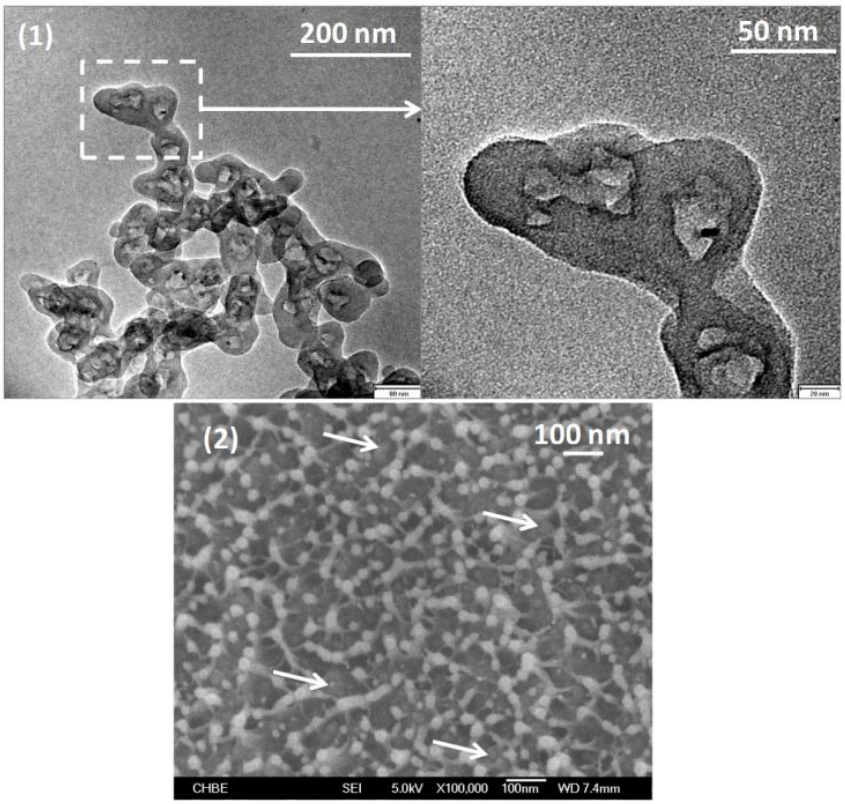

Figure 4.3 Morphology images of ZIF-7/PBI nano-composite
(1): TEM micrograph of the 50/50 (w/w) ZIF-7/PBI mixture; (2): FESEM micrograph from the cross-section of 50/50 (w/w) ZIF-7/PBI membrane

Figure 4.4 shows the appearance of the 50/50 (w/w) ZIF-7/PBI nano-composite membrane placed on an NUS logo and bended with fingers. It is obvious that the logo can be clearly seen through the membrane. This indicates that the membrane is maintained its transparency even containing a higher loading of ZIF-7 particles, which is commonly lost in mixed matrix membranes of loadings above 20 wt %. This appearance provides a visualized proof of a very low level of agglomeration in the 50/50 (w/w) ZIF-7/PBI nano-composite membrane. Meanwhile, acceptable mechanical strength is shown in the bending test. To best of our knowledge, the 50/50

(w/w) ZIF-7/PBI membrane is the highest loading reported so far for ZIF-based functional nano-composite membranes.

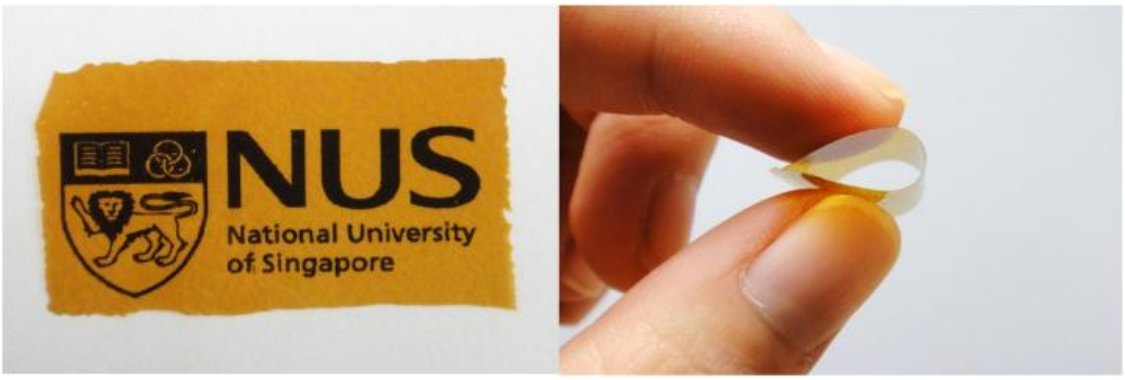

Figure 4.4 The appearance of 50/50 (w/w) ZIF-7/PBI nano-composite membrane **Left**: Tiled on an NUS logo; **Right**: Bended with fingers.

4.2.2 Characterizations

Figure 4.5 shows Fourier transform infrared spectroscopy (FTIR) spectra of the chemical structure of composite membranes. All the spectra of membranes containing PBI are normalized by the peak at 1443 cm^{-1}, which is assigned to the in-plane ring vibration of 2,6-disubstituted benzimidazole [69]. It is shown that with the increasing of ZIF-7 nano particle loadings, the peaks of N-H bond (3415cm^{-1} for 'free' non-hydrogen-bonded N-H stretching, and 3145cm^{-1} for self-associated N-H stretching) become weaker. These results indicate that there may be a strong interaction between PBI and ZIF-7 nano particles in which the reactive hydrogen atom is replaced by the zinc ion on the surface of ZIF-7, forming a sub-nano interphase structure between ZIF-7 and PBI as an extension of ZIF-7 frameworks. Interestingly, the N-H group can be also observed in the spectrum of ZIF-7 powder as shown in Figure 4.5. This is resulted from the synthesis environment where an excess amount of benzimidazole

was used. The benzimidazole can act both as a linker in its deprotonated form and as a terminating and stabilizing unit in its neutral form [67].

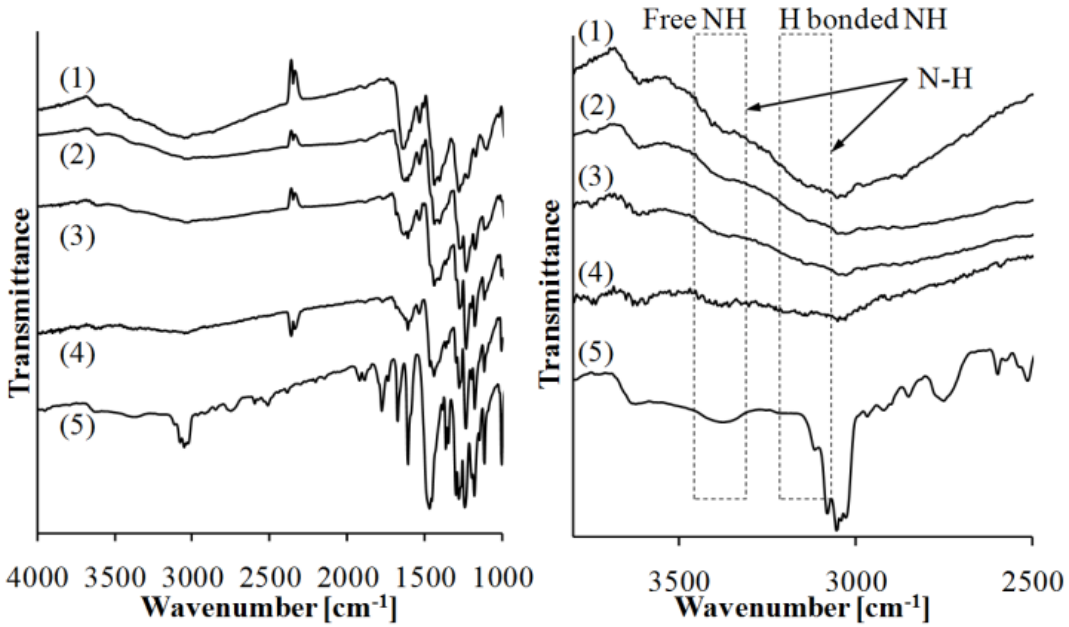

Figure 4.5 FTIR spectra of pure PBI and ZIF-7/PBI nano-composite membranes (1): Pure PBI; (2): 10/90 (w/w) ZIF-7/PBI; (3): 25/75 (w/w) ZIF-7/PBI; (4): 50/50 (w/w) ZIF-7/PBI; (5): Pure ZIF-7 powder in KBr pallet. (Left: spectra of the original range; Right: enlarged spectra at the N-H region)

Figure 4.6 shows thermo gravimetric analysis (TGA) thermograms of PBI and ZIF-7/PBI nano-composite membranes with different ZIF-7 loadings. Because PBI absorbs water and exhibits a visible weight loss below 200 °C [30, 70], the TGA thermograms were calibrated using the weight at 200 °C as the starting point. From 350 °C to 450 °C, there is a weight loss of less than 10% in pure PBI spectra, which may represent additives or impurities in commercial polymer powders, as reported by Jaffe et al. [70]. It is shown that PBI, ZIF-7 and composite membranes all exhibit good thermal stability up to 550 °C in air. After heating up to 710 °C at atmosphere in air, PBI is completely decomposed and remaining only zinc oxide, a derivative of zinc

based ZIFs [67]. As a result, the accurate loadings of ZIF-7 in the membranes can be calculated based on the stoichiometry amount of remaining zinc oxide and the results are tabulated in Table 4.1.

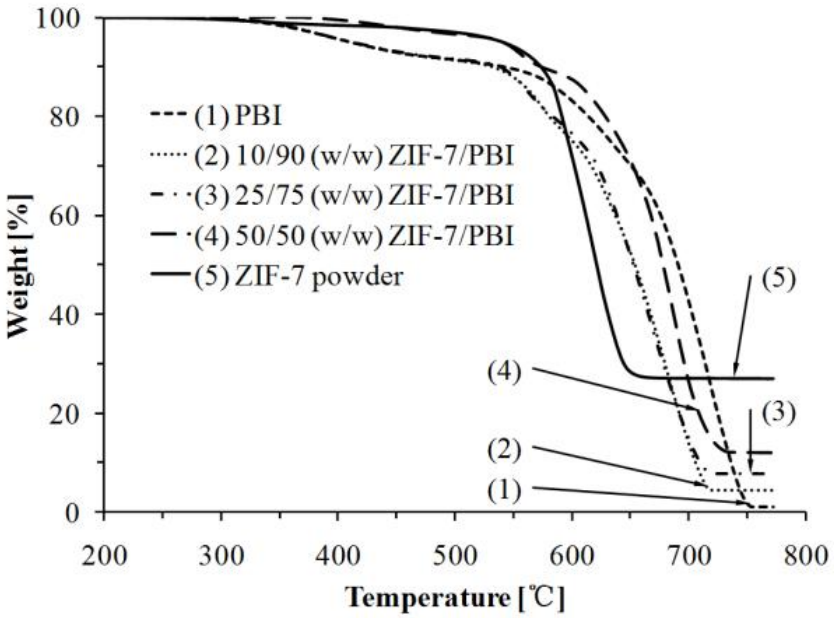

Figure 4.6 TGA thermograms of pure PBI, ZIF-7, and ZIF-7/PBI nano-composite membranes under air atmosphere

Table 4.1 Thermo properties and particle loadings of pure PBI, ZIF-7 and ZIF-7/PBI nano-composite membranes

Membrane name	Ash content weight [%]	ZIF-7 loading [wt%]	Glass transition temperature [℃]
PBI	0.0	0.0	427
10/90 (w/w) ZIF-7/PBI	3.7	13.7	444
25/75(w/w) ZIF-7/PBI	7.1	26.1	452
50/50 (w/w) ZIF-7/PBI	11.4	42.1	462
ZIF-7 powder	27.0	99.7	—

Table 4.1 also summarizes the glass transition temperatures of all membranes determined by differential scanning calorimetry (DSC). The pure PBI shows a T_g of

427 °C which is consistent with the value in the literature [32, 33, 35, 70, 71]. The T_g of the composite membranes increases with an increase in ZIF-7 loading. This result indicates that there are changes of PBI polymer chain packing structure after loaded with ZIF-7 nano-particles. Thus, the rigidification of polymer chain could be one of the reasons for the enhanced permselectivity of ZIF-7/PBI nano-composite membranes, which will be discussed in subsequent section (section 4.3.3).

Wide-angle X-ray diffraction (WAXRD) measurements between 5 °to 30 °were conducted to determine the crystalline structure in each nano-composite membrane. The XRD patterns are shown in Figure 4.7. The patterns of pure PBI and ZIF-7 are included in Figure 4.7 for comparison purpose. The XRD pattern of pure PBI shows a broad peak from 10 °to 26 °, which is a characteristic of amorphous structure and consistent with the reported XRD pattern for PBI in the literature [38]. The diffraction patterns of PBI/ZIF-7 nano-composite membranes exhibit intense, characteristic ZIF-7 crystalline peaks matching extremely well with pure ZIF-7 and PBI patterns and confirm that ZIF-7 and PBI structures are present in the membranes.

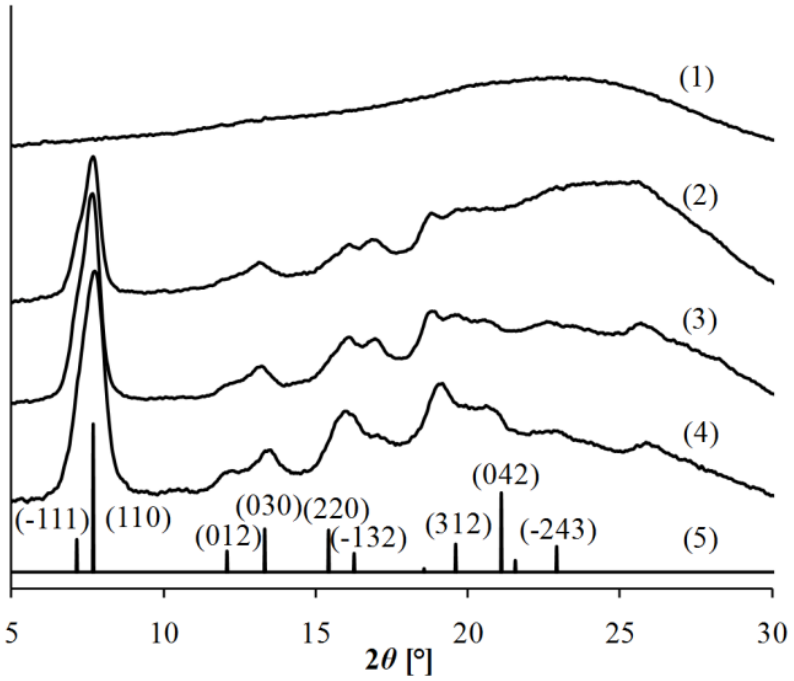

Figure 4.7 XRD spectra of pure PBI, ZIF-7, and ZIF-7/PBI nano-composite membranes
(1) Pure PBI; (2) 10/90 (w/w) ZIF-7/PBI; (3) 25/75 (w/w) ZIF-7/PBI; (4) 50/50 (w/w) ZIF-7/PBI; (5) ZIF-7 (theoretical).

The positron annihilation lifetime spectroscopy (PALS) results such as intensity (I_3), lifetime (τ_3), free volume radius (R) and free volume fraction (FV) of the nano-composite membranes are shown in Table 4.2. It should be mentioned that the free volume fraction measured by PALS is methodologically different from the fractional free volume calculated by the Bondi method [72]. The lifetime between 2 and 3.5 ns is attributed to the o-Ps annihilation (τ_3) in the amorphous region of the polymeric membranes [73, 74], thus τ_3 is a useful parameter for the determination of the average free volume cavity size in the range of 2.9 Å to 4.0 Å (in radius) for polymers. Since the cavity radius of ZIF-7 is equal to 2.15 Å, which is smaller than polymer free volume cavities, the lifetime correlating with ZIF-7 is not present in this range of lifetime. The τ_3 of the membranes became larger with the presence of ZIF-7, and it is

relatively constant with an increase in ZIF-7 loading. On the other hand, the free volume fraction increases with an increasing in ZIF-7 loading. This indicates that a larger free volume cavity has been formed in the PBI phase resulted from interactions between the PBI phase and ZIF-7. However, the number of cavities, not their size is increased with increasing ZIF-7 loading.

Table 4.2 Positron annihilation lifetime spectroscopy (PALS) data of pure PBI and ZIF-7/PBI nano-composite membranes

Membrane name	I_3 **[%]**	τ_3 **[ns]**	R **[Å]**	**FV [%]**
PBI	17.23 ±0.30	2.07 ±0.02	2.92 ±0.02	3.24 ±0.11
25/75 (w/w) ZIF-7/PBI	16.99 ±0.29	2.18 ±0.03	3.01 ±0.02	3.51 ±0.14
50/50 (w/w) ZIF-7/PBI	18.41 ±0.31	2.17 ±0.03	3.00 ±0.02	3.76 ±0.13

4.2.3 Gas transport properties

Table 4.3 summarizes pure gas permeabilities of H_2 and CO_2 of PBI and ZIF-7/PBI nano-composite membranes with different loadings under 35 °C. The gas permeation data of pure PBI reported in the literatures show large diversity [30, 38, 75]. This may be due to (1) the use of different solvents, molecular weights, and fabricating methods for membrane preparation, and (2) unknown impurities presence in commercial polymer powders. In this work, the permeability of each gas was obtained by measuring three different pieces of PBI membranes. The average deviation was found to be less than 5%. For the nano-composite membranes, the gas permeability of H_2 exhibits significant enhancement with increasing ZIF-7 loadings, from 3.7 Barrer of pure PBI to 26.2 Barrer of 50/50 (w/w) ZIF-7/PBI, while the ideal selectivity of H_2/CO_2 improves from 8.7 to 14.9. These results clearly support the assumptions in

the previous discussion. The extra-introduced free volume provides more sub-nano channels for gas transportation, thus the permeability of the resultant membranes are higher than the simple combination of two phases. Meanwhile, though the mean free volume size becomes slightly larger, the rigidified chains may amplify the molecular sieve effect and result in an undiminished or even enhanced selectivity. Since this structure become more dominant in membranes with a higher loading of ZIF-7, the enhancement of permeability and selectivity can be also more apparent.

Table 4.3 Pure gas and mixed gas permeation properties of pure PBI and ZIF-7/PBI nano-composite membranes with different ZIF-7 loadings at 35 ℃

Membrane name	**Single gas permeability[a] [Barrer[b]]**		**Ideal selectivity**	**Mixed gas permeability[c] [Barrer]**		**Separation factor**
	H_2	**CO_2**	**H_2/CO_2**	**H_2**	**CO_2**	**H_2/CO_2**
PBI	3.7	0.4	8.7	2.9	0.3	7.1
10/90 (w/w) ZIF-7/PBI	7.7	0.6	12.9	—	—	—
25/75(w/w) ZIF-7/PBI	15.4	1.3	11.9	6.3	0.9	6.8
50/50 (w/w) ZIF-7/PBI	26.2	1.8	14.9	13.3	1.8	7.2

[a] Single gas tests were performed in 3.5 atm, at 35 ℃.
[b] 1 Barrer=1×10^{-10} cm^3 (STP) cm cm^{-2} s^{-1} $cmHg^{-1}$.
[c] Mixed gas tests were performed in 7 atm with 50% H_2 and 50% CO_2, at 35 ℃.

The Maxwell model as shown below has been widely used for the performance prediction of mixed matrix membranes [54]:

$$P_{eff} = P_C\left[\frac{P_D + 2P_C - 2\phi_D(P_C - P_D)}{P_D + 2P_C + \phi_D(P_C - P_D)}\right] \quad (4\text{-}1)$$

where P_{eff} is the effective permeability, P_C and P_D represent the permeabilities of the continuous phase and dispersed phase, respectively, and φ_D is the volume fraction of the dispersed phase. Figure 4.8 shows a comparison of the current permeation data and the prediction curve by the Maxwell model using the permeation data of pure

ZIF-7 membrane with the aid of methodology developed by Li et al. [63]. It is found that the experimental value of H_2 permeability is well above the prediction by the Maxwell model, and the difference becomes more significant with an increase in ZIF-7 loading. The deviation of experimental value of CO_2 permeability is much less from the Maxwell prediction curve. The different deviations for the predication of H_2 and CO_2 permeabilities are well consistent with previous characterization results because (1) the FTIR results provide the explanation for good interactions between PBI and ZIF-7 particles; (2) the increased glass transition temperature implies the existence of interphase and chain rigidification; and (3) the PALS results further prove a larger amount of free volume with increasing ZIF-7 loadings in addition to a slightly bigger pore size. All above data suggest that sub-nano transportation channels are formed in ZIF-7/PBI membranes that favor the permeation of H_2.

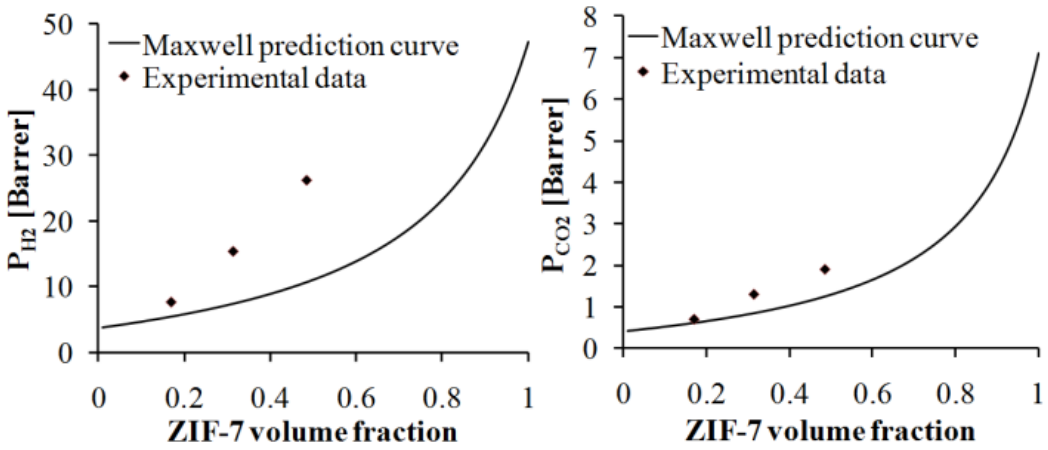

Figure 4.8 Comparison between the Maxwell predicted values and experimental data of ZIF-7/PBI nano-composite membranes

For possible applications to separate gas streams from the production of steam reforming or syngas, gas mixture tests from 35 ℃ to 180 ℃ were conducted using pure PBI and nano-composite membranes with 25% and 50% loadings of ZIF-7 nano-

particles. Figure 4.9 shows the results using a 50/50 H_2/CO_2 mixture as the feed. Compared with pure gas data, a significant decrease of H_2 permeability is observed in all membranes in the present of CO_2 at 35 °C. This phenomenon becomes obvious with an increase in ZIF-7 loadings. This may due to the fact that CO_2 is likely to be adsorbed into the free volume and pores, and subsequently blocks the transportation of H_2 molecules, leading to the simultaneously reduction of H_2 permeability and selectivity. While at higher temperatures, CO_2 adsorption is largely restrained and diffusion became more dominant.

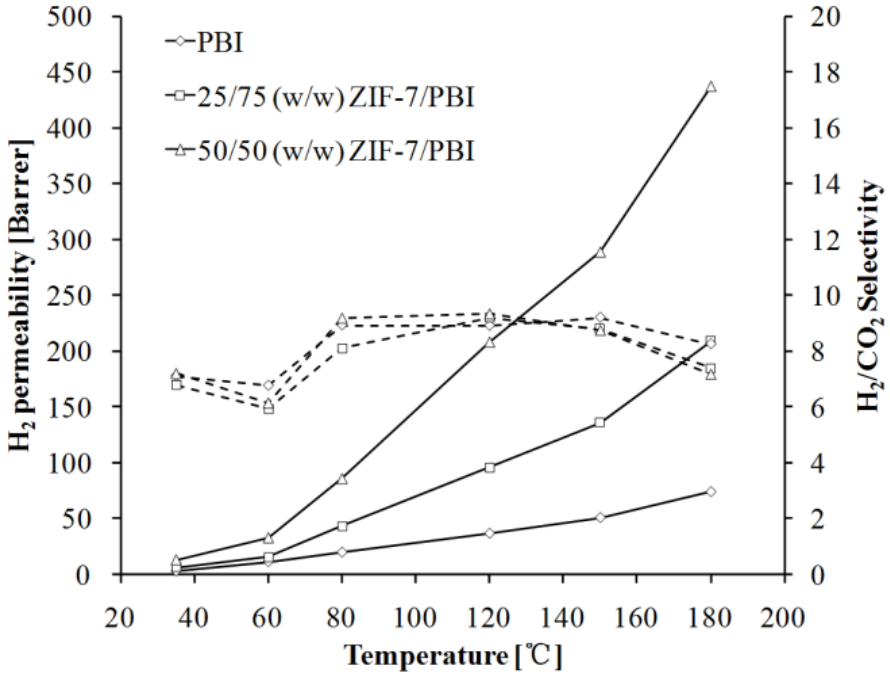

Figure 4.9 Mixed gas permeation test results of pure PBI and ZIF-7/PBI nano-composite membranes
(Solid line: H_2 permeability; dotted line: H_2/CO_2 selectivity).

For all membranes, the separation factors decrease from 35 °C to 60 °C, increase in the subsequent temperatures, and decrease again at 180 °C. This is a result of the balance between the diffusivity selectivity and solubility selectivity for the H_2 and CO_2 pair.

Generally, accompanying with increasing temperature, the D_{H2}/D_{CO2} ratio decreases since the polymer chains become more flexible at higher temperatures. On the other hand, the S_{H2}/S_{CO2} ratio becomes larger due to a greater decrease in CO_2 solubility than that of H_2. From 35 °C to 60 °C, the effect of D_{H2}/D_{CO2} reduction is more dominant, thus the selectivity decreases; from 60 °C to 150 °C. The augment of S_{H2}/S_{CO2} overcome the reduction of D_{H2}/D_{CO2}, thus the selectivity become higher. Finally, at temperatures above 150 °C, there is almost no CO_2 solubility in the membranes. Therefore the contribution of S_{H2}/S_{CO2} is diminished and the effect of D_{H2}/D_{CO2} became dominant again, resulted in the reduction of selectivity.

Figure 4.10 shows the gas permeation results and compares with the Roberson upper bound [76]. The ideal H_2 permeability and selectivity at 35 °C of the 50/50 (w/w) ZIF-7/PBI has surpassed the upper bound. Although the mixed gas result at 35 °C dips slightly below the upper bound, a remarkable performance rebound is observed when the membrane is tested at 180 °C.

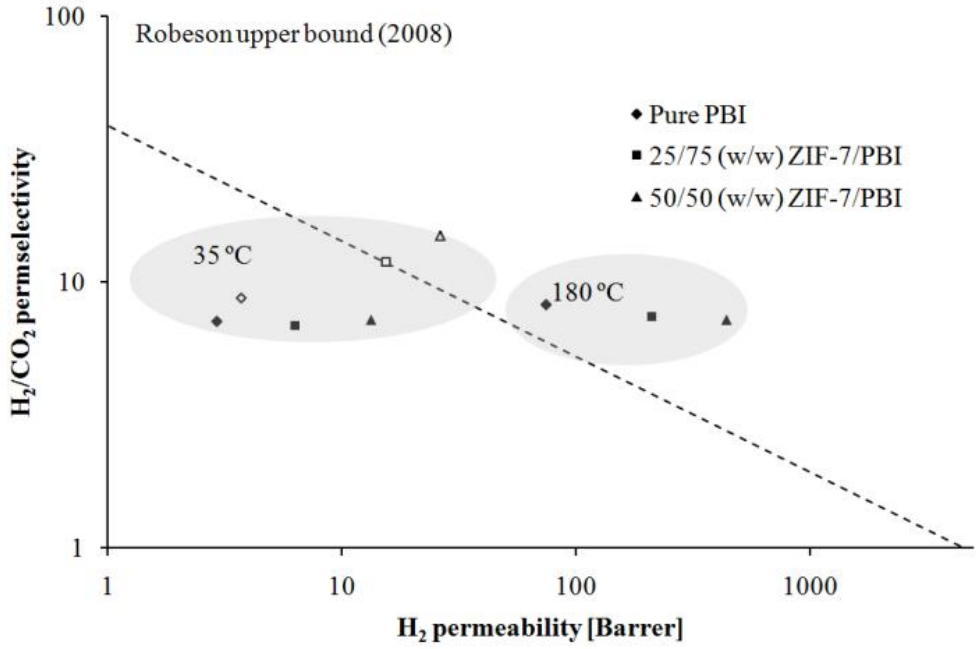

Figure 4.10 H_2/CO_2 separation performance of pure PBI and ZIF-7/PBI nano-composite membranes compared to the Robeson upper bound
(Hollow marks: pure gas separation performance; Solid marks: mixed gas separation performance.)

4.3 Conclusions

We have demonstrated, for the first time, the incorporation of ZIF-7 nano-particles into the PBI polymer matrix without much ZIF agglomeration by using an excess amount of benzimidazole during the ZIF-7 synthesis. In addition to exhibiting characteristics of highly transparency and mechanical flexibility, the resultant nano-composite membranes show superior separation performance with enhanced H_2 permeability and ideal H_2/CO_2 permselectivity compared to both neat PBI and ZIF-7 membranes. Experimental results from advanced analytic instruments confirm that the superior performance is a combinative result of (1) strong chemical interactions between ZIF-7 surface and PBI, (2) minimal non-selective voids, (3) rigidified PBI chains on ZIF nano-particles, and (4) the creation of more free volume and slightly larger pores as sub-nano interphase channels for gas transport. Mixed gas results were conducted from ambient temperature to 180°C and show a significant increase in H_2 permeability but without compromising H_2/CO_2 selectivity. The newly developed scheme to prepare ZIF-7/PBI mixed matrix membranes with well dispersed nano-size particles has great potential to be scaled up for industrial productions of asymmetric hollow fibers and flat-sheet membranes for gas separation and CO_2 capture.

4.4 References

[1] L. Schlapbach, A. Zuttel, Hydrogen-storage materials for mobile applications, Nature, 414 (2001) 353-358.

[2] N. W. Ockwig, T. M. Nenoff, Membranes for hydrogen separation, Chemical Reviews, 107 (2007) 4078-4110.

[3] L. Shao, B. T. Low, T. S. Chung, A. R. Greenberg, Polymeric membranes for the hydrogen economy: Contemporary approaches and prospects for the future, Journal of Membrane Science, 327 (2009) 18-31.

[4] J. Dong, Y. S. Lin, M. Kanezashi, Z. Tang, Microporous inorganic membranes for high temperature hydrogen purification, Journal of Applied Physics, 104 (2008) 121301-121317.

[5] D. Grainger, M. B. Hägg, Evaluation of cellulose-derived carbon molecular sieve membranes for hydrogen separation from light hydrocarbons, Journal of Membrane Science, 306 (2007) 307-317.

[6] D. Grainger, M. B. Hagg, The recovery by carbon molecular sieve membranes of hydrogen transmitted in natural gas networks, International Journal of Hydrogen Energy, 33 (2008) 2379-2388.

[7] J. D. Perry, K. Nagai, W. J. Koros, Polymer membranes for hydrogen separations, MRS Bulletin, 31 (2006) 745-749.

[8] R. Baker, Future directions of membrane gas-separation technology, Membrane Technology, 138 (2001) 5-10.

[9] J. G. Wijmans, R. W. Baker, The solution-diffusion model: A review, Journal of Membrane Science, 107 (1995) 1-21.

[10] M. Kawakami, H. Iwanaga, Y. Hara, M. Iwamoto, S. Kagawa, Gas permeabilities of cellulose nitrate/poly(ethylene glycol) blend membranes, Journal of Applied Polymer Science, 27 (1982) 2387-2393.

[11] W. Yave, A. Car, S. S. Funari, S. P. Nunes, K. -V. Peinemann, CO_2-Philic polymer membrane with extremely high separation performance, Macromolecules, 43 (2010) 326-333.

[12] S. R. Reijerkerk, M. H. Knoef, K. Nijmeijer, M. Wessling, Poly(ethylene glycol) and poly(dimethyl siloxane): Combining their advantages into efficient CO_2 gas separation membranes, Journal of Membrane Science, 352 (2010) 126-135.

[13] A. Car, C. Stropnik, W. Yave, K. -V. Peinemann, Pebax®/polyethylene glycol blend thin film composite membranes for CO_2 separation: Performance with mixed gases, Separation and Purification Technology, 62 (2008) 110-117.

[14] K. I. Okamoto, M. Fujii, S. Okamyo, H. Suzuki, K. Tanaka, H. Kita, Gas permeation properties of poly(ether imide) segmented copolymers, Macromolecules, 28 (1995) 6950-6956.

[15] H. Chen, Y. Xiao, T. S. Chung, Synthesis and characterization of poly (ethylene oxide) containing copolyimides for hydrogen purification, Polymer, 51 (2010) 4077-4086.

[16] H. Lin, E. Van Wagner, B. D. Freeman, L. G. Toy, R. P. Gupta, Plasticization-enhanced hydrogen purification using polymeric membranes, Science, 311 (2006) 639-642.

[17] L. Shao, T. S. Chung, In situ fabrication of cross-linked PEO/silica reverse-selective membranes for hydrogen purification, International Journal of Hydrogen Energy, 34 (2009) 6492-6504.

[18] L. Shao, T. S. Chung, S. H. Goh, K. P. Pramoda, Transport properties of cross-linked polyimide membranes induced by different generations of diaminobutane (DAB) dendrimers, Journal of Membrane Science, 238 (2004) 153-163.

[19] T. S. Chung, L. Shao, P. S. Tin, Surface modification of polyimide membranes by diamines for H_2 and CO_2 separation, Macromolecular Rapid Communications, 27 (2006) 998-1003.

[20] Y. Liu, R. Wang, T. S. Chung, Chemical cross-linking modification of polyimide membranes for gas separation, Journal of Membrane Science, 189 (2001) 231-239.

[21] L. Shao, T. S. Chung, S. H. Goh, K. P. Pramoda, The effects of 1,3-cyclohexanebis(methylamine) modification on gas transport and plasticization resistance of polyimide membranes, Journal of Membrane Science, 267 (2005) 78-89.

[22] L. Shao, L. Liu, S. X. Cheng, Y. D. Huang, J. Ma, Comparison of diamino cross-linking in different polyimide solutions and membranes by precipitation observation and gas transport, Journal of Membrane Science, 312 (2008) 174-185.

[23] P. S. Tin, T. S. Chung, Y. Liu, R. Wang, S. L. Liu, K. P. Pramoda, Effects of cross-linking modification on gas separation performance of Matrimid membranes, Journal of Membrane Science, 225 (2003) 77-90.

[24] B. T. Low, Y. Xiao, T. S. Chung, Y. Liu, Simultaneous occurrence of chemical grafting, cross-linking, and etching on the surface of polyimide membranes and their impact on H_2/CO_2 separation, Macromolecules, 41 (2008) 1297-1309.

[25] J. D. Wind, C. Staudt-Bickel, D. R. Paul, W. J. Koros, Solid-state covalent cross-linking of polyimide membranes for carbon dioxide plasticization reduction, Macromolecules, 36 (2003) 1882-1888.

[26] P. Bernardo, E. Drioli, G. Golemme, Membrane gas separation: A review/state of the art, Industrial & Engineering Chemistry Research, 48 (2009) 4638-4663.

[27] H. Vogel, C. S. Marvel, Polybenzimidazoles, new thermally stable polymers, Journal of Polymer Science, 50 (1961) 511-539.

[28] Y. Tsur, H. H. Levine, M. Levy, Effects of structure on properties of some new aromatic-aliphatic polybenzimidazoles, Journal of Polymer Science Part A: Polymer Chemistry, 12 (1974) 1515-1529.

[29] D. R. Pesiri, B. Jorgensen, R. C. Dye, Thermal optimization of polybenzimidazole meniscus membranes for the separation of hydrogen, methane, and carbon dioxide, Journal of Membrane Science, 218 (2003) 11-18.

[30] S. C. Kumbharkar, P. B. Karadkar, U. K. Kharul, Enhancement of gas permeation properties of polybenzimidazoles by systematic structure architecture, Journal of Membrane Science, 286 (2006) 161-169.

[31] G. Krishnan, D. Steele, K. O'Brien, R. Callahan, K. Berchtold, J. Figueroa, Simulation of a process to capture CO_2 from IGCC syngas using a high temperature PBI membrane, in *Energy Procedia*, Vol. 1 (Eds.: J. Gale, H. Herzog, J. Braitsch), Elsevier, Amsterdam, (2009) pp. 4079-4088.

[32] S. S. Hosseini, N. Peng, T. S. Chung, Gas separation membranes developed through integration of polymer blending and dual-layer hollow fiber spinning process for hydrogen and natural gas enrichments, Journal of Membrane Science, 349 (2010) 156-166.

[33] T. S. Chung, Z. L. Xu, Asymmetric hollow fiber membranes prepared from miscible polybenzimidazole and polyetherimide blends, Journal of Membrane Science, 147 (1998) 35-47.

[34] T. S. Chung, C. M. Tun, K. P. Pramoda, R. Wang, Novel hollow fiber membranes with defined unit-step morphological change, Journal of Membrane Science, 193 (2001) 123-128.

[35] S. S. Hosseini, M. M. Teoh, T. S. Chung, Hydrogen separation and purification in membranes of miscible polymer blends with interpenetration networks, Polymer, 49 (2008) 1594-1603.

[36] S. H. Han, J. E. Lee, K. J. Lee, H. B. Park, Y. M. Lee, Highly gas permeable and microporous polybenzimidazole membrane by thermal rearrangement, Journal of Membrane Science, 357 (2010) 143-151.

[37] S. C. Kumbharkar, U. K. Kharul, Investigation of gas permeation properties of systematically modified polybenzimidazoles by N-substitution, Journal of Membrane Science, 357 (2010) 134-142.

[38] M. Sadeghi, M. A. Semsarzadeh, H. Moadel, Enhancement of the gas separation properties of polybenzimidazole (PBI) membrane by incorporation of silica nano particles, Journal of Membrane Science, 331 (2009) 21-30.

[39] C. M. Zimmerman, A. Singh, W. J. Koros, Tailoring mixed matrix composite membranes for gas separations, Journal of Membrane Science, 137 (1997) 145-154.

[40] Y. Li, T. S. Chung, C. Cao, S. Kulprathipanja, The effects of polymer chain rigidification, zeolite pore size and pore blockage on polyethersulfone (PES)-zeolite A mixed matrix membranes, Journal of Membrane Science, 260 (2005) 45-55.

[41] H. M. Guan, T. S. Chung, Z. Huang, M. L. Chng, S. Kulprathipanja, Poly(vinyl alcohol) multilayer mixed matrix membranes for the dehydration of ethanol-water mixture, Journal of Membrane Science, 268 (2006) 113-122.

[42] S. Kim, T. W. Pechar, E. Marand, Poly(imide siloxane) and carbon nanotube mixed matrix membranes for gas separation, Desalination, 192 (2006) 330-339.

[43] L. Y. Jiang, T. S. Chung, C. Cao, Z. Huang, S. Kulprathipanja, Fundamental understanding of nano-sized zeolite distribution in the formation of the mixed matrix single- and dual-layer asymmetric hollow fiber membranes, Journal of Membrane Science, 252 (2005) 89-100.

[44] E. Okumus, T. Gurkan, L. Yilmaz, Development of a mixed-matrix membrane for pervaporation, Separation Science and Technology, 29 (1994) 2451-2473.

[45] Y. Li, T. S. Chung, S. Kulprathipanja, Novel Ag^{+}-zeolite/polymer mixed matrix membranes with a high CO_2/CH_4 selectivity, AICHE Journal, 53 (2007) 610-616.

[46] M. D. Jia, K. V. Peinemann, R. D. Behling, Molecular-sieving effect of the zeolite-filled silicone-rubber membranes in gas permeation, Journal of Membrane Science, 57 (1991) 289-296.

[47] L. Shao, J. Samseth, M. B. Hagg, Crosslinking and stabilization of nanoparticle filled PMP nanocomposite membranes for gas separations, Journal of Membrane Science, 326 (2009) 285-292.

[48] S. P. Nunes, K. V. Peinemann, K. Ohlrogge, A. Alpers, M. Keller, A. T. N. Pires, Membranes of poly(ether imide) and nanodispersed silica, Journal of Membrane Science, 157 (1999) 219-226.

[49] M. L. Sforça, I. V. P. Yoshida, S. P. Nunes, Organic-inorganic membranes prepared from polyether diamine and epoxy silane, Journal of Membrane Science, 159 (1999) 197-207.

[50] R. A. Zoppi, S. das Neves, S. P. Nunes, Hybrid films of poly(ethylene oxide-b-amide-6) containing sol-gel silicon or titanium oxide as inorganic fillers: effect of morphology and mechanical properties on gas permeability, Polymer, 41 (2000) 5461-5470.

[51] W. X. Li, X. J. Zhang, W. H. Xing, W. Q. Jin, N. P. Xu, Hydrolysis of ethyl lactate coupled by vapor permeation using polydimethylsiloxane/ceramic composite membrane, Industrial & Engineering Chemistry Research, 49 (2010) 11244-11249.

[52] F. J. Xiangli, Y. W. Chen, W. Q. Jin, N. P. Xu, Polydimethylsiloxane (PDMS)/ceramic composite membrane with high flux for pervaporation of ethanol-water mixtures, Industrial & Engineering Chemistry Research, 46 (2007) 2224-2230.

[53] S. Kulprathipanja, R. W. Neuzil, N. N. Li, Separation of fluids by means of mixed matrix membranes, US Patent 4740219, (1988).

[54] T. S. Chung, L. Y. Jiang, Y. Li, S. Kulprathipanja, Mixed matrix membranes (MMMs) comprising organic polymers with dispersed inorganic fillers for gas separation, Progress in Polymer Science, 32 (2007) 483-507.

[55] J. L. C. Rowsell, O. M. Yaghi, Metal-organic frameworks: A new class of porous materials, Microporous and Mesoporous Materials, 73 (2004) 3-14.

[56] Y. Hu, X. Dong, J. Nan, W. Jin, X. Ren, N. Xu, Y. M. Lee, Metal-organic framework membranes fabricated via reactive seeding, Chemical Communications, 47 (2011) 737-739.

[57] K. S. Park, Z. Ni, A. P. Côté, J. Y. Choi, R. Huang, F. J. Uribe-Romo, H. K. Chae, M. O'Keeffe, O. M. Yaghi, Exceptional chemical and thermal stability of

zeolitic imidazolate frameworks, Proceedings of the National Academy of Sciences of the United States of America, 103 (2006) 10186-10191.

[58] M. C. McCarthy, V. Varela-Guerrero, G. V. Barnett, H. K. Jeong, Synthesis of zeolitic imidazolate framework films and membranes with controlled microstructures, Langmuir, 26 (2010) 14636-14641.

[59] Y. S. Li, F. Y. Liang, H. Bux, A. Feldhoff, W. S. Yang, J. Caro, Molecular sieve membrane: Supported metal-organic framework with high hydrogen selectivity, Angewandte Chemie - International Edition, 49 (2010) 548-551.

[60] A. Huang, H. Bux, F. Steinbach, J. Caro, Molecular-sieve membrane with hydrogen permselectivity: ZIF-22 in LTA topology prepared with 3-aminopropyltriethoxysilane as covalent linker, Angewandte Chemie - International Edition, 49 (2010) 4958-4961.

[61] A. S. Huang, W. Dou, J. Caro, Steam-stable zeolitic imidazolate framework ZIF-90 membrane with hydrogen selectivity through covalent functionalization, Journal of the American Chemical Society, 132 (2010) 15562-15564.

[62] H. Bux, C. Chmelik, J. M. Van Baten, R. Krishna, J. Caro, Novel MOF-membrane for molecular sieving predicted by IR-diffusion studies and molecular modeling, Advanced Materials, 22 (2010) 4741-4743.

[63] Y. S. Li, F. Y. Liang, H. G. Bux, W. S. Yang, J. Caro, Zeolitic imidazolate framework ZIF-7 based molecular sieve membrane for hydrogen separation, Journal of Membrane Science, 354 (2010) 48-54.

[64] E. V. Perez, K. J. Balkus Jr, J. P. Ferraris, I. H. Musselman, Mixed-matrix membranes containing MOF-5 for gas separations, Journal of Membrane Science, 328 (2009) 165-173.

[65] M. J. C. Ordoñez, K. J. Balkus, J. P. Ferraris, I. H. Musselman, Molecular sieving realized with ZIF-8/Matrimid® mixed-matrix membranes, Journal of Membrane Science, 361 (2010) 28-37.

[66] C. Courteille, C. Hollenstein, J. L. Dorier, P. Gay, W. Schwarzenbach, A. A. Howling, E. Bertran, G. Viera, R. Martins, A. Macarico, Particle agglomeration study in rf silane plasmas: In situ study by polarization-sensitive laser light scattering, Journal of Applied Physics, 80 (1996) 2069-2078.

[67] J. Cravillon, S. Münzer, S. J. Lohmeier, A. Feldhoff, K. Huber, M. Wiebcke, Rapid room-temperature synthesis and characterization of nanocrystals of a prototypical zeolitic imidazolate framework, Chemistry of Materials, 21 (2009) 1410-1412.

[68] Y. Li, W. B. Krantz, T. S. Chung, A novel primer to prevent nanoparticle agglomeration in mixed matrix membranes, AICHE Journal, 53 (2007) 2470-2475.

[69] Z. H. Chang, H. T. Pu, D. C. Wan, L. Liu, J. J. Yuan, Z. L. Yang, chemical oxidative degradation of polybenzimidazole in simulated environment of fuel cells, Polymer Degradation and Stability, 94 (2009) 1206-1212.

[70] M. Jaffe, M. I. Haider, J. Menczel, J. Rafalko, Thermal characterization of high-performance PBI and 6F polymers and their alloys, Polymer Engineering and Science, 32 (1992) 1236-1241.

[71] M. Jaffe, P. Chen, E. W. Choe, T. S. Chung, S. Makhija, High-performance polymer blends, in Advances in Polymer Science, Vol. 117 (Ed: P. Hergenroth), Springer Verlag, N.Y. (1994) pp. 297-329.

[72] Y. Yampolskii, V. Shantarovich, Positron annihilation lifetime spectroscopy and other methods for free volume evaluation in polymers, in: Y. Yampolskii, I.

Pinnau, B. D. Freeman (Eds.) Materials science of membranes for gas and vapor separation, John Wiley & Sons, Ltd., England, (2006) pp. 191-210.

[73] G. Dlubek, J. Pionteck, V. Bondarenko, G. Pompe, C. Taesler, K. Petters, R. Krause-Rehberg, Positron annihilation lifetime spectroscopy (PALS) for interdiffusion studies in disperse blends of compatible polymers: A quantitative analysis, Macromolecules, 35 (2002) 6313-6323.

[74] H. M. Chen, W. S. Hung, C. H. Lo, S. H. Huang, M. L. Cheng, G. Liu, K. R. Lee, J. Y. Lai, Y. M. Sun, C. C. Hu, R. Suzuki, T. Ohdaira, N. Oshima, Y. C. Jean, Free-volume depth profile of polymeric membranes studied by positron annihilation spectroscopy: Layer structure from interfacial polymerization, Macromolecules, 40 (2007) 7542-7557.

[75] B. S. Jorgensen, J. S. Young, B. F. Espinoza, Cross-linked polybenzimidazole membrane for gas separation, US patent 6946015 (2006).

[76] L. M. Robeson, The upper bound revisited, Journal of Membrane Science, 320 (2008) 390-400.

CHAPTER 5

ZIF-8/PBI NANO-COMPOSITE MEMBRANES FOR HIGH TEMPERATURE HYDROGEN PURIFICATION CONSISTING OF CARBON MONOXIDE AND WATER VAPOR

This chapter is published as a journal paper

Tingxu Yang, Tai Shung Chung, High performance ZIF-8/PBI nano-composite membranes for high temperature hydrogen separation consisting of carbon monoxide and water vapor, International Journal of Hydrogen Energy (2012) DOI: 10.1016/j.ijhydene.2012.10.045.

5.1 Introduction

Hydrogen production is a large and an emerging industry. The economic value of hydrogen produced worldwide was around $135 billion in 2005 [1, 2]. Typically, a large portion of hydrogen is consumed to convert heavy crude oil into useable fuels via hydrocracking in the petroleum and chemical industries. Other major applications include ammonia production via Haber–Bosch process for fertilizer [3], food production (e.g., hydrogenation), metals treatment, and other purposes. Due to the growing global awareness of energy security and sustainability, hydrogen has attracted much industrial attention as an effective and green energy carrier [4].

To date, commercially available hydrogen is mainly produced from steam reforming followed by the water-gas shift reaction using fossil fuels such as natural gas, oil, or coal as the reactor feed [5, 6]. CO_2 is the main by-product of this process and needs to be captured in order to produce high purity hydrogen as well as reduce the green house effect. Conventional technologies for CO_2 capture include cold absorption, amine-based absorption, pressure-swing adsorption and cryogenic distillation. Recently, membrane technology has shown great promising for H_2/CO_2 separation with advantages of low energy consumption, small footprint and easy operation over conventional ones [7-9]. In addition, there are plenty of organic and inorganic materials available for membrane fabrication. Among them, polymers are the most practical and economical candidate not only at present but also in the foreseeable future [10]. Comparing with membranes made from inorganic materials, polymeric membranes made from organic materials are low-cost, easy fabrication, mechanically

flexible, which make them usable for fabricating large and defect-free membrane modules.

The gas permeation in polymeric membranes is controlled by the solution-diffusion mechanism [11] in which gas pair selectivity is the product of diffusion selectivity and solubility selectivity. The diffusion selectivity favors the transport of smaller gas molecules such as H_2 (kinetic diameter: 2.89Å) over larger ones such as CO_2 (kinetic diameter: 3.30 Å), while the solubility selectivity favors the sorption of more condensable gases such as CO_2 (critical temperature: 304K) over the less condensable gases such as H_2 (critical temperature: 33K). Since the diffusion selectivity and solubility selectivity show opposite preference for H_2 and CO_2 transports, the separation of H_2 and CO_2 mixture by polymeric membranes is complicated and challenging as compared with other gas pairs. Generally, rubbery materials are CO_2-selective while glassy materials are H_2-selective. A significant number of rubbery membranes with good CO_2/H_2 separation performance have been developed in recent years [12-18]. However, rubbery membranes show declining CO_2/H_2 selectivity at high temperatures and low stability under high operating pressures. Therefore, these membranes are unsuitable for industrial applications where harsh and extreme conditions are operated.

Conversely, H_2-selective membranes are often made from glassy polymers and the H_2/CO_2 diffusion selectivity dominates the overall permeation selectivity. Several methods, such as new polymer designs, mixed matrix membranes, polymer blending, doping, and post-modifications (e.g., chemical cross-linking), have been proposed to enhance the performance of H_2-selective membranes [6, 19]. Some chemically cross-

linked membranes showed significantly improved H_2/CO_2 selectivity and resistance to CO_2-induced plasticization [20-27]. However, their hydrothermal stability needs improvement in order to expand their applications in high temperature and humid environments.

For syngas separation, an ideal H_2-selective membrane should possess the following features: 1) It can operate continuously at elevated temperatures (around 200 ℃) and directly separate the production stream from the low-temperature water-gas shift reactor, thus eliminating the additional processes and cost to cool the syngas and remove a large amount of water; 2) It can also effectively remove impurities such as CO, N_2 and CH_4 from the feed stream; and 3) It is able to withstand high pressures from the feed gas stream [7]. Compared to other polymers, polybenzimidazole (PBI) is a promising material to meet the aforementioned requirements because it possesses remarkable thermal stability, good chemical resistance, impressive compression strength, and high intrinsic H_2/CO_2 selectivity. However, the major drawbacks of PBI are (1) low H_2 permeability and (2) brittleness [28]. The former is resulted from the inherent characteristics of rigid polymeric backbone and high degree of chain packing, while the latter makes impossible in fabricating ultrathin PBI membranes. Several approaches have been taken to overcome the these bottlenecks such as polymer blending [29], replacing PBI acid moiety [30], chemical cross-linking [31], thermally rearranging of precursor polymer [32], N-substitution modification [33], and incorporating with inorganic particles [34, 35]. Among them, increasing PBI gas permeability by incorporating high free volume nano-particles appears promising.

Zeolitic imidazolate frameworks (ZIFs) are a subfamily of metal-organic frameworks (MOFs) which refer to a group of crystalline transition metal complexes with one-, two-, or three-dimensional nano-porous networks. In addition to typical properties of MOFs such as high porosity, tailorable cavity sizes and good affinity with organic polymers, ZIFs also have characteristics of exceptional thermal stability and outstanding chemical resistance. Many studies have reported the encouraging gas separation performance of crystalline ZIF membranes grown on inorganic supports for various gas pairs such as H_2/CO_2 [36-38], CO_2/CH_4 [39], CO_2/CO [40], and C2/C3 hydrocarbons [41]. However, similar to inorganic membranes, disadvantages such as high fabrication cost, mechanical brittleness, and difficulties to prepare robust and large-scale membrane modules have deterred the commercial uses of ZIF membranes. To circumvent these weaknesses, one practical way is to utilize ZIFs by incorporating their nano-particles into organic polymers and synergistically combine the merits of both materials. This material design strategy has been demonstrated and novel ZIFs/PBI nano-composite materials for H_2/CO_2 separation have been invented [35, 42]. The best ZIFs/PBI dense membrane had a H_2 permeability of 105.4 Barrer and a H_2/CO_2 selectivity of 12.3 at 35 °C [42]. Even though this performance is far superior to other polymer systems, it is still far below from metallic and inorganic membranes.

Therefore, the purposes of this work are to investigate the science and engineering on how to molecularly design the ZIF-8/PBI nano-composite material with much superior separation performance for hydrogen purification at high temperatures. We aim to double the H_2/CO_2 selectivity and H_2 permeability in order to develop market viable H_2–selective membranes. Since most CO_2-selective membranes show better CO_2/H_2 selectivity at low temperatures [43-49], while most H_2-selecive membranes

exhibit better H_2/CO_2 selectivity at high temperatures [50-54] possibly because of opposite variations of H_2/CO_2 diffusion selectivity and solubility selectivity with temperature, this makes our aim possible if the separation takes place at high temperatures. In addition, conventional syngas is produced with many byproducts as impurities. They must be removed simultaneously with CO_2 at elevated temperatures. As a consequence, besides investigating the temperature-dependent separation performance, we will examine the effects of impurities such as CO and H_2O vapor on the newly developed membrane. So far, there are many reports on the effects of CO [55, 56], water [55, 57], H_2S [58], NO [56], ethane [59] and toluene [60] on CO_2/CH_4 and CO_2/N_2 separations, and CO on CO_2/H_2 separation [61], but almost no studies were focused on the influences of CO and H_2O vapor to high temperature H_2/CO_2 separation. Therefore, advanced characterizations and measurements will be carried out to study membrane morphology, permeation mechanism, and performance evolution at high temperatures in the presence of impurities.

5.2 Results and discussion

5.2.1 Characterizations

To eliminate the effect of absorbed water and gas in the membranes, the starting point of all the thermogravimetric curves is set at 200 ℃ (Figure 5.1). It is very clear that all the membranes show good thermal stability up to 500 ℃ in air. From the ash content remained at 800 ℃, the actual weight loadings of ZIF-8 nano-particles are determined as 31.1 wt% in the 30/70 (w/w) ZIF-8/PBI membrane and 56.1 wt% in the 60/40 (w/w) ZIF-8/PBI membrane, respectively (Table 5.1). Since the density of PBI

is 1.30g/cm^3 [30] and the density of ZIF-8 is 0.95g/cm^3 based on the theoretical density of the framework without guest molecules [62], the 30/70 (w/w) ZIF-8/PBI and 60/40 (w/w) ZIF-8/PBI membranes are estimated to have 38.2 vol% and 63.6 vol% volume loadings of ZIF-8 nano-particles, respectively (Table 5.1). To the best of our knowledge, a ZIF-8 loading of 63.6 vol% in the 60/40 (w/w) ZIF-8/PBI membrane is the highest ever reported volume loading of nano-particles in mixed matrix membranes.

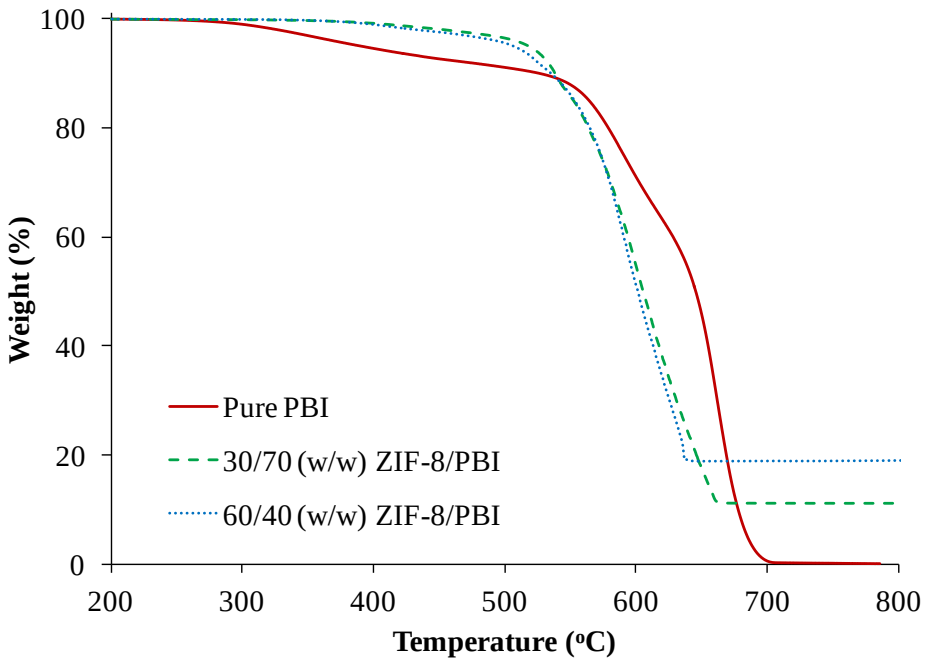

Figure 5.1 TGA thermograms of pure PBI and ZIF-8/PBI nano-composite membranes under air atmosphere

Table 5.1 ZIF-8 particle loadings of the nano-composite membranes determined from TGA

Sample ID	Ash content weight (%)	ZIF-8 weight (%)	ZIF-8 volume (%)
Pure PBI	0	0	0
30/70 (w/w) ZIF-8/PBI	11.1	31.1	38.2

60/40 (w/w) ZIF-8/PBI	20.0	56.1	63.6

It can be clearly seen from the FESEM images of the membrane cross-section in Figure 5.2 that ZIF-8 nano-particles are homogenously dispersed in the 30/70 (w/w) ZIF-8/PBI membrane. At a magnification of 20,000, neither inter-phase voids nor particle agglomeration can be observed in this membrane. A relatively non-uniform particle distribution is visible in the 60/40 (w/w) ZIF-8/PBI membrane which has a higher ZIF-8 loading possibly due to particle agglomeration [63]. A homogenously dispersed morphology is particularly important for fabricating defect-free asymmetric thin film composite membranes and hollow fibers because it can effectively use the function of each particle. Figure 5.3 reconfirms the uniform dispersion of ZIF-8 particles in the 30/70 (w/w) ZIF-8/PBI membrane by mappings C, N, and Zn elements with the aid of the energy-dispersive X-ray spectroscopy (EDX). Since zinc element only exists in ZIF-8 particles, the uniform distribution of the Zn element clearly verifies the uniform dispersion of ZIF-8 nano-particles in the PBI matrix.

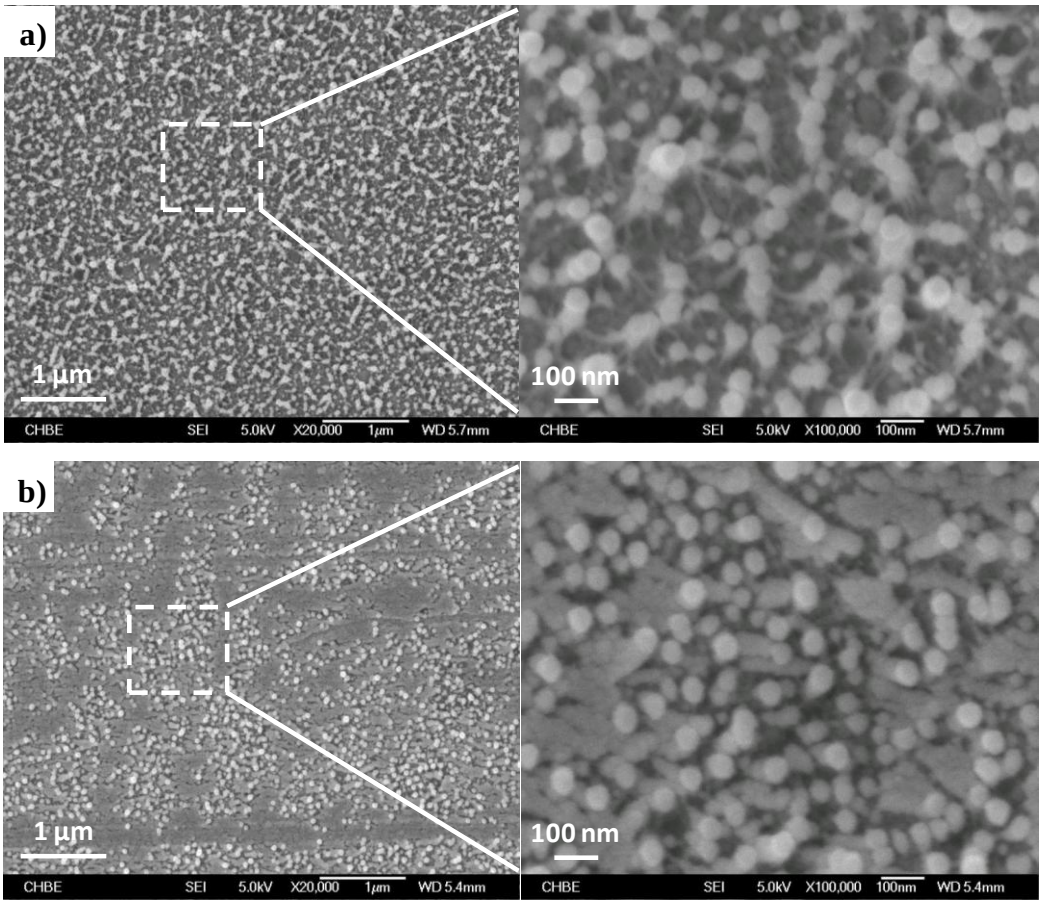

Figure 5.2 FESEM images from cross-section views of a) 30/70 (w/w) ZIF-8/PBI and b) 60/40 (w/w) ZIF-8/PBI membranes

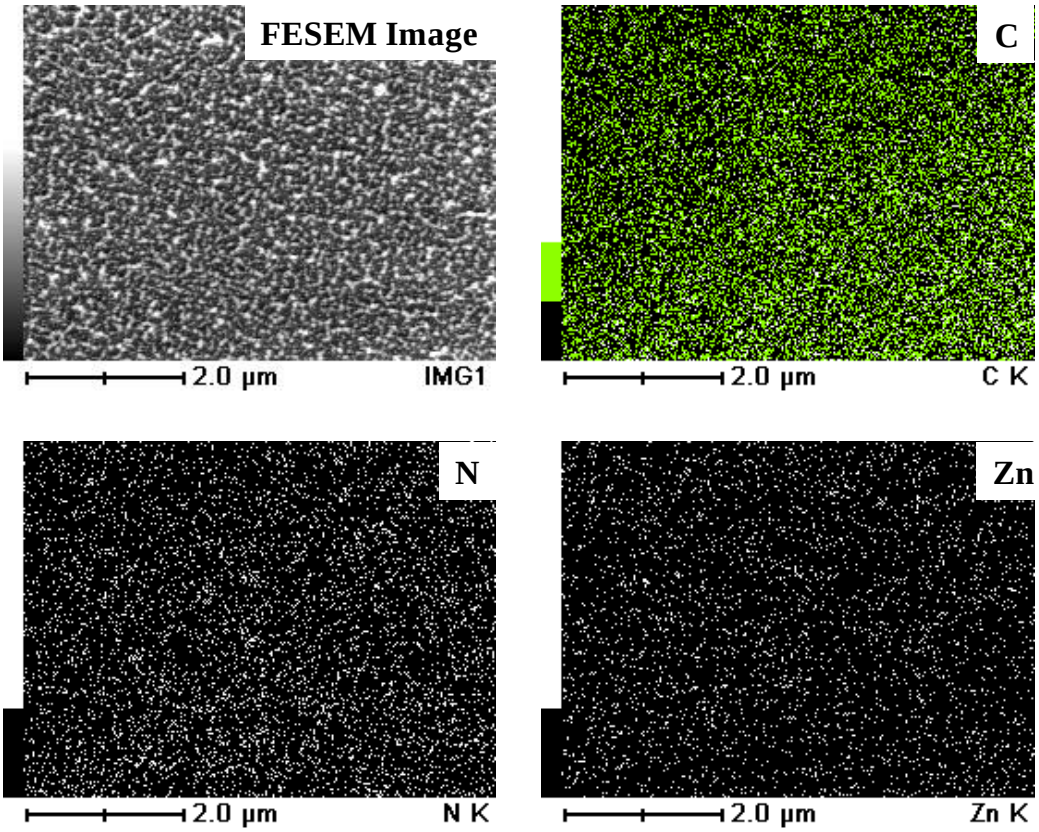

Figure 5.3 EDX element mappings for C, N and Zn from the cross-section of 30/70 (w/w) ZIF-8/PBI membrane

5.2.2 Pure gas transport properties at ambient temperature

Table 5.2 summarizes the single-gas permeability and ideal selectivity of ZIF-8/PBI nano-composite membranes for H_2 and CO_2 at 35 ℃ and 3.5 atm. These data are in good agreement with those membranes with similar ZIF-8 loadings reported previously [42]. The 30/70 (w/w) ZIF-8/PBI membrane shows a high H_2/CO_2 selectivity of 12.0 and a moderate H_2 permeability of 82.5 Barrer, while the 60/40 (w/w) ZIF-8/PBI membrane shows a lower H_2/CO_2 selectivity of 4.1 with a superior H_2 permeability of 1612.8 Barrer. Since the 60/40 (w/w) ZIF-8/PBI membrane shows a comparable H_2/CO_2 selectivity to that of the ZIF-8 crystalline membrane whose H_2/CO_2 selectivity is 4.5 [64], this indicates that ZIF-8 nano-particles are the major

gas transportation channels in this nano-composite membrane. In other words, intercalation may occur in this high particle loaded membrane [42] because the polymer phase cannot fully seal all the nano-particles. As a result, gas transports take place directly among closely connected ZIF-8 nano-particles and exhibit gas transportation properties very similar to ZIF-8 crystals. This phenomenon is in consistent with our observation from FESEM images as shown in Figure 5.2.

Table 5.2 Pure and mixed gas separation performances of pure PBI and ZIF-8/PBI nano-composite membranes at 35 ℃

Sample ID	Permeability[a] (Barrer[b])		Selectivity (H_2/CO_2)	Mixed gas Permeability (Barrer)		Mixed gas Selectivity (H_2/CO_2)
	H_2	CO_2		H_2	CO_2	
Pure PBI	4.1	0.46	8.9	2.9	0.41	7.1
30/70 (w/w) ZIF-8/PBI	82.5	6.9	12.0	39.0	5.7	6.8
60/40 (w/w) ZIF-8/PBI	1612.8	397.6	4.1	669.9	238.0	2.8

[a] Single gas tests were performed in 3.5 atm, at 35 ℃.
[b] 1 Barrer = 1×10^{-10} cm^3(STP)cm /(cm^2 s cmHg).
[c] Mixed gas tests were performed in 2 atm with 50 mol% H_2 and 50 mol% CO_2, at 35 ℃.

Due to competitive sorption between highly condensable CO_2 (critical temperature: 304K) and less condensable H_2 (critical temperature: 33K) [35, 42, 61], the mixed gas data in terms of H_2 permeability and H_2/CO_2 selectivity are lower than those of pure gas tests, as shown in Table 5.2. To further explore the contributions of solubility and diffusivity on the overall permeability, CO_2 sorption tests were conducted on pure PBI and ZIF-8/PBI nano-composite membranes. Figure 5.4 illustrates the sorption curves, while Table 5.3 shows the calculated transportation coefficients (i.e., P, S and D). Compared with PBI, membranes comprising ZIF-8 nano-particles show

significantly increased CO_2 solubility due to the high porosity and strong CO_2 adsorption in ZIF-8 cavities. On the other hand, tens and hundreds times of increment are achieved in diffusion coefficients when adding ZIF-8 nano-particles into PBI membranes. These results indicate that both solubility and diffusivity are significantly enhanced with the addition of ZIF-8 particles, and a higher ZIF-8 loading results in a much higher increment in diffusivity.

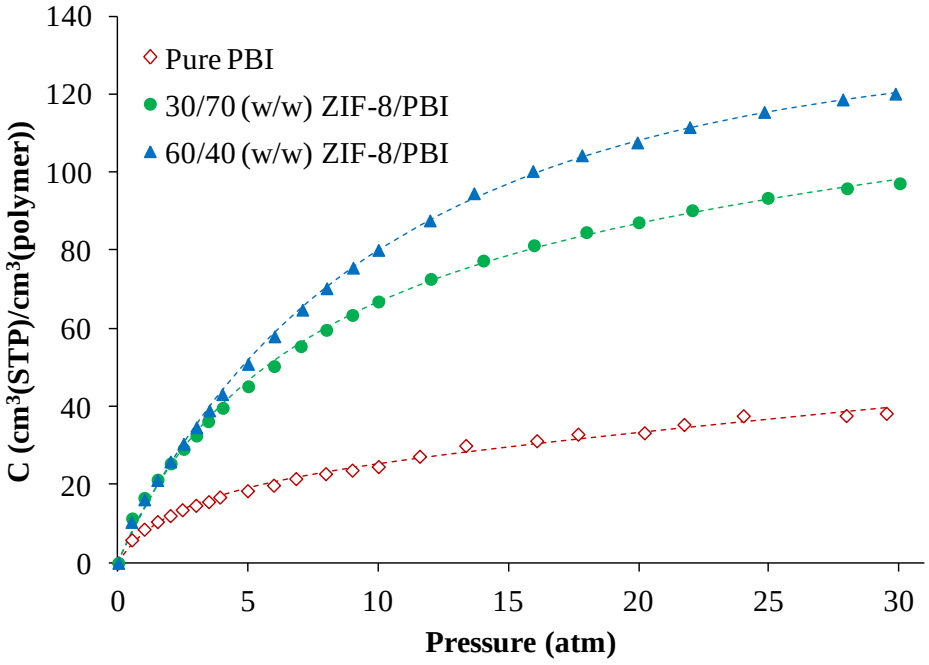

Figure 5.4 CO_2 sorption isotherms of pure PBI and ZIF-8/PBI nano-composite membranes

Table 5.3 P, D and S coefficents of CO_2 in pure PBI and ZIF-8/PBI nano-composite membranes at 35 ℃ in 3.5 atm

Sample ID	Permeability (Barrer), *P*	Solubility (cm^3 (STP)/cm^3 atm), *S*	Diffusivity ($\times 10^{-8}$ cm^2/s), *D*
Pure PBI	0.46	4.65	0.0753
30/70 (w/w) ZIF-8/PBI	6.9	10.36	0.506

60/40 (w/w) ZIF-8/PBI	397.6	11.14	27.1

5.2.3 Membrane performance at high temperature mixed gas tests

To evaluate the gas separation performance of the ZIF-8/PBI membranes at temperatures similar to industrial applications, mixed gas permeation tests were conducted at 35-230 ℃ with a 50/50 (mol/mol) H_2/CO_2 gas mixture as the feed stream. Figure 5.5 presents the H_2/CO_2 separation performance of 30/70 (w/w) ZIF-8/PBI and 60/40 (w/w) ZIF-8/PBI membranes at different temperatures. Obviously, both membranes show increased H_2/CO_2 selectivity with increasing test temperature. To our best knowledge, the 30/70 (w/w) ZIF-8/PBI membrane has the highest ever reported H_2/CO_2 selectivity of 26.3 in those polymer membranes with permeability of around 470 Barrer at 230 °C, while the 60/40 (w/w) ZIF-8/PBI membranes the highest ever reported H_2 permeability of 2015 Barrer in those polymer membranes with H_2/CO_2 selectivity of around 12.3 at 230 °C. This unique performance arises from the synergistic combination of (1) a substantial increase in H_2/CO_2 solubility selectivity due to a significant drop in CO_2 sorption in ZIF-8 nano-particles at elevated temperatures and (2) a minor drop in H_2/CO_2 diffusivity selectivity due to the relatively rigid backbone and high thermal stability of the PBI polymer.

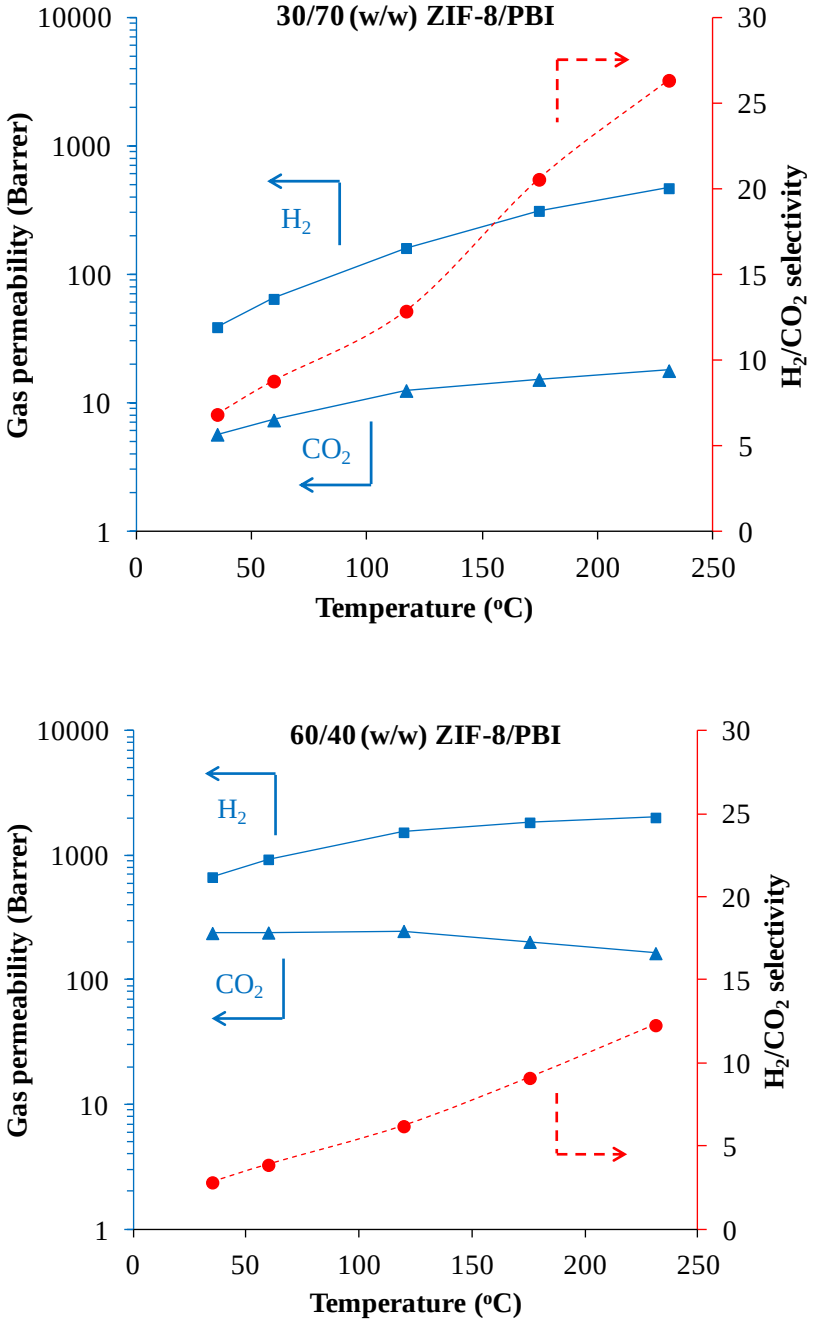

Figure 5.5 H_2/CO_2 mixed gas permeation results of ZIF-8/PBI nano-composite membranes
(Solid lines: H_2 and CO_2 permeability; dotted lines: H_2/CO_2 selectivity)

The permeation of H_2 or CO_2 through ZIF-8/PBI membranes is a thermally activated process; therefore, the permeability of each gas can be correlated with the temperature

through the Van't Hoff-Arrhenius equation [65]:

$$P = P_0 \exp\left(\frac{-E_p}{RT}\right) \tag{5-1}$$

where P is the gas permeability, P_0 is the pre-exponential coefficients, E_P is the apparent activation energy for the permeation process, R is the gas constant, and T is the absolute temperature. Figure 5.6 shows straight lines by fitting H_2 and CO_2 permeation data as a function of temperature using the Van't Hoff equation. The activation energies (E_p) for H_2 and CO_2 permeation across the 30/70 (w/w) ZIF-8/PBI membrane are 15.5 and 5.1 kJ/mol, respectively. These values become 4.0 and -5.8 kJ/mol, respectively, for the 60/40 (w/w) ZIF-8/PBI membrane. Clearly, the apparent activation energy drops significantly with increasing ZIF-8 loading, indicating a drastic reduction in the energy barrier for permeation with more ZIF-8 particles incorporated inside the membranes.

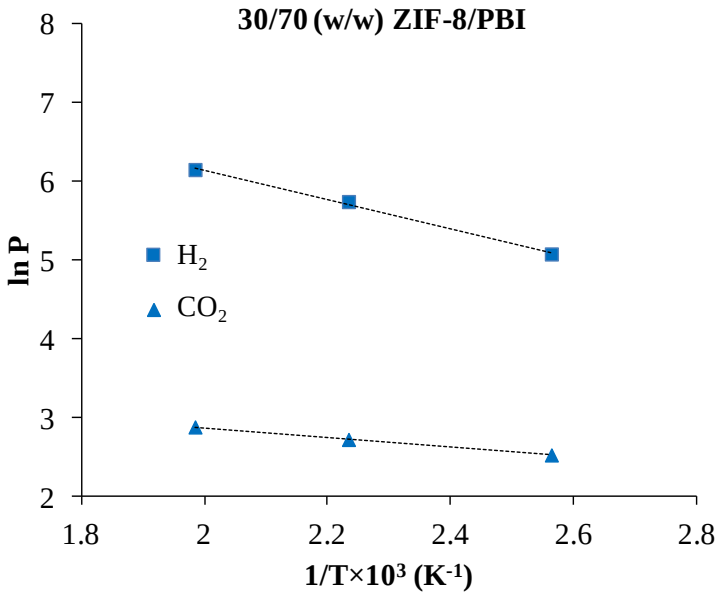

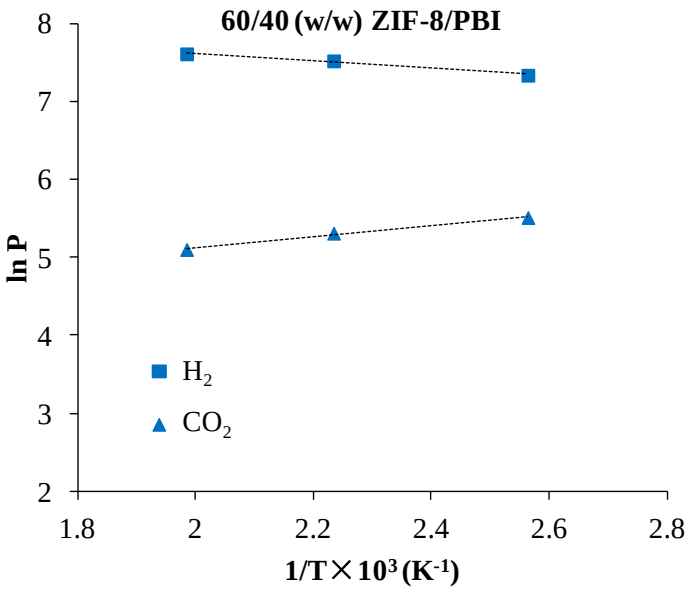

Figure 5.6 Temperature dependence on gas permeability (P) in ZIF-8/PBI nano-composite membranes

Since gas transport through membrane materials generally follows the solution-diffusion model, the activation energy for the permeation can be expressed as:

$$E_p = E_D + \Delta H_S \qquad (5\text{-}2)$$

where E_D is the activation energy of diffusion and is always positive, while ΔH_S is the enthalpy of sorption and is usually negative. Whether E_p is positive or negative depends on the relative value of E_D and ΔH_S. For the 30/70 (w/w) ZIF-8/PBI membrane, the values of E_p for H_2 and CO_2 are all positive, indicating an obvious diffusion sieving effect similar to that of pure PBI polymer. For the 60/40 (w/w) ZIF-8/PBI membrane with a much higher ZIF-8 volume fraction, however, the values of E_p for both H_2 and CO_2 drop significantly, i.e., being close to or even below zero. This great transformation might be resulted from the decreased energy barrier for diffusion and increased ΔH_S with higher ZIF-8 loadings in the membrane.

Figure 5.7 compares pure gas and mixed gas permeation results with the latest Robeson upper bound [66] for the H_2/CO_2 gas pair. The ideal H_2/CO_2 separation performance of both 30/70 (w/w) ZIF-8/PBI and 60/40 (w/w) ZIF-8/PBI membranes at 35 ℃ has surpassed the upper bound. Encouragingly, both membranes also show much enhanced mixed gas separation performance at 230 ℃ that is far beyond the upper bound.

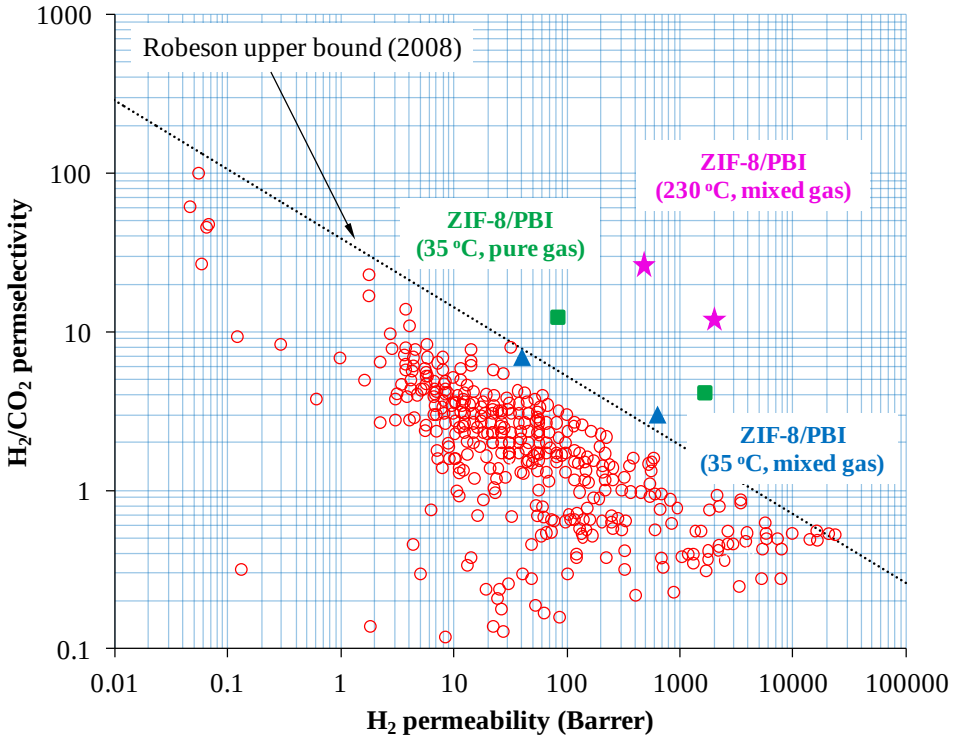

Figure 5.7 H_2/CO_2 separation performance of ZIF-8/PBI nano-composite membranes compared to the Robeson upper bound
(Square marks: 35 ℃, pure gas; triangle marks: 35 ℃, mixed gas; star marks: 230 ℃, mixed gas.)

5.2.4 Effects of CO and water vapor on mixed gas separation performance

To examine the influence of a trace amount of CO on H_2/CO_2 separation performance, mixed gas tests with a tertiary gas mixture containing 49.5 mol% H_2, 49.5 mol% CO_2

and 1 mol% CO were performed. A CO fraction of 1 mol% was chosen because this is a typical concentration of CO in the syngas stream discharged from the water-gas shift reactor. Figure 5.8 compares the H_2/CO_2 mixed gas separation performance with and without the presence of CO from ambient to high temperatures. For the 30/70 (w/w) ZIF-8/PBI membrane, the presence of 1 mol% CO in the feed stream almost does not affect the CO_2 permeability but results in a slight reduction in the H_2 permeability. The latter may account for the slightly decreased H_2/CO_2 selectivity. However, both H_2 and CO_2 permeabilities decrease for the 60/40 (w/w) ZIF-8/PBI membrane while the change in the CO_2 permeability is more significant. Therefore, the observed H_2/CO_2 selectivity does not decline but goes up. This trend is quite different from the observation from the 30/70 (w/w) ZIF-8/PBI membrane probably due to (1) the competitive sorption of gas molecules inside the membrane matrix and (2) the CO induced pore blocking effect [67]. CO has a kinetic diameter of 3.76 Å and is the largest gas component in these 3 gases, while ZIF-8 cavities have very small connection windows (i.e., 3.4 Å in diameter) for gas molecules to pass through. As a result, the presence of CO in the mixed gas feed stream might affect both the activation energy of diffusion (E_D) and the enthalpy of sorption (ΔH_S) for H_2 and CO_2 but in varying degrees at different ZIF-8 loadings. Further studies will focus on the solution and diffusion behavior of H_2, CO_2 and CO in the membranes at different temperatures to elucidate this interesting phenomenon.

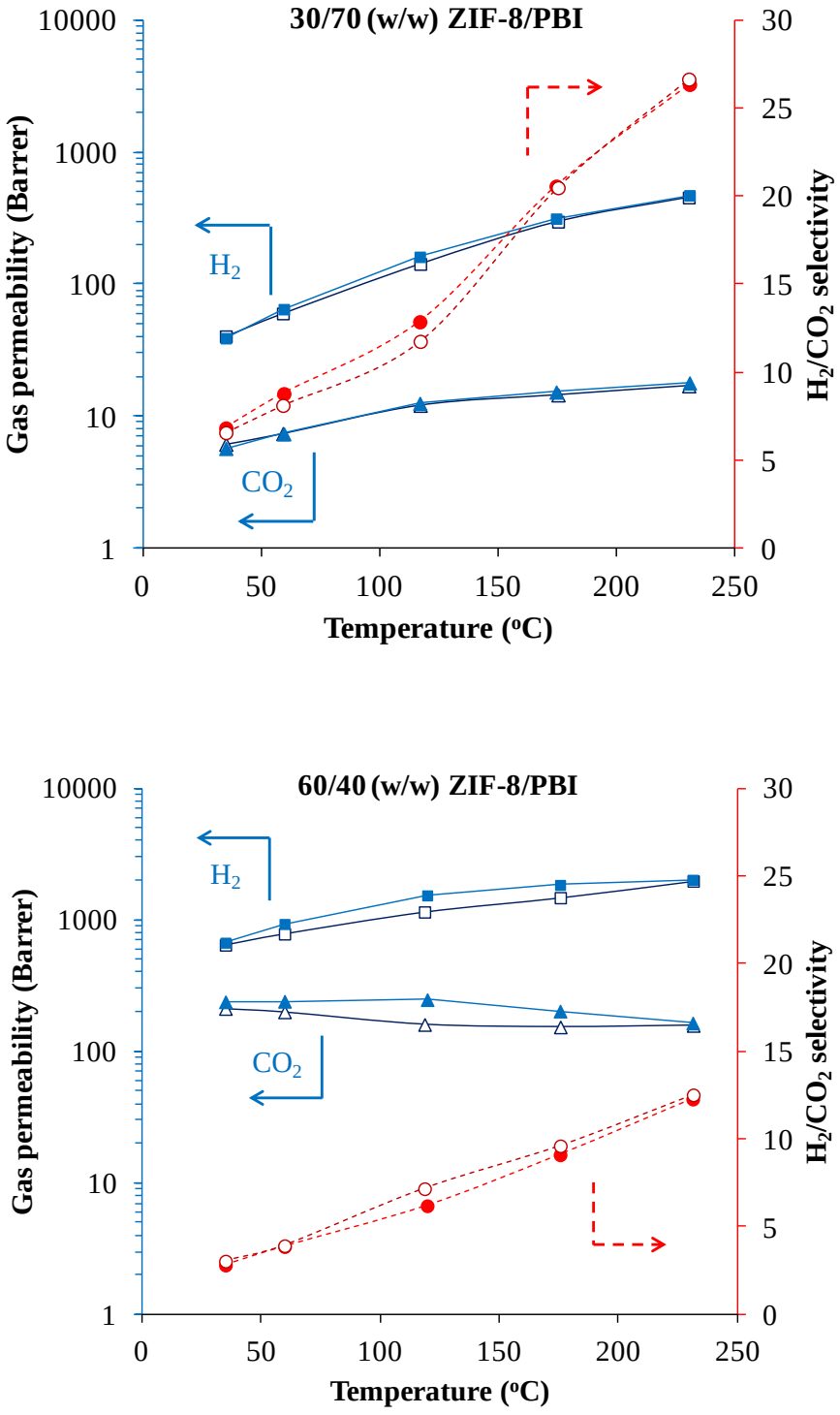

Figure 5.8 Effect of CO on H_2/CO_2 mixed gas separation performance (Solid symbols: without CO; Hollow symbols: with 1.0 mol % CO.)

Water vapor is another major impurity in the syngas stream. By varying water vapor content in H_2/CO_2 mixed gases up to about 11 mol% which is similar to the typical water vapor content in syngas streams, Figure 5.9 shows the separation performance of both 30/70 (w/w) ZIF-8/PBI and 60/40 (w/w) ZIF-8/PBI membranes conducted at 230 ℃. For both membranes, the addition of water vapor in the feed gas stream does not significantly change the H_2 and CO_2 permeabilities as well as the H_2/CO_2 selectivity. This remarkable performance stability may arise from three factors: (1) the ZIF-8/PBI nano-composite material has super thermal stability in hot steams, (2) the high temperature (i.e., 230 ℃) limits water condensation in the membranes, and (3) water has the smallest kinetic diameter compared to both H_2 and CO_2. Therefore, water induced sorption competition and pore block are minimized.

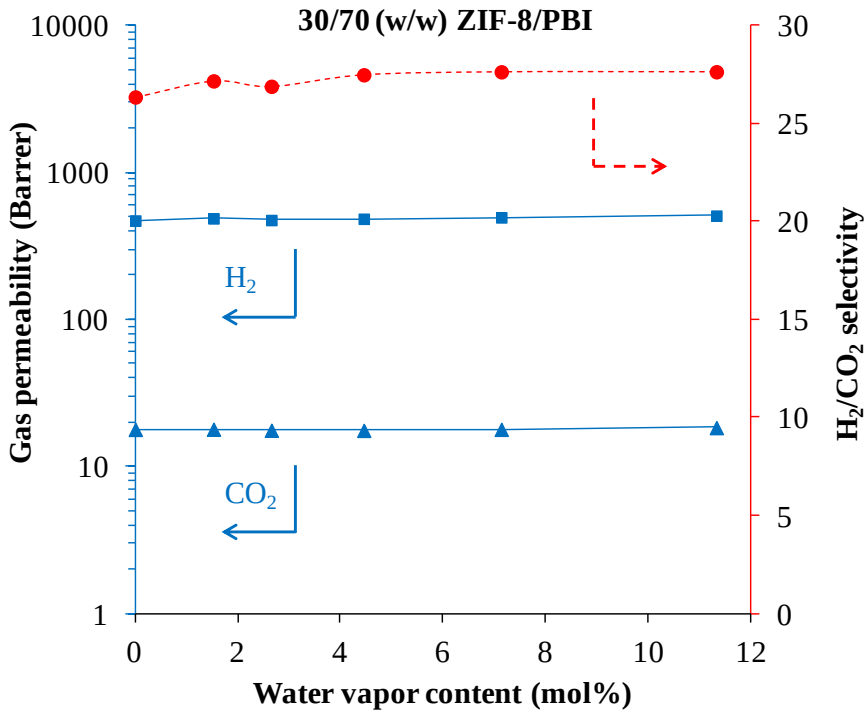

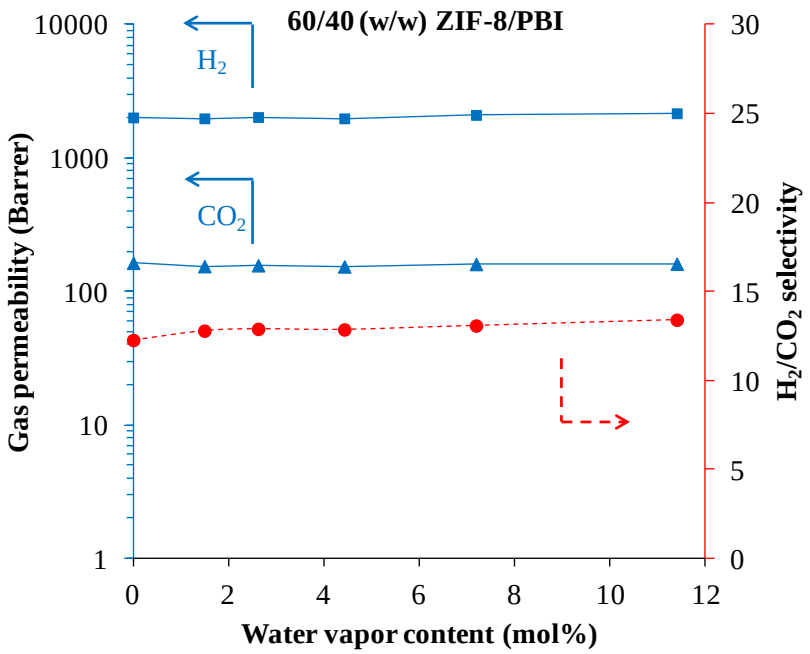

Figure 5.9 Effect of water vapor content on H_2/CO_2 mixed gas separation performance

5.3 Conclusions

In this work, we have reported the separation performance of ZIF-8/PBI nano-composite materials for hydrogen purification from 35 to 230 ℃. Detailed investigations were carried out in the aspects of material characterizations, gas permeation mechanism, as well as performance evolution using feed streams containing CO or water impurities. The following conclusions can be made from this study:

(1) The ZIF-8/PBI nano-composite material possesses high thermal and separation stability under elevated temperatures and hot steams in a testing duration of 10

days. A long term evaluation is required to further verify its stability under industrial conditions.

(2) Based on FESEM and EDX observation, ZIF-8 nano-particles are homogeneously dispersed in the 30/70 (w/w) ZIF-8/PBI membrane but non-uniformly dispersed in the 60/40 (w/w) ZIF-8/PBI membrane. Gas permeation results suggest that intercalation occurs when the ZIF-8 loading reaches 63.6 vol %.

(3) The incorporation of ZIF-8 particles in PBI-based membranes promotes both solubility and diffusion coefficients, thus enhancing the overall gas permeability. However, the degree of enhancement is much higher for diffusion than for solubility.

(4) The ZIF-8/PBI nano-composite membranes perform impressively in terms of H_2 permeability and H_2/CO_2 selectivity at elevated operation temperatures. Both pure gas and mixed gas permeation results at 230 °C have surpassed the latest Robeson upper bound.

(5) Impurities such as CO and water vapor existing in the model syngas stream have insignificant impact on the H_2/CO_2 separation performance.

In summary, the ZIF-8/PBI nano-composite membrane materials show very encouraging H_2/CO_2 separation performance and excellent stability at high temperatures. No significant degradation has been found by common impurities in syngas streams. Further studies are needed to understand the CO effect on sorption and convert this material into hollow fibers with a much thinner selective layer for industrial applications.

5.4 References

[1] T. Abbasi, S. A. Abbasi, 'Renewable' hydrogen: Prospects and challenges. Renewable & Sustainable Energy Reviews, 15 (2011) 3034-3040.

[2] http://reporter.leeds.ac.uk/press_releases/current/biodiesel.htm, last accessed on 04/08/2012.

[3] M. Appl, Ammonia, 1. Introduction. in: ed. B. Elvers, S. D. Kean, S. Hawkins, R. Harrer, M. Hammer-Altmann, N. Kirsch-Pietz, Ullmann's Encyclopedia of Industrial Chemistry, Wiley-VCH Verlag GmbH & Co. KGaA, Weinheim, (2012) pp.107-137.

[4] M. Momirlan, T. N. Veziroglu, The properties of hydrogen as fuel tomorrow in sustainable energy system for a cleaner planet, International Journal of Hydrogen Energy, 30 (2005) 795-802.

[5] N. W. Ockwig, T. M. Nenoff, Membranes for hydrogen separation, Chemical Reviews, 107 (2007) 4078-4110.

[6] L. Shao, B. T. Low, T. S. Chung, A. R. Greenberg, Polymeric membranes for the hydrogen economy: Contemporary approaches and prospects for the future, Journal of Membrane Science, 327 (2009) 18-31.

[7] T. C. Merkel, M. Zhou, R. W. Baker, Carbon dioxide capture with membranes at an IGCC power plant, Journal of Membrane Science, 389 (2012) 441-450.

[8] S. A. Stern, Polymers for gas separations: The next decade, Journal of Membrane Science, 94 (1994) 1-65.

[9] P. Bernardo, E. Drioli, G. Golemme, Membrane gas separation: A review/state of the art, Industrial & Engineering Chemistry Research, 48 (2009) 4638-4663.

[10] R. W. Baker, Future directions of membrane gas separation technology, Industrial & Engineering Chemistry Research, 41 (2002) 1393-1411.

[11] D. R. Paul, Y. P. Yampol'skii, Polymeric gas separation membranes, 1st ed., CRC Press, Boca Raton (1994).

[12] M. Kawakami, H. Iwanaga, Y. Hara, M. Iwamoto, S. Kagawa, Gas permeabilities of cellulose nitrate/poly(ethylene glycol) blend membranes, Journal of Applied Polymer Science, 27 (1982) 2387-2393.

[13] H. Lin, E. Van Wagner, B. D. Freeman, L. G. Toy, R. P. Gupta, Plasticization-enhanced hydrogen purification using polymeric membranes, Science, 311 (2006) 639-642.

[14] L. Shao, T. S. Chung, In situ fabrication of cross-linked PEO/silica reverse-selective membranes for hydrogen purification, International Journal of Hydrogen Energy, 34 (2009) 6492-6504.

[15] H. Chen, Y. C. Xiao, T. S. Chung, Synthesis and characterization of poly (ethylene oxide) containing copolyimides for hydrogen purification, Polymer, 51 (2010) 4077-4086.

[16] A. Car, C. Stropnik, W. Yave, K. -V. Peinemann, Pebax®/polyethylene glycol blend thin film composite membranes for CO_2 separation: Performance with mixed gases, Separation and Purification Technology, 62 (2008) 110-117.

[17] J. Z. Xia, S. L. Liu, C. H. Lau, T. S. Chung, Liquidlike poly(ethylene glycol) supported in the organic-inorganic matrix for CO_2 removal, Macromolecules, 44 (2011) 5268-5280.

[18] C. H. Lau, S. L. Liu, D. R. Paul, J. Z. Xia, Y. C. Jean, H. Chen, Silica nanohybrid membranes with high CO_2 affinity for green hydrogen purification, Advanced Energy Materials, 1 (2011) 634-642.

[19] L. Shao, J. Samseth, M. B. Hägg, Crosslinking and stabilization of nanoparticle filled PMP nanocomposite membranes for gas separations, Journal of Membrane Science, 326 (2009) 285-292.

[20] Y. Liu, R. Wang, T. S. Chung, Chemical cross-linking modification of polyimide membranes for gas separation, Journal of Membrane Science, 189 (2001) 231-239.

[21] J. D. Wind, C. Staudt-Bickel, D. R. Paul, W. J. Koros, Solid-state covalent cross-linking of polyimide membranes for carbon dioxide plasticization reduction, Macromolecules, 36 (2003) 1882-1888.

[22] C. H. Lau, B. T. Low, L. Shao, T. S. Chung, A vapor-phase surface modification method to enhance different types of hollow fiber membranes for industrial scale hydrogen separation, International Journal of Hydrogen Energy, 35 (2010) 8970-8982.

[23] B. T. Low, Y. C. Xiao, T. S. Chung, Y. Liu, Simultaneous occurrence of chemical grafting, cross-linking, and etching on the surface of polyimide membranes and their impact on H_2/CO_2 separation, Macromolecules, 41 (2008) 1297-1309.

[24] L. Shao, C. H. Lau, T. S. Chung, A novel strategy for surface modification of polyimide membranes by vapor-phase ethylenediamine (EDA) for hydrogen purification, International Journal of Hydrogen Energy, 34 (2009) 8716-8722.

[25] B. T. Low, T. S. Chung, H. Chen, Y. C. Jean, K. P. Pramoda, Tuning the free volume cavities of polyimide membranes via the construction of pseudo-interpenetrating networks for enhanced gas separation performance, Macromolecules, 42 (2009) 7042-7054.

[26] B. T. Low, Y. C. Xiao, T. S. Chung, Amplifying the molecular sieving capability of polyimide membranes via coupling of diamine networking and molecular architecture, Polymer, 50 (2009)3250-3258.

[27] C. E. Powell, X. J. Duthie, S. E. Kentish, G. G. Qiao, G. W. Stevens, Reversible diamine cross-linking of polyimide membranes, Journal of Membrane Science, 291 (2007) 199-209.

[28] T. S. Chung, A critical review of polybenzimidazoles: Historical development and future R&D, Journal of Macromolecular Science, Part C: Polymer Review, 37 (1997) 277-301.

[29] T. S. Chung, Z. L. Xu, Asymmetric hollow fiber membranes prepared from miscible polybenzimidazole and polyetherimide blends, Journal of Membrane Science, 147 (1998) 35-47.

[30] S. C. Kumbharkar, P. B. Karadkar, U. K Kharul, Enhancement of gas permeation properties of polybenzimidazoles by systematic structure architecture, Journal of Membrane Science, 286 (2006) 161-169.

[31] S. S.Hosseini, M. M. Teoh, T. S. Chung, Hydrogen separation and purification in membranes of miscible polymer blends with interpenetration networks, Polymer, 49 (2008) 1594-1603.

[32] S. H. Han, J. E. Lee, K. J. Lee, H. B. Park, Y. M. Lee, Highly gas permeable and microporous polybenzimidazole membrane by thermal rearrangement, Journal of Membrane Science, 357 (2010) 143-151.

[33] S. C. Kumbharkar, U. K. Kharul, Investigation of gas permeation properties of systematically modified polybenzimidazoles by N-substitution, Journal of Membrane Science, 357 (2010) 134-142.

[34] M. Sadeghi, M. A. Semsarzadeh, H. Moadel, Enhancement of the gas separation properties of polybenzimidazole (PBI) membrane by incorporation of silica nano particles, Journal of Membrane Science, 331 (2009) 21-30.

[35] T. Yang, Y. C. Xiao, T. S. Chung, Poly-/metal-benzimidazole nano-composite membranes for hydrogen purification, Energy & Environmental Science, 4 (2011) 4171-4180.

[36] Y. S. Li, F. Y. Liang, H. Bux, A. Feldhoff, W. S. Yang, J. Caro, Molecular sieve membrane: Supported metal-organic framework with high hydrogen selectivity, Angewandte Chemie-International Edition, 49 (2010) 548-551.

[37] A. Huang, H. Bux, F. Steinbach, J. Caro, Molecular-sieve membrane with hydrogen permselectivity: ZIF-22 in LTA topology prepared with 3-aminopropyltriethoxysilane as covalent linker, Angewandte Chemie-International Edition, 49 (2010) 4958-4961.

[38] A. Huang, W. Dou, J. Caro, Steam-stable zeolitic imidazolate framework ZIF-90 membrane with hydrogen selectivity through covalent functionalization. Journal of The American Chemical Society, 132 (2010) 15562-15564.

[39] S. R. Venna, M. A. Carreon, Highly permeable zeolite imidazolate framework-8 membranes for CO_2/CH_4 separation, Journal of The American Chemical Society, 132 (2010) 76-78.

[40] Y. Liu, E. Hu, E. A. Khan, Z. Lai, Synthesis and characterization of ZIF-69 membranes and separation for CO_2/CO mixture, Journal of Membrane Science, 353 (2010) 36-40.

[41] Y. Pan, Z. Lai, Sharp separation of C2/C3 hydrocarbon mixtures by zeolitic imidazolate framework-8 (ZIF-8) membranes synthesized in aqueous solutions, Chemical Communication, 47 (2011) 10275-10277.

[42] T. Yang, G. M. Shi, T. S. Chung, Symmetric and asymmetric zeolitic imidazolate frameworks (ZIFs)/polybenzimidazole (PBI) nano-composite membranes for hydrogen purification at high temperatures, Advanced Energy Materials, 2 (2012) 1358-1367.

[43] C. A. Scholes, J. Bacus, G. Q. Chen, W. X. Tao, G. Li, A. Qader, Pilot plant performance of rubbery polymeric membranes for carbon dioxide separation from syngas, Journal of Membrane Science, 389 (2012) 470-477.

[44] M. K. Barillas, R. M Enick, M. O'Brien, R. Perry, D. R. Luebke, B. D. Morreale, The CO_2 permeability and mixed gas CO_2/H_2 selectivity of membranes composed of CO_2-philic polymers, Journal of Membrane Science, 372 (2011) 29-39.

[45] H. Bai, W. S. W. Ho, New carbon dioxide-selective membranes based on sulfonated polybenzimidazole (SPBI) copolymer matrix for fuel cell applications, Industrial & Engineering Chemistry Research, 48 (2009) 2344-2354.

[46] J. A. de Sales, P. S. O. Patrício, J. C. Machado, G. G. Silva, D. Windmöller, Systematic investigation of the effects of temperature and pressure on gas transport through polyurethane/poly(methylmethacrylate) phase-separated blends, Journal of Membrane Science, 310 (2008) 129-140.

[47] T. Komatsuka, K. Nagai, Temperature dependence on gas permeability and permselectivity of poly(lactic acid) blend membranes, Polymer Journal, 41 (2009) 455-458.

[48] M. L. Chua, L. Shao, B. T. Low, Y. C. Xiao, T. S. Chung, Polyetheramine-polyhedral oligomeric silsesquioxane organic-inorganic hybrid membranes for CO_2/H_2 and CO_2/N_2 separation, Journal of Membrane Science, 385 (2011) 40-48.

[49] M. B. Hägg, R. Quinn, Polymeric facilitated transport membranes for hydrogen purification, MRS Bulletin, 31 (2006) 750-755.

[50] O. C. David, D. Gorri, A. Urtiaga, I. Ortiz, Mixed gas separation study for the hydrogen recovery from $H_2/CO/N_2/CO_2$ post combustion mixtures using a Matrimid membrane, Journal of Membrane Science, 378 (2011) 359-368.

[51] B. T. Low, N. Widjojo, T. S. Chung, Polyimide/polyethersulfone dual-layer hollow fiber membranes for hydrogen enrichment, Industrial & Engineering Chemistry Research, 49 (2010) 8778-8786.

[52] A. L. Khan, A. Cano-Odena, B. Gutiérrez, C. Minguillón, I. F. J. Vankelecom, Hydrogen separation and purification using polysulfone acrylate-zeolite mixed matrix membranes, Journal of Membrane Science, 350 (2010) 340-346.

[53] D. R. Pesiri, B. Jorgensen, R. C. Dye, Thermal optimization of polybenzimidazole meniscus membranes for the separation of hydrogen, methane, and carbon dioxide, Journal of Membrane Science, 218 (2003) 11-18.

[54] S. Choi, J. Coronas, Z. Lai, D. Yust, F. Onorato, M. Tsapatsis, Fabrication and gas separation properties of polybenzimidazole (PBI)/nanoporous silicates hybrid membranes, Journal of Membrane Science, 316 (2008) 145-152.

[55] L. Deng, M. B. Hägg, Swelling behavior and gas permeation performance of PVAm/PVA blend FSC membrane, Journal of Membrane Science, 363 (2010) 295-301.

[56] C. A. Scholes, G. Q. Chen, G. W. Stevens, S. E. Kentish, Nitric oxide and carbon monoxide permeation through glassy polymeric membranes for carbon dioxide separation, Chemical Engineering Research & Design, 89 (2011) 1730-1736.

[57] J. R. Pauls, D. Fritsch, T. Klassen, K. -V. Peinemann, Gas permeation measurement under defined humidity via constant volume/variable pressure method, Journal of Membrane Science, 389 (2012) 343-348.

[58] C. A. Scholes, G. W. Stevens, S. E. Kentish, Permeation through CO_2-selective glassy polymeric membranes in the presence of hydrogen sulfide, AIChE Journal, 58 (2012) 967-973.

[59] M. P. Chenar, H. Savoji, M. Soltanieh, T. Matsuura, S. Tabe, The effect of ethane on the performance of commercial polyphenylene oxide and cardo-type polyimide hollow fiber membranes in CO_2/CH_4 separation applications, Korean Journal of Chemical Engineering, 27 (2010) 1876-1881.

[60] J. K. Ward, W. J. Koros, Crosslinkable mixed matrix membranes with surface modified molecular sieves for natural gas purification: II. Performance characterization under contaminated feed conditions, Journal of Membrane Science, 377 (2011) 82-88.

[61] H. Z. Chen, T. S. Chung, CO_2-selective membranes for hydrogen purification and the effect of carbon monoxide (CO) on its gas separation performance. International Journal of Hydrogen Energy, 37 (2012) 6001-6011.

[62] J. C. Tan, T. D. Bennett, A. K. Cheetham, Chemical structure, network topology, and porosity effects on the mechanical properties of zeolitic imidazolate frameworks, Proceedings of the National Academy of Sciences of the United States of America, 107 (2010) 9938-9943.

[63] Y. Li, T. S. Chung, S. Kulprathipanja. Novel Ag^+-zeolite/polymer mixed matrix membranes with a high CO_2/CH_4 selectivity, AIChE Journal, 53 (2007) 610-616.

[64] H. Bux, F. Liang, Y. Li, J. Cravillon, M. Wiebcke, J. Caro, Zeolitic imidazolate framework membrane with molecular sieving properties by microwave-assisted

solvothermal synthesis, Journal of the American Chemical Society, 131 (2009) 16000-16001.

[65] Y. Yampolskii, I. Pinnau, B. D. Freeman, Materials Science of Membranes for Gas and Vapor Separation, John Wiley & Sons, Ltd., Chichester (2006).

[66] L. M. Robeson, The upper bound revisited, Journal of Membrane Science, 320 (2008) 390-400.

[67] C. A. Scholes, S. E. Kentish, G. W. Stevens, Effects of minor components in carbon dioxide capture using polymeric gas separation membranes, Separation & Purification Reviews, 38 (2009) 1-44.

CHAPTER 6

ZIF-90/PBI NANO-COMPOSITE MEMBRANES FOR HYDROGEN PURIFICATION

This chapter contains unpublished work

6.1 Introduction

Besides the particle size, the particle synthesis method and the particle-polymer mixing procedure also significantly affect the properties of the resultant MMMs. Preliminary studies have demonstrated that the direct-mixing of as-synthesized wet-state nanoparticles in polymer solutions shows much better particle-polymer adhesion and more uniform particle dispersion than the traditional dry-state mixing method [1-4].

Recently, zeolitic imidazolate frameworks (ZIF) have been intensively studied as a promising candidate for MMMs fabrication due to its high intrinsic gas and vapor permeability [5-10], good chemical and thermal stability [11] and remarkable affinity toward polymeric materials [12]. Comparing with common ZIFs such as ZIF-7 and ZIF-8, ZIF-90 offers more chemical versatility due to the extra aldehyde group on the imidazolate linkers [13, 14]. Moreover, experimental [7] and simulation [15] data of ZIF-90 crystalline membranes have indicated the superior H_2 permeability, remarkable H_2/CO_2 diffusion selectivity and excellent thermal and steam stabilities of this material, which are beneficial for high temperature H_2/CO_2 separation. Existing ZIF-90 particle synthesis methods include hydrothermal, vapor diffusion [13], and nonsolvent-induced crystallization [16]. These methods produce large particles with sizes from 0.8 um to 100 um, and are not suitable for MMMs fabrication. The normal room-temperature colloidal chemistry route works well for ZIF-7 [5] and ZIF-8 [17] particle syntheses, producing nanocrystals with a narrow size distribution between 40 nm and 100 nm. However, for the ZIF-90 synthesis, nanocrystals cannot automatically form in the solution at room temperature because the α-hydrogen in the

aldehyde group (pKa near 17) is far more acidic than the C-H bond in the alkyl group (pKa about 50) [18] thus the reactivity toward ZIF-90 construction is much reduced.

In this work, we report a novel room-temperature synthesis method of nanoscale ZIF-90 particles and demonstrate its applicability by fabricating ZIF-90/PBI nano-composite membranes for hydrogen purification. The resultant membranes show homogeneous particle dispersion, high thermal stability and superior H_2/CO_2 ideal selectivity and high mixed gas separation factor at high temperatures. This study indicates the feasibility of introducing nano-science and nano-technology into advanced materials development for chemical engineering applications.

6.2 Results and discussion

6.2.1 Characterizations of ZIF-90 nanocrystals

In this work, the ZIF-90 nanocrystals were synthesized by a novel method which was specially developed to obtain ZIF-90 particles with a nano scale particle size. Figure 6.1 shows their apparent particle size distribution after the 3rd centrifugation and dispersion in a NMP solvent using dynamic light scattering (DLS) measurements. About 60 vol% of the ZIF-90 particles are between 85 and 105 nm, while the rest are between 198 and 245 nm.

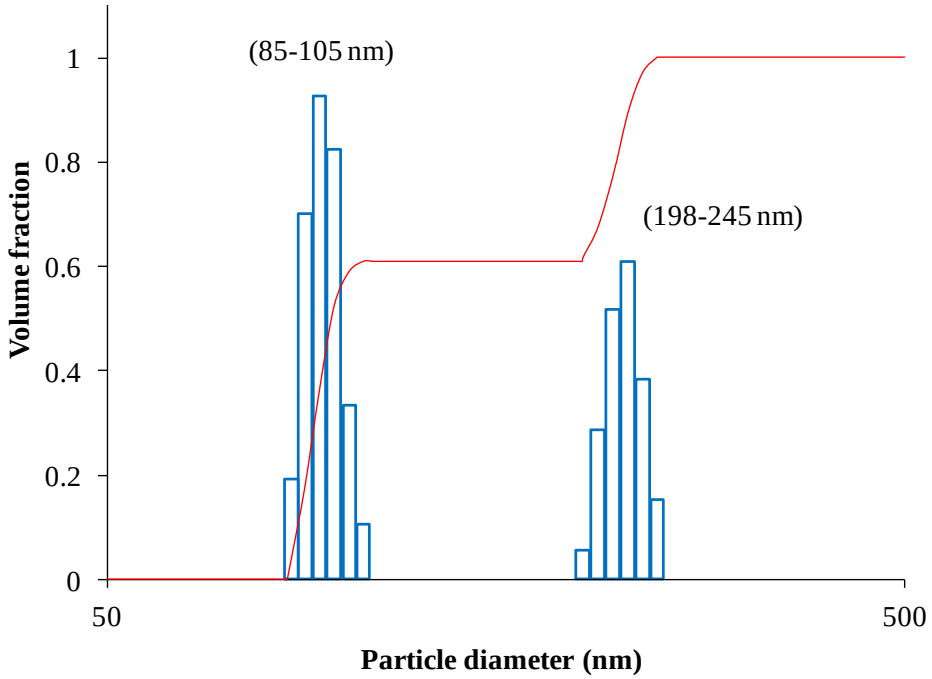

Figure 6.1 The particle distribution pattern of the as-synthesized ZIF-90 nanocrystals measured by DLS

Figure 6.2 shows the FESEM morphology of ZIF-90 particles and further confirm its size distribution. The particle sizes generally fall within range of 80 to 200 nm and are well consistent with the DLS results. The as-synthesized ZIF-90 nanoparticles have a typical cubic crystalline morphology, which is similar to the ZIF-90 particles synthesized via hydrothermal method by Morris et al. [13] and nonsolvent-induced crystallization by Bae et al. [16].

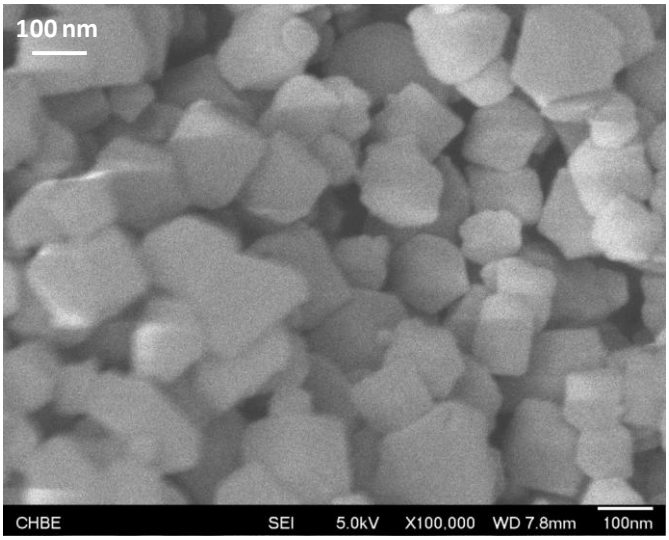

Figure 6.2 A FESEM image of ZIF-90 nanocrystals. (dry state powders)

Figure 6.3 shows the XRD spectrum between 2.5 ° to 50 ° from the dry state ZIF-90 powders. The ZIF-90 nanocrystals possess well matched peaks with the simulated ZIF-90 XRD pattern in the literature [13], confirming the successful formation of the ZIF-90 crystalline structure. The structure of ZIF-90 framework is correlated to the sodalite (**SOD**) topology of zeolite, and shows extended 3-D networks with a large pore size of 11.2 Å and a small aperture size of 3.5 Å in diameters.

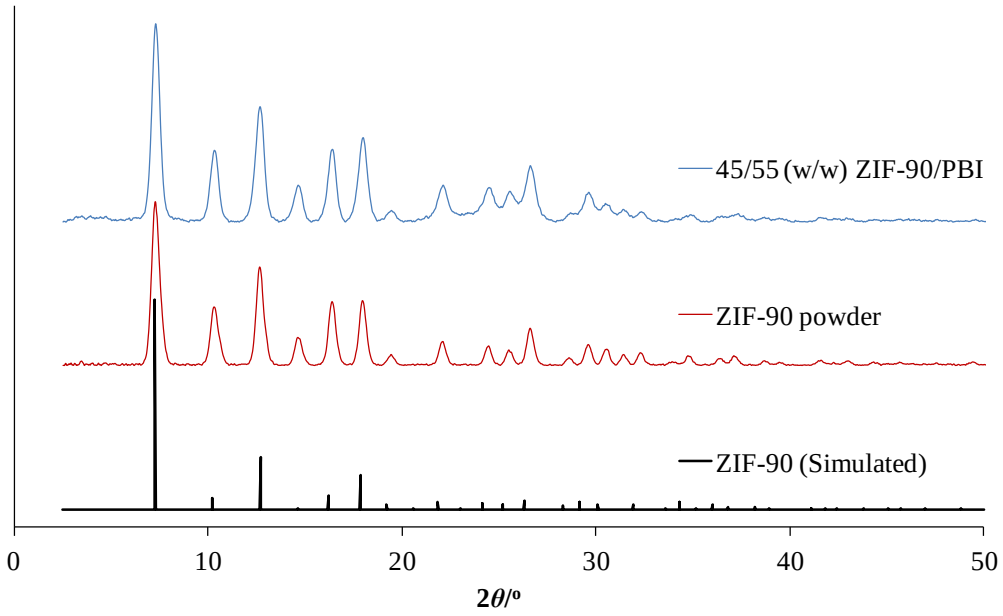

Figure 6.3 XRD spectra of ZIF-90 powders and ZIF-90/PBI nano-composite membrane comparing with literature data

Figure 6.4 confirms the chemical structure of ZIF-90 using solid state ^{13}C cross polarization magic angle spinning (CP/MAS) NMR. The NMR spectrum displays resonances at 178, 150, and 130 ppm from the aldehyde carbon atom, the 2-carbon atom of the imidazolate ring, and the symmetrically equivalent 4- and 5-carbon atoms of imidazolate ring, respectively [13]. The NMR spectrum is consistent with the expected structure.

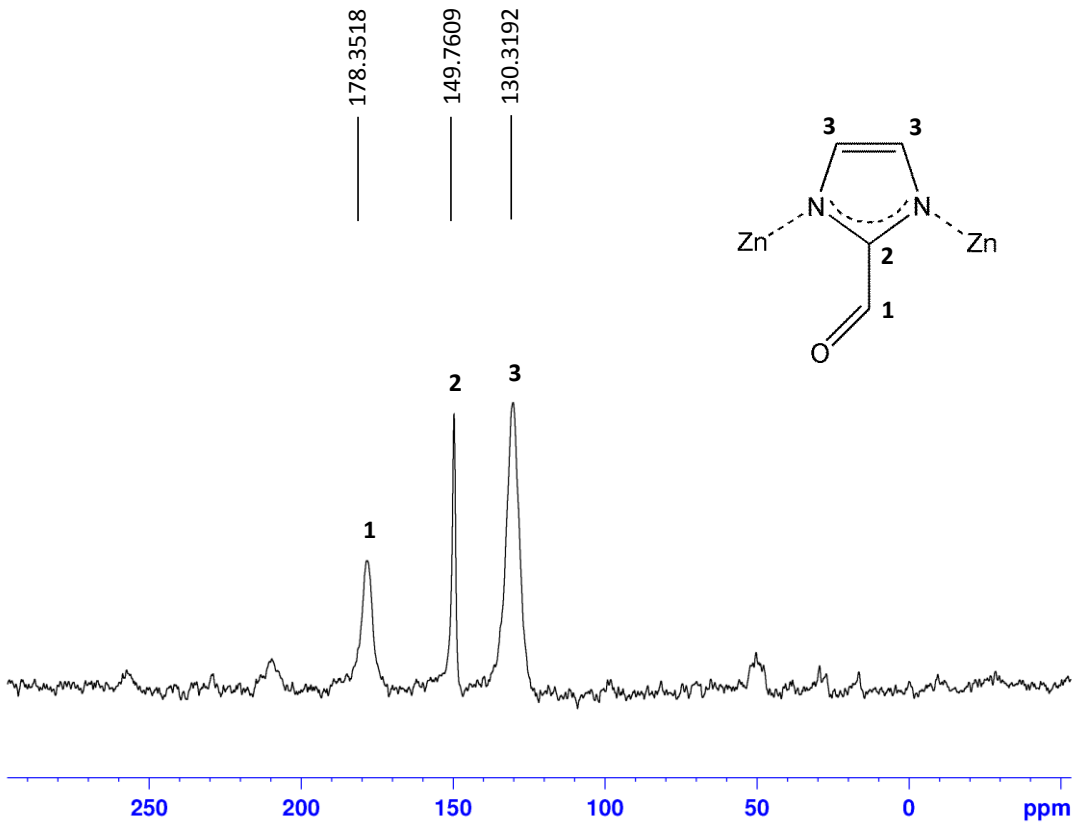

Figure 6.4 The solid state ^{13}C CP/MAS NMR spectrum of ZIF-90 nanocrystals

Figure 6.5 depicts the FTIR spectrum of the ZIF-90 dry powders in a KBr pallet tested under the transmission mode. The spectrum shows peaks identical with the previous report [13], providing further evidence for the correct chemical structure. The most representative bond at 1668 cm^{-1} as pointed by the arrow refers to the aldehyde stretch from the imidazole ligands. The weak peaks at 1258, 1095, and 656 cm^{-1} can be ascribed to the residue solvents inside the cavities.

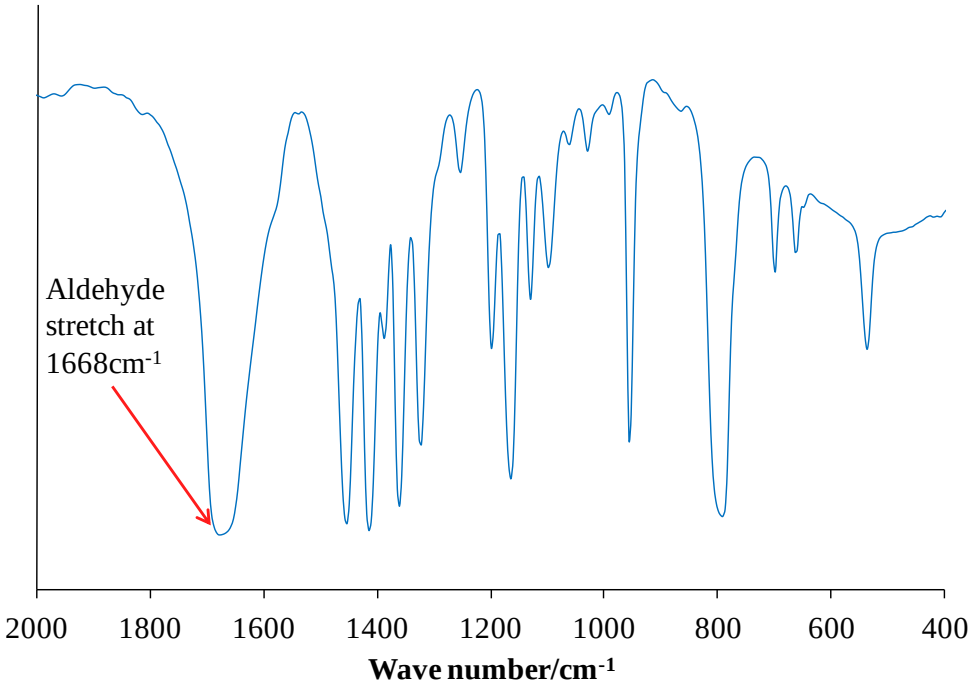

Figure 6.5 The FTIR spectrum of pure ZIF-90 powders

6.2.2 Characterizations of ZIF-90/PBI nano-composite membranes

The weight loadings of ZIF-90 in the nano-composite membranes were measured by TGA analyses under air atmosphere. The ash content was obtained from the residual weight of zinc oxide powders at 800 ℃, and was further calculated back to the weight of ZIF-90 nanoparticles according to the stoichiometry relationship. As listed in Table 6.1, the exact weight loadings of ZIF-90 nanoparticles in the 10/90 (w/w) ZIF-90/PBI, 25/75 (w/w) ZIF-90/PBI and 45/55 (w/w) ZIF-90/PBI nano-composite membranes are 9.8 wt%, 24.5 wt% and 43.7 wt%, respectively. Subsequently, the volume loadings are estimated from the weight loadings and their density data. According to the literatures, the density of PBI is 1.30 g/cm^3 based on experiments and the density of ZIF-90 is 0.974 g/cm^3 based on the atomically detailed calculation [15]. Thus the

volume loadings of the above three membranes are calculated as 12.7 vol%, 30.2 vol%, and 50.9 vol%, respectively.

Table 6.1 ZIF-90 particle loadings of the nano-composite membranes determined from TGA

Sample ID	Ash content weight (%)	ZIF-90 weight (%)	ZIF-90 volume (%)
Pure PBI	0	0	0
10/90 (w/w) ZIF-90/PBI	3.1	9.8	12.7
25/75 (w/w) ZIF-90/PBI	7.8	24.5	30.2
45/55 (w/w) ZIF-90/PBI	13.9	43.7	50.9

Wide-angle XRD measurements between 2.5 °to 50 °were conducted to determine the crystalline structure inside the 45/55 (w/w) ZIF-90/PBI nano-composite membrane. As shown in Figure 6.3, the diffraction pattern of the membrane shows identical ZIF-90 crystalline peaks matching well with pure ZIF-90 particles, indicating that the ZIF-90 crystalline structure remains unchanged after being incorporated into the PBI matrix.

Field emission scanning electron microscopy (FESEM) observation was conducted on the ZIF-90/PBI membrane with the highest ZIF-90 loading to determine the particle dispersion state. Figure 6.6 clearly shows that the ZIF-90 nanoparticles are uniformly dispersed in the 45/55 (w/w) ZIF-90/PBI membrane. At a magnification of x100,000 neither particle agglomeration nor interphase voids can be observed in this membrane. This homogenously dispersed morphology proves excellent interphase affinity between ZIF-90 nanoparticles and the PBI polymer matrix, and also indicates the

feasibility for fabricating defect-free asymmetric hollow fibers and thin film composite membranes using the ZIF-90/PBI nano-composite material.

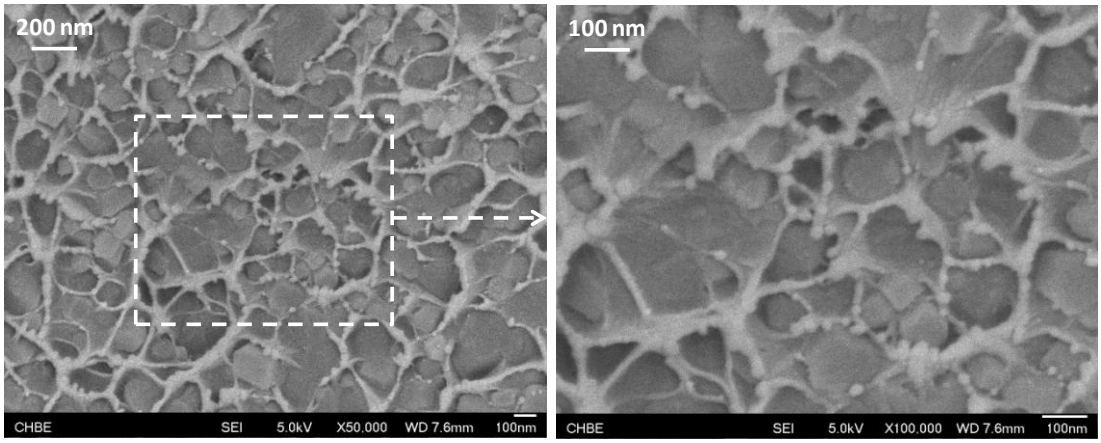

Figure 6.6 FESEM images of the 45/55 (w/w) ZIF-90/PBI nano-composite membrane

6.2.3 Pure gas transport properties at ambient temperature

The single-gas permeability and ideal selectivity for H_2 and CO_2 of ZIF-90/PBI nano-composite membranes were measured at 35 ℃ with a 3.5 atm trans-membrane pressure and the results are listed in Table 6.2. Both H_2 permeability and H_2/CO_2 ideal selectivity show significant improvements with increasing ZIF-90 loadings. Particularly, the 45/55 (w/w) ZIF-90/PBI membrane with the highest ZIF-90 loading shows the best performance with a H_2 permeability of 24.5 Barrer and a H_2/CO_2 ideal selectivity of 25.0. The increase of the H_2 permeability comes from the high porosity of ZIF-90 particles and the sub-nano transportation channels formed at the PBI-ZIF interphase [1]. Comparing with previously studies about ZIF-8/PBI nano-composite membranes [2, 3], the ZIF-90/PBI membranes show extremely high ideal selectivity, mainly due to the following facts: 1) ZIF-90 exhibits a much higher H_2/CO_2 diffusion

selectivity according to the atomically detailed simulation results [15]; and 2) the aldehyde group in ZIF-90 shows more acidity in its enolate form [19] and thus possesses interaction with the N-3 atom on the PBI imidazole ring, which shows alkalinity [20]. The enhancements in both permeability and selectivity become more notable with increased ZIF-90 loading because of superior particle dispersion in the polymer matrix.

Table 6.2 Pure gas separation performance of pure PBI and ZIF-90/PBI nano-composite membranes at 35 ℃.

Sample ID	ZIF-90 weight %	Permeability[a] (Barrer[b])		Selectivity (H_2/CO_2)
		H_2	CO_2	
Pure PBI	0	4.1	0.46	8.9
10/90 (w/w) ZIF-90/PBI	9.8	12.7	0.87	14.6
25/75 (w/w) ZIF-90/PBI	24.5	18.3	0.89	20.6
45/55 (w/w) ZIF-90/PBI	43.7	24.5	0.98	25.0

[a] Single gas tests were performed in 3.5 atm, at 35 ℃.

[b] 1 Barrer = 1×10^{-10} cm^3(STP)cm /(cm^2 s cmHg).

To understand the contributions of solubility and diffusivity changes to the overall permeability, CO_2 sorption curves of pure PBI and ZIF-90/PBI nano-composite membranes were measured at 35 ℃ from 0 to 30 atm. Figure 6.7 shows the sorption curves, and Table 6.3 lists the relative transportation parameters calculated from the sorption results. Comparing with pure PBI, ZIF-90/PBI membranes exhibit about three times enhancement in CO_2 solubility because of the high porosity and CO_2 adsorption capacity of ZIF-90 particles [13, 15]. However, the diffusivity of CO_2 decreases slightly in the ZIF-90/PBI nano-composite membranes. This decreasing phenomenon is unique because other ZIFs based nano-composite materials usually

show an increase in CO_2 diffusivity with increasing ZIFs loading [3, 4, 21, 22]. The reduction of CO_2 diffusivity may indicate a narrowing of gas transport pathways due to the special interaction between ZIF-90 particles and PBI chains.

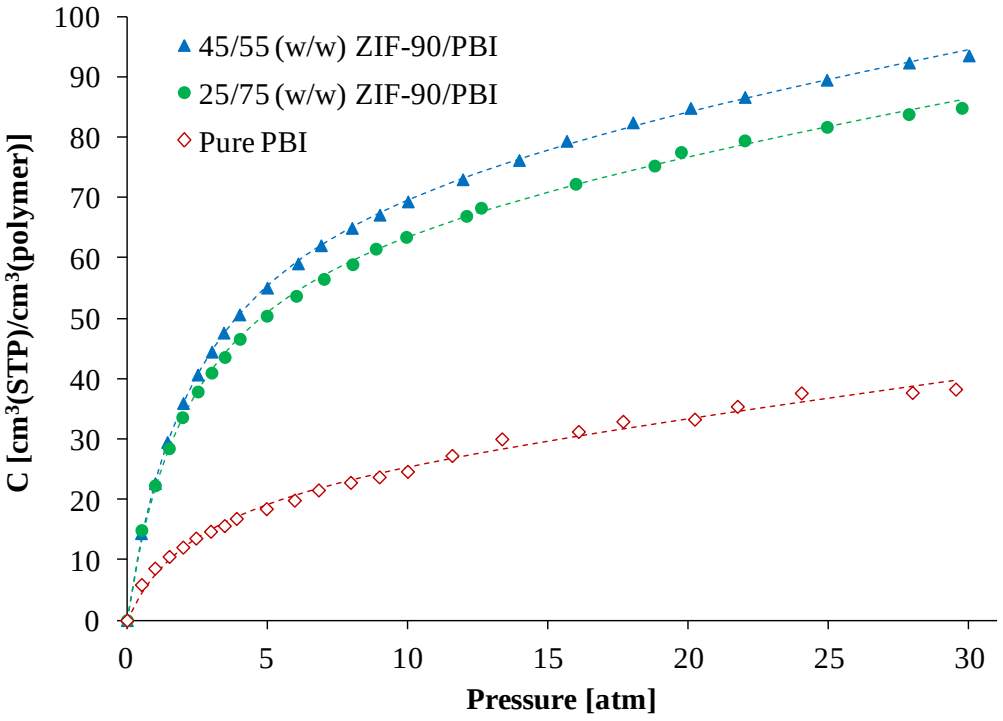

Figure 6.7 CO_2 sorption isotherms of pure PBI and ZIF-90/PBI nano-composite membranes

Table 6.3 P, D and S coefficients of CO_2 in pure PBI and ZIF-90/PBI nano-composite membranes at 35 ℃ and 3.5 atm

Sample ID	Permeability (Barrer)	Solubility (cm^3 (STP)/cm^3 atm)	Diffusivity ($\times 10^{-8}$ cm^2/s)
Pure PBI	0.46	4.65	0.0753
25/75 (w/w) ZIF-90/PBI	0.89	12.52	0.0541
45/55 (w/w) ZIF-90/PBI	0.98	13.84	0.0539

6.2.4 Mixed gas performance at high temperatures

Figure 6.8 shows the mixed gas permeation results of the 45/55 (w/w) ZIF-90/PBI membrane from 35 to 180 ℃ using a 50/50 (mol/mol) H_2/CO_2 binary gas mixture as the feed gas. At 35 ℃, the membrane shows obviously a reduced mixed gas selectivity comparing with pure gas data. This phenomenon may be due to the plasticization by the more condensable component (CO_2 in this study) and competitive sorption [23-25]. The CO_2 in the gas mixture may plasticize the membrane, decrease the diffusivity selectivity, and decrease the gas pair selectivity. Both H_2 permeability and H_2/CO_2 selectivity increase significantly with an increase in temperature. At 180 ℃, the membrane shows impressive mixed gas separation performance with a H_2 permeability of 226.9 Barrer and a H_2/CO_2 separation factor of 13.3.

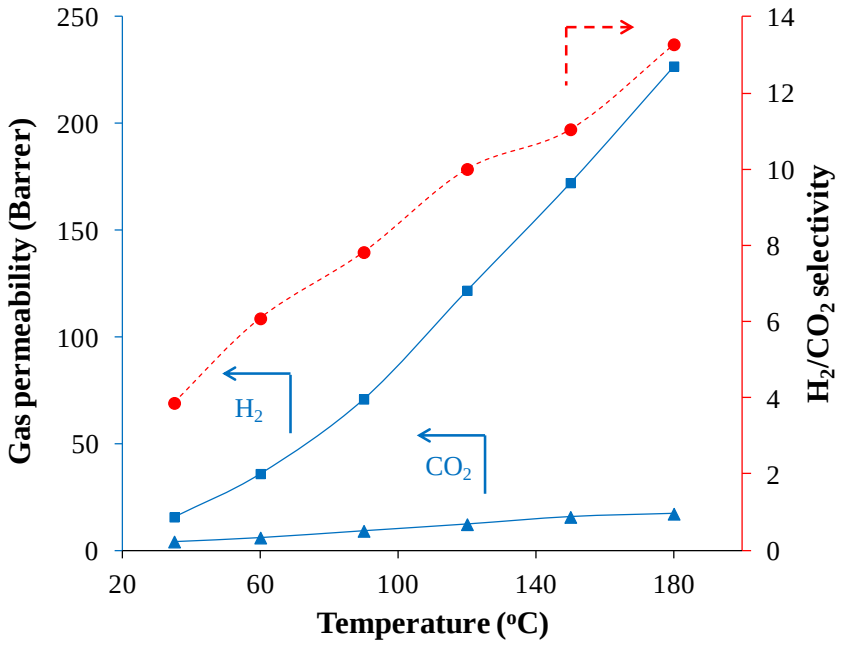

Figure 6.8 H_2/CO_2 mixed gas permeation results of ZIF-90/PBI nano-composite membranes

The permeation of H_2 or CO_2 across ZIF-90/PBI membranes is a thermally activated process. The temperature dependence of gas permeability can be described by the Arrhenius-van't Hoff equation [23]:

$$P = P_0 \exp\left(\frac{-E_p}{RT}\right) \quad (6\text{-}1)$$

where P refers to the gas permeability, P_0 represents the pre-exponential coefficient, E_P indicates the apparent activation energy in the permeation process, R is the gas constant, and T stands for the absolute temperature. Based on the solution-diffusion model, E_P can be expressed in terms of two contributions:

$$E_p = E_D + \Delta H_S \quad (6\text{-}2)$$

where E_D refers to the activation energy of diffusion and is always positive, while ΔH_S represents the enthalpy of sorption and is usually negative. For strongly size-sieving membranes, E_D is larger than the absolute value of ΔH_S, thus the total value E_P is positive and the gas permeability increases as temperature increases.

Figure 6.9 shows the temperature dependence of individual gas permeability (P) across the 45/55 (w/w) ZIF-90/PBI nano-composite membrane by means of the Arrhenius-van't Hoff equation and mixed gas data. The activation energies (E_p) of H_2 and CO_2 permeation through the 45/55 (w/w) ZIF-90/PBI membrane are 15.4 and 8.4 kJ/mol, respectively, indicating a strong size-sieving effect for both H_2 and CO_2 gas molecules, which is consistent with the results of diffusion coefficients in section 6.2.3. The activation energy of CO_2 permeation is lower than H_2 because CO_2 exhibits a far more negative enthalpy of sorption (ΔH_S) in the membrane. As a result, the H_2 permeability increases faster than CO_2 as temperature going up, thus the H_2/CO_2

selectivity becomes higher with increasing temperature. The gas separation performance of the 45/55 ZIF-90/PBI membrane at 400 ℃ can be therefore predicted from their individual activation energy and gas permeability at room temperature. The predicted H_2 permeability is 864.6 Barrer while the calculated H_2/CO_2 selectivity is 23.8 at 400 ℃.

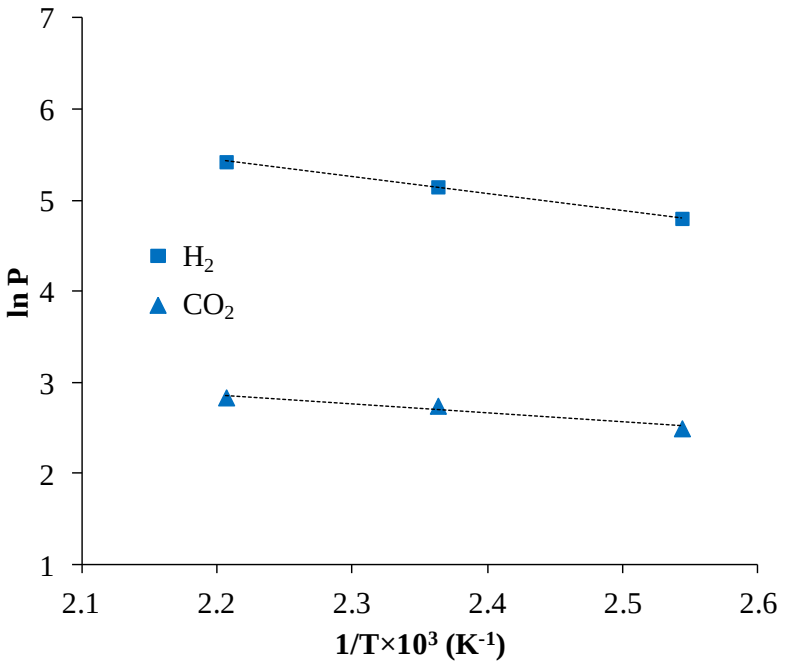

Figure 6.9 Temperature dependence of gas permeability (P) in the 45/55 (w/w) ZIF-90/PBI nano-composite membrane

Figure 6.10 compares the pure gas and mixed gas permeation results of the 45/55 ZIF-90/PBI nano-composite membrane with the latest Robeson upper bound [26] for H_2/CO_2 separation. The ideal H_2 permeability and H_2/CO_2 selectivity at 35 ℃ of the 45/55 (w/w) ZIF-90/PBI has surpassed the upper bound. Although the mixed gas result at 35 ℃ drops significantly comparing with pure gas results, an encouraging performance recovery shows up when the membrane is tested under mixed gases at elevated temperatures.

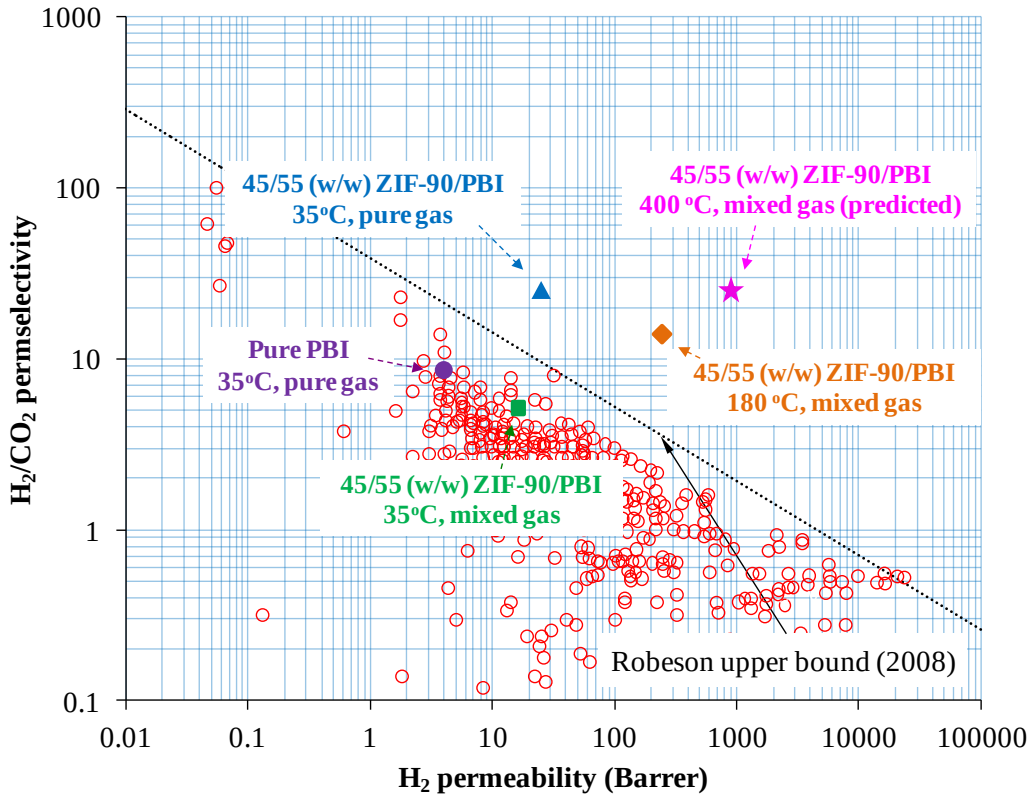

Figure 6.10 H_2/CO_2 separation performance of ZIF-90/PBI nano-composite membranes compared to the Robeson upper bound

6.3 Conclusions

In this work, we have successfully synthesized ZIF-90 nanocrystals via a specially designed route in order to keep particles small and maximize the separation performance of ZIF-90/PBI nano-composite membranes for H_2/CO_2 separation. Investigations on the properties of ZIF-90 nanoparticles and the derived nano-composite membranes were carried out using advanced instrumental analyses and gas permeation tests. The following conclusions can be made from this study:

(1) Comparing with the ZIF-90 particles in the previous literatures, the ZIF-90 nanoparticles in this study exhibit identical morphology, crystalline and chemical structure, but with a significantly reduced particle size (around 100 nm). As a result, no visible particle agglomeration was observed and the derived ZIF-90/PBI nano-composite membranes possess homogeneous particle dispersion and fine particle-polymer adhesion as observed by FESEM.

(2) The incorporation of ZIF-90 nanoparticles into PBI-based membranes promotes CO_2 solubility coefficients while reduces CO_2 diffusion coefficients. This transition may indicate an increased H_2/CO_2 diffusion selectivity which explains the enhancement of ideal H_2/CO_2 selectivity. The 45/55 (w/w) ZIF-90/PBI membrane achieves the highest ZIF-90 volume loading up to 50.9 vol%. This membrane possesses the best ideal H_2/CO_2 separation performance with a moderate H_2 permeability of 24.5 Barrer and a high H_2/CO_2 selectivity of 25.0 in pure gas permeation tests at 35 ℃.

(3) Mixed gas permeation results show that the 45/55 (w/w) ZIF-90/PBI membrane suffers a significant performance drop possibility due to competitive sorption and plasticization phenomenon in strong size-sieving glassy polymeric membranes. Nevertheless, the membrane still possesses impressive mixed gas separation performance with a H_2 permeability of 226.9 Barrer and a H_2/CO_2 separation factor of 13.3 at 180 ℃. Based on activation energy calculations, the membrane may have a H_2 permeability of 864.6 Barrer and a H_2/CO_2 selectivity of 23.8 at 400 ℃. Both the experimental and calculated mixed gas data of the 45/55 ZIF-

90/PBI nano-composite membrane surpass the latest Robeson upper bound for H_2/CO_2 separation.

6.4 References

[1] G. M. Shi, T. Yang, T. S. Chung, Polybenzimidazole (PBI)/zeolitic imidazolate frameworks (ZIF-8) mixed matrix membranes for pervaporation dehydration of alcohols, Journal of Membrane Science, 415-416 (2012) 577-586.

[2] T. Yang, G. M. Shi, T. S. Chung, Symmetric and asymmetric zeolitic imidazolate frameworks (ZIFs)/polybenzimidazole (PBI) nano-composite membranes for hydrogen purification at high temperatures, Advanced Energy Materials, 2 (2012) 1358-1367.

[3] T. Yang, T. S. Chung, High performance ZIF-8/PBI nano-composite membranes for high temperature hydrogen separation consisting of carbon monoxide and water vapor, International Journal of Hydrogen Energy, (2012) doi: 10.1016/j.ijhydene.2012.10.045.

[4] Q. Song, S. K. Nataraj, M. V. Roussenova, J. C. Tan, D. J. Hughes, W. Li, P. Bourgoin, M. A. Alam, A. K. Cheetham, S. A. Al-Muhtaseb, E. Sivaniah, Zeolitic imidazolate framework (ZIF-8) based polymer nanocomposite membranes for gas separation, Energy and Environmental Science, 5 (2012) 8359-8369.

[5] Y. S. Li, F. Y. Liang, H. Bux, A. Feldhoff, W. S. Yang, J. Caro, Molecular sieve membrane: Supported metal-organic framework with high hydrogen selectivity, Angewandte Chemie - International Edition, 49 (2010) 548-551.

[6] A. Huang, H. Bux, F. Steinbach, J. Caro, Molecular-sieve membrane with hydrogen permselectivity: ZIF-22 in LTA topology prepared with 3-aminopropyltriethoxysilane as covalent linker, Angewandte Chemie - International Edition, 49 (2010) 4958-4961.

[7] A. Huang, W. Dou, J. Caro, Steam-stable zeolitic imidazolate framework ZIF-90 membrane with hydrogen selectivity through covalent functionalization, Journal of the American Chemical Society, 132 (2010) 15562-15564.

[8] S. R. Venna, M. A. Carreon, Highly permeable zeolite imidazolate framework-8 membranes for CO_2/CH_4 separation, Journal of the American Chemical Society, 132 (2010) 76-78.

[9] G. M. Shi, H. M. Chen, Y. C. Jean, T. S. Chung, Sorption, swelling, and free volume of polybenzimidazole (PBI) and PBI/zeolitic imidazolate framework (ZIF-8) nano-composite membranes for pervaporation, submitted to Polymer (2012).

[10] Y. Pan, Z. P. Lai, Sharp separation of C2/C3 hydrocarbon mixtures by zeolitic imidazolate framework-8 (ZIF-8) membranes synthesized in aqueous solutions, Chemical Communications, 47 (2011) 10275-10277.

[11] K. S. Park, Z. Ni, A. P. Côté, J. Y. Choi, R. Huang, F. J. Uribe-Romo, H. K. Chae, M. O'Keeffe, O. M. Yaghi, Exceptional chemical and thermal stability of zeolitic imidazolate frameworks, Proceedings of the National Academy of Sciences of the United States of America, 103 (2006) 10186-10191.

[12] J. Caro, Are MOF membranes better in gas separation than those made of zeolites, Current Opinion in Chemical Engineering, 1 (2011) 77-83.

[13] W. Morris, C. J. Doonan, H. Furukawa, R. Banerjee, O. M. Yaghi, Crystals as molecules: Postsynthesis covalent functionalization of zeolitic imidazolate frameworks, Journal of the American Chemical Society, 130 (2008) 12626-12627.

[14] A. Huang, J. Caro, Covalent post-functionalization of Zeolitic imidazolate framework ZIF-90 membrane for enhanced hydrogen selectivity, Angewandte Chemie - International Edition, 50 (2011) 4979-4982.

[15] E. Atci, S. Keskin, Understanding the potential of zeolite imidazolate framework membranes in gas separations using atomically detailed calculations, Journal of Physical Chemistry C, 116 (2012) 15525-15537.

[16] T. H. Bae, J. S. Lee, W. Qiu, W. J. Koros, C. W. Jones, S. Nair, A high-performance gas-separation membrane containing submicrometer-sized metal-organic framework crystals, Angewandte Chemie - International Edition, 49 (2010) 9863-9866.

[17] J. Cravillon, S. Münzer, S. J. Lohmeier, A. Feldhoff, K. Huber, M. Wiebcke, Rapid room-temperature synthesis and characterization of nanocrystals of a prototypical zeolitic imidazolate framework, Chemistry of Materials, 21 (2009) 1410-1412.

[18] F. A. Carey and R. J. Sundberg, Advanced Organic Chemistry Part B: Reactions and Synthesis, Springer Science+Business Media, New York (2007).

[19] A. Burrows, J. Holman, A. Parsons, G. Pilling and G. Price, Chemistry 3: Introducing Inorganic, Organic and Physical Chemistry, Oxford University Press, Oxford (2009).

[20] X. Zhang and J. Jiang, N-Based rare earth complexes, in Rare Earth Coordination Chemistry: Fundamentals and Applications, ed. C. H. Huang, John Wiley & Sons (Asia) Pte Ltd, Singapore (2010) ch.4, pp.137-192.

[21] K. Díaz, L. Garrido, M. López-González, L. F. Del Castillo, E. Riande, CO_2 transport in polysulfone membranes containing zeolitic imidazolate frameworks

as determined by permeation and PFG NMR techniques, Macromolecules, 43 (2010) 316-325.

[22] K. Díaz, M. López-González, L. F. Del Castillo, E. Riande, Effect of zeolitic imidazolate frameworks on the gas transport performance of ZIF8-poly(1,4-phenylene ether-ether-sulfone) hybrid membranes, Journal of Membrane Science, 383 (2011) 206-213.

[23] S. Matteucci, Y. Yampolskii, B. D. Freeman and I. Pinnau, Transport of gases and vapors in glassy and rubbery polymers, in Materials Science of Membranes for Gas and Vapor Separation, ed. Y. Yampolskii, I. Pinnau and B. D. Freeman, John Wiley & Sons, Ltd., Chichester (2006) ch.1, pp.1-47.

[24] C. Staudt-Bickel, W. J. Koros, Improvement of CO_2/CH_4 separation characteristics of polyimides by chemical crosslinking, Journal of Membrane Science, 155 (1999) 145-154.

[25] L. S. White, T. A. Blinka, H. A. Kloczewski, I. F. Wang, Properties of a polyimide gas separation membrane in natural gas streams, Journal of Membrane Science, 103 (1995) 73-82.

[26] L. M. Robeson, The upper bound revisited, Journal of Membrane Science, 320 (2008) 390-400.

CHAPTER 7

ZIF-8-PBI/MATRIMID DUAL-LAYER HOLLOW FIBER MEMBRANES FOR HYDROGEN PURIFICATION

This chapter is published as a journal paper

Tingxu Yang, Gui Min Shi, Tai Shung Chung, Symmetric and asymmetric zeolitic imidazolate frameworks (ZIFs)/polybenzimidazole (PBI) nanocomposite membranes for hydrogen purification at high temperatures, Advanced Energy Materials, 2 (2012) 1358-1367.

7.1 Introduction

Energy security and sustainability have attracted enormous attention globally because resource depletion, high oil price and global warming are threatening the living quality, survivability and development of human beings in the future [1]. New energy resources are required to meet the demands from rapid growths in both population and industries [2]. Among many energy alternatives, hydrogen is one of the most strategically important sustainable fuel sources. In addition to be viable and versatile in widely applications such as fuel for transportation and feedstock for chemical industries, a hydrogen-based energy system has other advantages including low emissions and environmentally friendly, clean, and efficient use [3, 4].

Currently, the favored route of hydrogen production is from the steam reforming of methane followed by the water-gas shift reaction [5, 6]. The main by-product in the leaving stream from the operation is carbon dioxide. The removal of CO_2 from H_2 or its sequestration is a critical requirement for hydrogen to be a sustainable energy system as well as for the minimization of environmental impact. Comparing with traditional CO_2 separation technologies including amine-based absorption, cryogenic distillation and pressure-swing adsorption, etc., which are highly energy and capital intensive, membrane separation technologies are more economical and environmental friendly since neither absorbent or phase change is needed during the separation process [7, 8].

Among materials for membrane fabrication, polymers remain to be the most practical and economical choice [9]. The gas permeation through polymeric membranes is

generally controlled by the solution-diffusion model [10] in which the selectivity of a gas pair is the product of diffusivity selectivity and solubility selectivity. The effective separation of H_2 and CO_2 mixtures is challenging because most polymers show undesirable counterbalance characteristics of H_2-selective diffusivity and CO_2-selective solubility. Generally, rubbery polymers are CO_2-selective, while glassy polymers are H_2-selective. For example, PEG or PEO-based blended membranes are typical CO_2-selective membranes. They have the advantages of requiring less membrane area, eliminating H_2 recompression and exhibiting no performance reduction under high pressure CO_2 induced plasticization [11-17]. However, similar to common rubbery materials, the applications of these CO_2-selective membranes in industrial syngas processes are limited by their drawbacks of weak mechanical strength, low thermal stability and easy crystallization. On the other hand, H_2-selective membranes are often made from glassy polymers in which the H_2/CO_2 diffusivity selectivity is much greater than the CO_2/H_2 solubility selectivity. Various approaches have been proposed to produce H_2-selectivite membranes such as new polymer designs, polymer blends, doping, chemical cross-linking and mixed matrix membranes [6, 18]. The chemical modification by means of diamino cross-linking reaction appears to be an effective way to improve H_2/CO_2 selectivity and enhance membrane resistance to CO_2-induced plasticization [19-25]. Nevertheless, although chemical cross-linked membranes exhibit good gas pair selectivity, they show severe sacrifice in permeability. In addition, the cross-linked membranes become brittle due to chain scission [22-25].

To sustain high H_2/CO_2 separation performance in harsh environments of high temperatures and pressures, membranes must possess impressive thermal stability,

good chemical resistance and high compression strength. Polybenzimidazole (PBI) is a specialty polymer that has been commercialized for fuel cells [26] and protective fibers [27], and studied for water reuse and desalination [28-30], solvent and protein dehydration [31-34]. Recently, PBI has been identified as a unique polymeric material for H_2 separation since it exhibits superior thermal stability and good intrinsic H_2/CO_2 selectivity under extreme high temperature environments [35]. However, due to the inherent characteristics of rigid polymeric backbone and high degree of chain packing, PBI shows very low gas permeance even in the hollow fiber configuration [36]. PBI membranes fabricated by means of non-solvent phase inversion processes are also very brittle. To overcome these deficiencies, various approaches have been proposed such as coating PBI on tube supports [37], spinning dual-layer hollow fibers [38], polymer blending [39], changing PBI acid moiety [40], cross-linking blended polymers [41], thermally rearranging PBI [42], N-substitution modification [43], and addition of inorganic particles [44].

Metal-organic frameworks (MOFs) are a group of crystalline materials which represent two-dimensional (2D) or three-dimensional (3D) nanoporous networks of transition metal complexes [45, 46]. Typically, MOFs show high porosity with exactly tailorable cavity sizes, and furthermore, due to the organic linkers present in the frameworks, it is believed that MOFs can achieve better affinity and interaction with polymeric materials [47]. As a subfamily of MOFs, zeolitic imidazolate frameworks (ZIFs) not only exhibit all the above advantages of MOFs, but also have exceptional high thermal and chemical stability [48]. Studies on ZIFs membranes with inorganic supports have shown promising intrinsic gas separation properties for various gas pairs [49-58]. Nonetheless, like other crystalline membranes, the

difficulties of preparing defect-free membranes on a large scale, the considerable material synthesis cost and the membrane mechanical brittleness make ZIFs less commercially attractive. Therefore, one affordable way to utilize ZIFs in gas separation membranes is to incorporate their nano-particles into a polymer matrix in order to take the strengths of both materials and minimize their weaknesses.

Mixed matrix membranes (MMMs) consisting of polymeric materials and inorganic components have been extensively studied since it was first invented by Kulprathipanja et al. [59] about 25 years ago. Some of MMMs have shown enhanced separation performance for gas and liquid pairs [60, 61]. However, challenges such as pore blockage, chain rigidification and interface voids still exist and restrain the potential separation performance of MMMs materials [60]. In addition, the oversize and agglomeration of nano-particles limit their applications in fabricating asymmetric hollow fibers. The hollow fiber configuration is favorable for gas separation due to its provision of high surface area per unit volume and high packing density in modules [62, 63].

Recently, we have reported the incorporation of as-synthesized ZIF-7 nano-particles into the PBI matrix. The resultant MMMs show synergized performance [64]. By controlling the synthesis conditions, we have controlled ZIF-7 particle sizes below 30-40 nm with limited agglomeration. As a result, the flat dense PBI/ZIF-7 nano-composite membranes not only display good particle-polymer interaction, but also have impressive mechanical strength and H_2/CO_2 separation properties at high temperatures [64]. However, the hydrogen permeability at room temperature is relatively low. Since ZIF-8 is much more porous than ZIF-7 [65] and asymmetric

hollow fiber configuration can significantly reduce the dense layer thickness and provide a large surface area, the objectives of this study are (1) to conduct fundamental research on the synthesis and characterization of novel PBI/ZIF-8 mixed matrix membranes and (2) to explore the feasibility of spinning this type of materials into defect-free asymmetric hollow fiber membranes. We aim to considerably improve the intrinsic H_2 permeability of the dense ZIFs/PBI membrane and fabricate it in a useful form for H_2/CO_2 separation. Compared to prior arts of mixed matrix hollow fibers, most of which mainly focused on developing membranes for O_2/N_2, H_2/N_2, He/N_2, and CO_2/CH_4 separations [66-69], this study focuses on more challenging H_2/CO_2 separation membranes. In addition, to our best knowledge, this work is the first successful case in the literature producing almost "defect-free" mixed matrix hollow fiber membranes without the aid of post annealing or silicone rubber coating. It may therefore have significant impact for the future development of high performance MMMs for hydrogen production and CO_2 capture.

7.2 Experimental

7.2.1 Spinning dope formulation

The spinning dope compositions are listed in Table 7.1. Based on the observation in a previous study [31], the outer layer dope composition was chosen as 24 wt% PBI in DMAc. The ZIF-8 nano-particles were added according to the targeted weight ratios to the PBI polymer. For the preparation of the outer-layer spinning dope, the as-synthesized ZIF-8 particles were firstly added into a certain amount of PBI/DMAc/LiCl dope (25.6 wt% PBI) with continuous stirring, followed by topping

up the dope with DMAc to the targeted composition. The solutions were stirred at room temperature for 24 hours to ensure the homogeneous dispersion of nano-particles in the dope. The inner layer spinning dope was a mixture of 21.6 wt% Matrimid and 78.4 wt% DMAc. For the preparation of the inner-layer spinning dope, Matrimid polymer powder was added gradually to DMAc under continuous agitation, and the solution was stirred for 24 hours to ensure complete dissolution of Matrimid. Both the outer layer dope and inner layer dope were left standing for another 24 hours for degassing before loading into the respective syringe pumps (ISCO 1000), followed by another degassing for overnight.

Table 7.1 Spinning conditions of ZIF-8-PBI/Matrimid dual-layer hollow fiber membranes

Parameters	**A**	**B**	**C**
Outer-layer dope composition	Pure PBI; PBI+ZIF-8(90:10); PBI+ZIF-8(80:20); PBI+ZIF-8(67:33)/DMAc/LiCl (PBI 24 wt% in DMAc)		
Inner-layer dope composition	Matrimid/DMAc: 21.6/78.4 wt%		
Bore fluid composition	NMP/Water: 90/10 wt%		
External coagulant	Water		
Outer layer dope flow rate [mL/min]	0.3	1.06	0.3
Inner layer dope flow rate [mL/min]	1.5	5.28	1.5
Bore fluid flow rate [mL/min]	0.6	2.11	0.6
Coagulation bath temperature [℃]	25		
Spinneret temperature [℃]	25		
Take-up rate [cm/min]	537.5 (free fall)	1624.4	792.6

Air gap [cm]	5

7.2.2 Co-extrusion of the dual-layer hollow fiber membranes and solvent exchange

Co-extrusion of dual layer hollow fibers was employed in this study for the following reasons: (1) PBI membranes are brittle when fabricated from the non-solvent phase-inversion process. This problem can be avoided by choosing a strong material as the inner layer during co-extrusion; (2) PBI has low gas permeability. By choosing an inner layer material with high permeability, the gas transport resistance of the support layer can be effectively reduced; (3) PBI/ZIF-8 is relatively expensive. By choosing a polymeric material as the supporting inner layer, the overall cost of hollow fibers can be significantly reduced. In addition, the de-lamination problem between the two layers can be eliminated because PBI and Matrimid are miscible [38, 41, 70].

All the dual layer hollow fibers with different ZIF-8 loadings in this study were fabricated using the same series of spinning parameters. The inner layer dope and outer layer dope were co-extruded together through a triple-orifice spinneret by a dry-jet/wet spinning process. The detailed description of the set up for dual-layer hollow fiber spinning and process can be found elsewhere [71]. The schematics for both side view and cross-section view of the dual-layer spinneret used in this work are shown in Figure 7.1. The detailed spinning parameters can be found in Table 7.1.

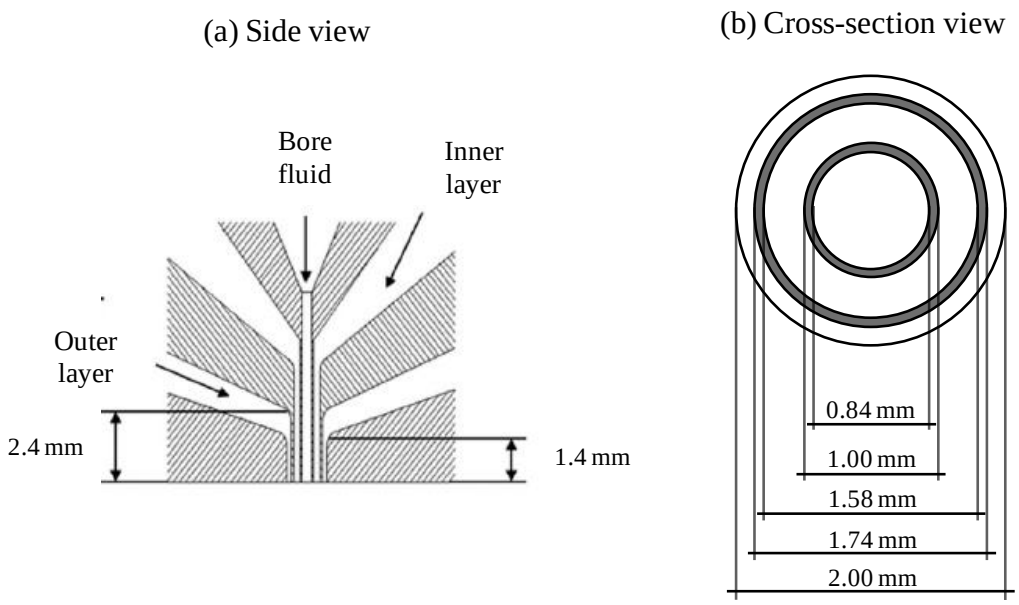

Figure 7.1 Dual-layer spinneret scheme in this study

After spinning, the as-spun hollow fibers were immersed in tap water to remove the residual solvent within the membranes. To further remove the residual solvent and study the effect of solvent exchange on hollow fiber morphology and separation performance, two series of solvent compositions were employed as shown in Table 7.2 during the solvent exchange for comparison. Series "M" has been described previously in the literatures [68, 69, 71, 72] using methanol as the second solvent, while Series "I" uses isopropanol as the second solvent. After finishing the solvent exchange process, the fibers were naturally dried at 25 ℃ for 24 hours.

Table 7.2 Solvent-exchange procedures for dual-layer hollow fibers

Solvent-exchange prototype code	**1st solvent**	**2nd solvent**	**3rd solvent**
M (Methanol)	Water: 1day ×3 times	Methanol: 30min ×3 times	Hexane: 30min ×3 times
I (Isopropanol)	Water: 1day ×3 times	Isopropanol: 30min ×3 times	Hexane: 30min ×3 times

7.3 Results and discussion

7.3.1 As-synthesized ZIF-8 particle properties

To obtain a defect-free hollow fiber membrane, the nano-composite material for the dense-selective layer must be uniformly dispersed in the polymer matrix and free of inter-phase voids between particles and the polymeric matrix. Since the thickness of the dense-selective layer is usually lower than several hundred nanometers [72-74], the dimension of nano-particles must be much smaller than this number to avoid defects and particle penetration. Figure 7.2 shows the apparent particle size distribution of the ZIF-8 suspension after the 2nd centrifugation. Above 70 volume percent of ZIF-8 particles are about 40 nm, while the rest is between 100 nm and 200 nm. This distribution is similar to that observed for the ZIF-7 nano-particles in the previous study [64], in which the small particles below 50 nm are single crystals, while the large ones above 100 nm are the clusters formed by single crystals. By mixing the as-synthesized wet ZIF-8 nano particles with the PBI solution, the problems of poor affinity, large particle size and serious particle agglomeration are minimized, thus reducing the formation of defects inside the membranes especially at high particle loadings. Figure 7.3 shows and compares the XRD patterns between 5 ° to 35 ° from the 30/70 ZIF-8/PBI flat-sheet membrane and the data from literature [48]. They match extremely well and confirm the successful synthesis of ZIF-8. The patterns also prove that the ZIF-8 crystalline structure remains the same after incorporating into the PBI matrix.

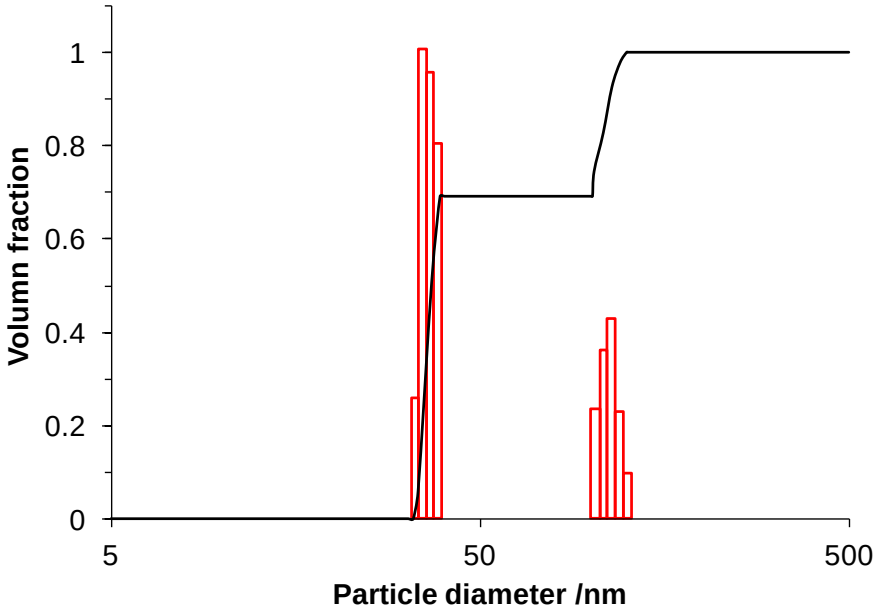

Figure 7.2 As-synthesized ZIF-8 particle distribution pattern from DLS measurement

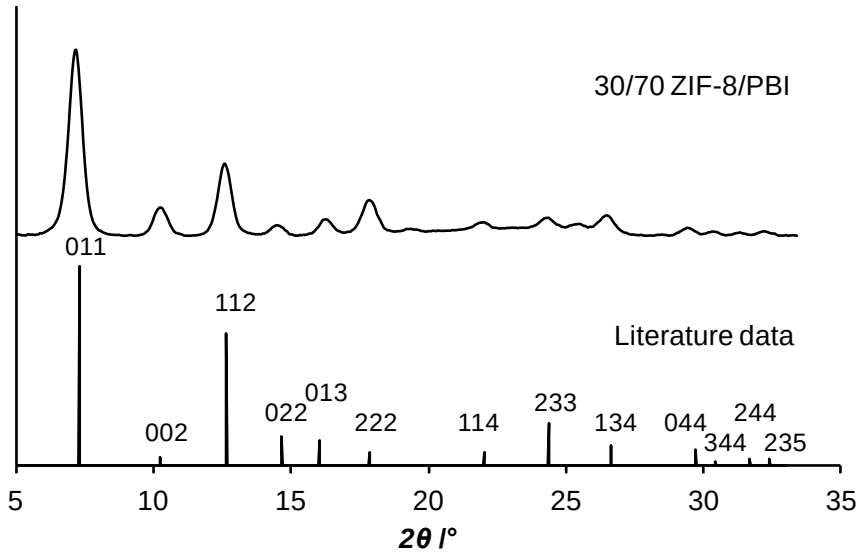

Figure 7.3 XRD spectrum of ZIF-8/PBI nano-composite membrane comparing with literature data

7.3.2 ZIF-8/PBI symmetric dense membranes

Table 7.3 summarizes the intrinsic gas permeability and ideal selectivity of flat ZIF-8/PBI nano-composite dense membranes for H_2 and CO_2 gas pair as a function of ZIF-8 nano-particle loading at 35 °C. Table 7.3 also includes the best gas performance of ZIF-7/PBI membranes under pure gas tests for comparison [64]. The highest ZIF-8 loading for this study is increased to 58.7 wt% compared with 42.1 wt% in the previous study of ZIF-7/PBI membranes. This is due to the fact that the molecular weight of PBI used in this study is higher than the previous one (IV of 1.0 vs. 0.55), thus the mechanical strength of the membranes at a high particle loading is stronger. The H_2 permeability of the ZIF-8/PBI dense membranes shows a tremendous increment with increasing ZIF-8 loading; namely, from 3.7 Barrer of the pure PBI to 1749.9 Barrer of the 60/40 ZIF-8/PBI. The H_2/CO_2 selectivity firstly increases to the maximum of about 13.2 at a ZIF-8 loading of 17.8 wt%. This selectivity is higher than both pure PBI and pure ZIF-8 membrane, indicating a possible formation of the unique interphase structure due to the chemical interaction of PBI chains and ZIF-8 particle surface [64]. The H_2/CO_2 selectivity stays above 12 till ZIF-8 loading of 28.6 wt%, and then decreases when the ZIF-8 loading is further increased. This trend is different from what we have observed in previous ZIF-7/PBI nano-composites [64] where no decrease on H_2/CO_2 selectivity as a function of ZIF-7 loading was noticed. In addition, the highest H_2 permeability increases from the previous 26.2 Barrer of 50/50 ZIF-7/PBI to the current 105.4 Barrer of 30/70 ZIF-8/PBI without severe dropping on selectivity. The H_2/CO_2 separation performances are compared with the Robeson upper bound in Figure 7.4 [25, 64, 75-77]. To our best knowledge, the 30/70 ZIF-8/PBI dense membrane with a H_2 permeability of 105.4 Barrer and a H_2/CO_2 selectivity of 12.3 has the best ever reported data for H_2-selective polymeric membranes in the literatures.

Table 7.3 Pure gas separation performance of flat ZIF-8/PBI dense membranes

Membrane ID	ZIFs wt% (from TGA)	Pure gas permeability[a)]		
		P_{H2} [Barrer[b)]]	P_{CO2} [Barrer]	Selectivity (H_2/CO_2)
Pure PBI	0.0	3.7	0.43	8.6
15/85 ZIF-8/PBI	17.8	28.5	2.2	13.0
20/80 ZIF-8/PBI	20.1	36.4	3.0	12.1
30/70 ZIF-8/PBI	28.6	105.4	8.6	12.3
35/65 ZIF-8/PBI	33.7	238.6	34.2	7.0
60/40 ZIF-8/PBI	58.7	1749.9	426.6	4.1
50/50 ZIF-7/PBI[c)]	42.1	26.2	1.8	14.6

[a)] Single gas tests were performed in 3.5 atm, at 35 ℃; [b)] 1 Barrer=1×10^{-10} cm^3 (STP) cm cm^{-2} s^{-1} $cmHg^{-1}$; [c)] From reference [64].

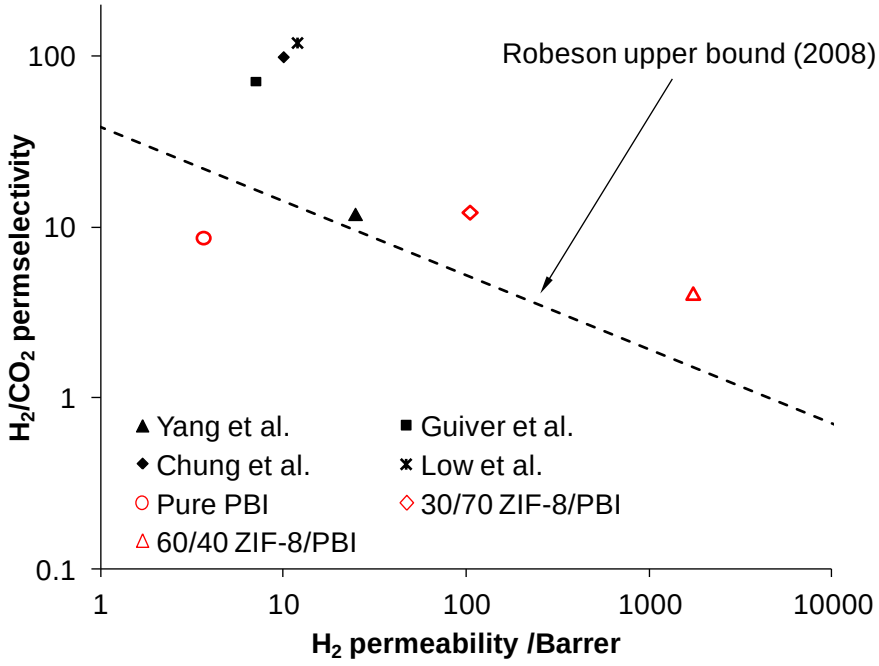

Figure 7.4 ZIF-8/PBI nano-composite membranes intrinsic gas separation performances (35 ℃) comparing with Robeson upper bound

Many factors contribute to the impressive gas separation performance of ZIF-8/PBI and its performance differences from ZIF-7/PBI. Since the kinetic diameters of H_2 and CO_2 are 2.9Å and 3.3Å, respectively, and the accessible cavity diameter of ZIF-7 is smaller than that of ZIF-8 (3.0 vs. 3.4Å) [48], ZIF-7/PBI may have a greater H_2/CO_2 selectivity but a lower permeability than ZIF-8/PBI. In addition, according to the literatures [78-80], the CO_2 adsorption capability of ZIF-8 is as high as 35 wt% at ambient temperature. This indicates that ZIF-8/PBI nano-composites may have a more CO_2 favorable solubility than ZIF-7/PBI. As a result, the former has a lower intrinsic H_2/CO_2 selectivity but a higher permeability than the latter.

7.3.3 Morphology of the asymmetric dual-layer hollow fiber membranes

For easy understanding, Figure 7.5 defines the sample name of dual-layer hollow fibers as a function of ZIF-8 particle loading, spinning condition and solvent exchange procedure, while Figure 7.6 illustrates the cross-section morphology. The effects of solvent-exchange procedures on the outer layer morphology can be clearly observed on hollow fibers spun from condition B with 10 wt% ZIF-8. Figure 7.6a exhibits a collapsed outer layer with less porosity after using methanol as the 2nd solvent during the multi-stage solvent change process, while Figure 7.6b shows a porous outer layer and a finger like macrovoid sub-structure after using isopropanol (IPA) as the 2nd solvent. Clearly, the immersion in isopropanol helps maintaining the outer layer morphology without collapse. Similar phenomena can be observed in all other fibers with different ZIF-8 loadings and spinning conditions (Figures are not shown). According to the literature [81, 82], the membrane skins on hollow fibers may be collapsed or densified due to capillary forces of higher surface tension

solvents during drying. As shown in Table 7.4 [39, 83, 84], the surface tension of hexane is the lowest among all the common solvents, which is one of the reasons that hexane is commonly used in the final step in multi-stage solvent-exchanges. Since IPA is more soluble in hexane than methanol and since PBI is a polymer exhibiting strong inter-chain hydrogen bonding, the outer layer would be more easily to collapse or densify after the solvent-exchange with methanol than IPA because the former has a higher surface tension and solubility parameter from hydrogen bonding than the latter.

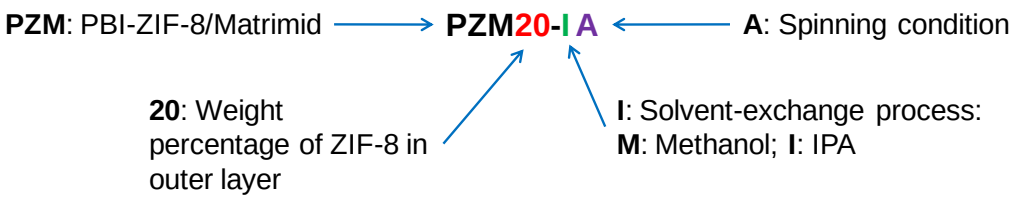

Figure 7.5 Definition of hollow fiber sample name

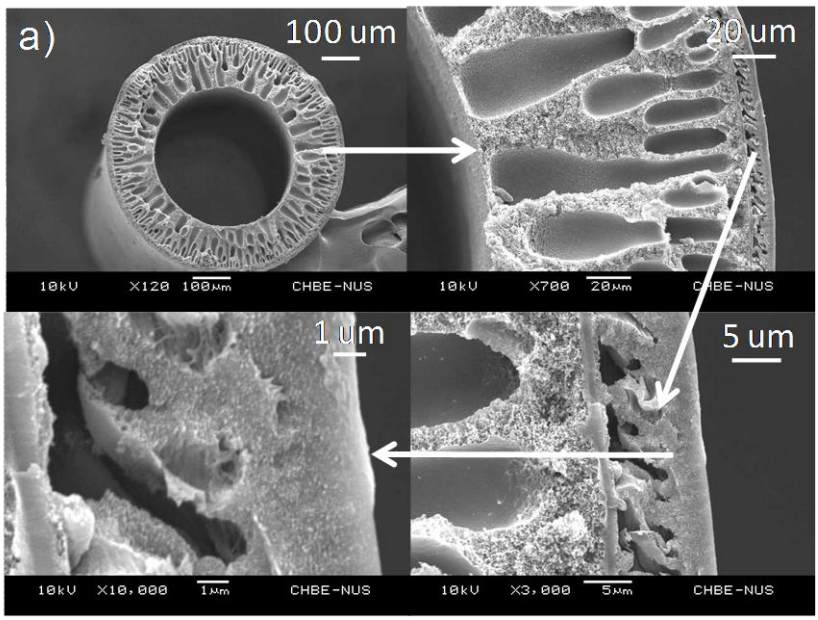

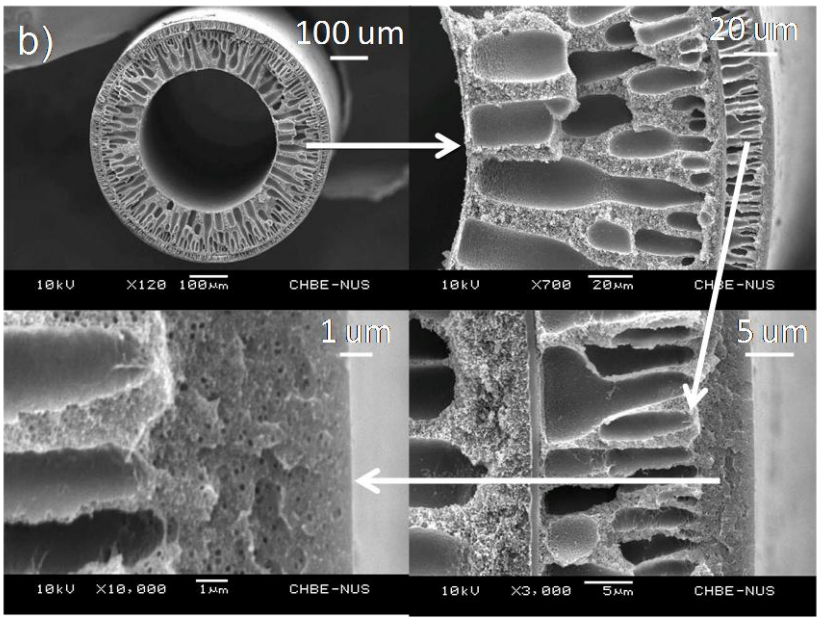

Figure 7.6 Cross sectional views of hollow fibers with different solvent-exchange procedures
(a) PZM10-M B; b) PZM10-I B.)

Table 7.4 Surface tension and solubility parameters of the solvents used for the hollow fiber solvent-exchange processes in this study

Solvent	**Surface tension at 25 ℃ [mJ m^{-2}]**	**Hansen solubility parameters[a] [MPa$^{1/2}$]**			
		δ_D	**δ_P**	**δ_H**	**δ_T**
Water	72.71	15.5	16.0	42.3	47.8
Methanol	22.09	15.1	12.3	22.3	29.6
Isopropanol	20.92	15.8	6.1	16.4	23.6
Hexane	17.98	14.9	0.0	0.0	14.9
PBI	--	20.8	6.7	8.0	23.3

[a] The total solubility parameter δ_T is the geometric mean of the three components δ_D (from dispersion interactions), δ_P (from polar attraction), and δ_H (from hydrogen bonding).

To examine the dispersion state of ZIF-8 nano-particles in the selective layer, FESEM images were taken from the outer edge of PZM33-I B hollow fibers, which not only have the highest ZIF-8 loading, but also show reasonable separation performance.

PZM10-I B fibers with the highest H_2/CO_2 selectivity were also included for comparison. As indicated in the right images of Figure 7.7, the tiny gray spheres are the PBI polymer nodules, while the bigger irregular shape particles are ZIF-8, as pointed by the small white arrows. There are no visible inter-phase voids and aggregation in the fiber whether in full or detailed views.

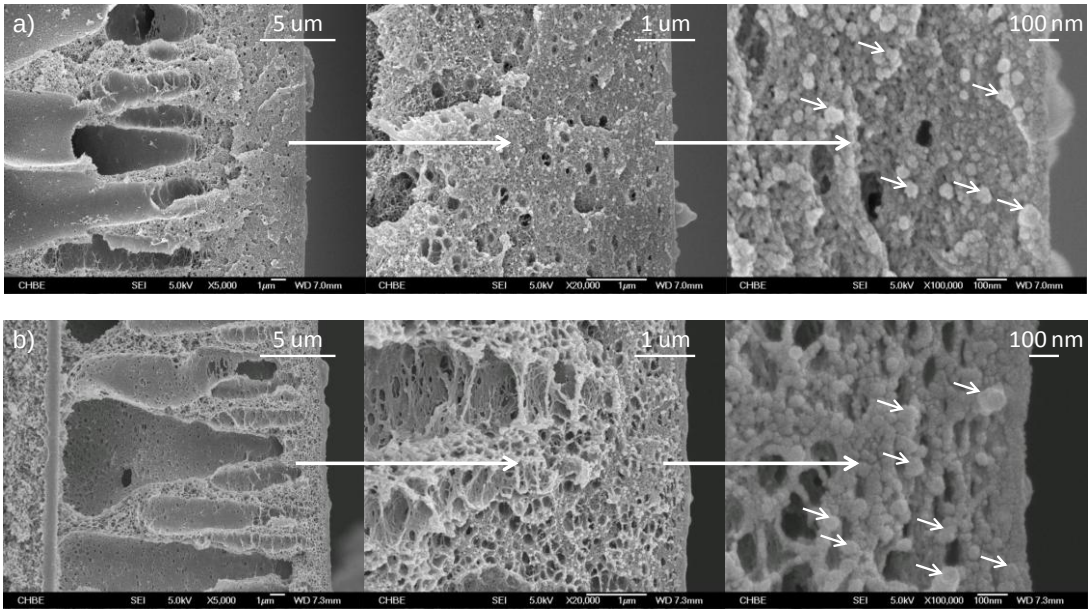

Figure 7.7 FESEM images taken from the outer edge of a) PZM10-I B, b) PZM33-I B hollow fibers
(Small white arrows indicate ZIF-8 nano-particles)

Figure 7.8 shows the R parameter from Doppler broadened energy spectra (DBES) of Positron Annihilation Spectroscopy (PAS) as a function of positron incident energy for hollow fibers after different solvent-exchange protocols. For PZM10-I B, the R parameter firstly exhibits a sharp decrease with an increase in positron incident energy from 0.1 to 4 keV, which covers the dense skin near the outer surface of the hollow fiber. After that, the R parameter gradually increases with an increase in positron incident energy from 4 to 9 keV (about 2000nm depth). This indicates a progressive transition from a dense to a porous structure with an increase in the depth distance

calculated from the outer skin of the hollow fiber. In contrast, PZM10-M B, which is the fiber spun from the same condition but solvent exchanged with methanol and then hexane, shows no significant transition layer and porous layer from its R parameter profile. The difference in R profile between these two fibers is in good agreement with the observation from SEM images. In summary, protocol I solvent exchange results in hollow fibers with a thinner dense skin and a porous sub-layer of the outer layer than protocol M using methanol in the 2nd step.

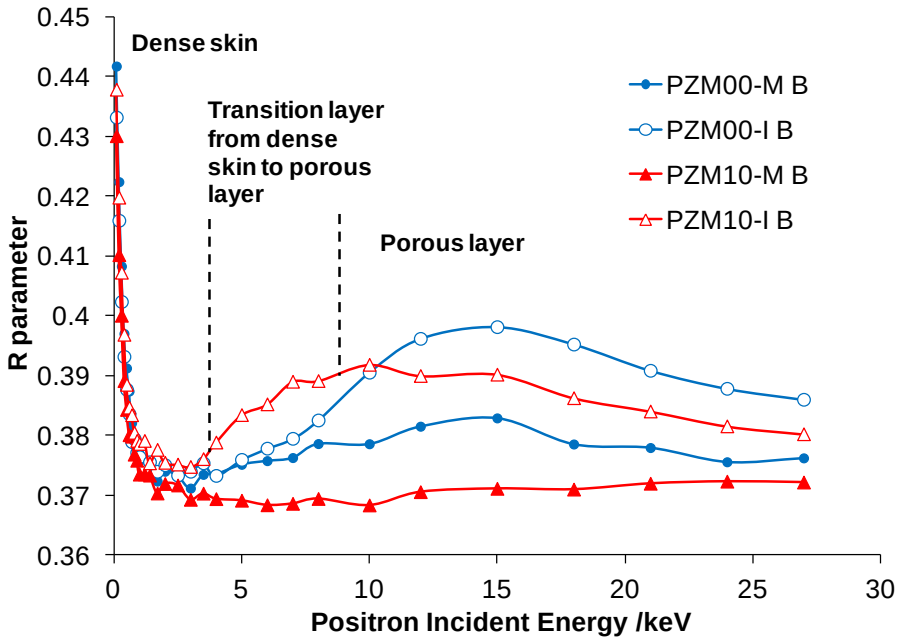

Figure 7.8 R parameters vs. positron incident energy in hollow fibers with different solvent-exchange protocols
(Vertical dot lines indicate the boundaries from layer to layer in PZM10-I B, only for guiding the eyes.)

7.3.4 Influence of particle loadings and spinning conditions on gas transport properties

The pure gas separation performances of ZIF-8-PBI/Matrimid dual-layer hollow fibers were tested at room temperature and listed in Table 7.5. The following trends can be observed: (1) Samples post-treated by protocol I have greater performance than those by protocol M; (2) H_2/CO_2 selectivity increases and then decreases with increasing particle loading; (3) Membranes spun from condition B show the best separation performance with the highest H_2/CO_2 selectivity among all the spinning conditions possibly due to a proper combination of dope flow rate and take-up speed. For easy comparison, only fibers spun under condition B are discussed thereafter.

Table 7.5 Pure gas permeation results of ZIF-8-PBI/Matrimid dual-layer hollow fibers tested at 25 ℃, 3.5 atm

a) Pure PBI/Matrimid

Sample name		**PZM00-M A**	**PZM00-M B**	**PZM00-M C**	**PZM00-I A**	**PZM00-I B**	**PZM00-I C**
Permeance [GPU [a)]]	**H_2**	1.3	0.81	0.84	1.7	2.1	1.8
	CO_2	0.26	0.13	0.12	0.22	0.34	0.22
Selectivity		5.0	6.2	7.0	7.7	6.2	8.0

b) 10% ZIF-8-PBI/Matrimid

Sample name		**PZM10-M A**	**PZM10-M B**	**PZM10-M C**	**PZM10-I A**	**PZM10-I B**	**PZM10-I C**
Permeance [GPU]	**H_2**	6.6	0.86	1.5	13.3	8.9	13.2
	CO_2	1.7	0.13	0.39	2.1	0.94	2.4
Selectivity		3.9	6.6	3.8	6.2	9.5	5.4

c) 20% ZIF-8-PBI/Matrimid

Sample name		**PZM20-M A**	**PZM20-M B**	**PZM20-M C**	**PZM20-I A**	**PZM20-I B**	**PZM20-I C**
Permeance [GPU]	**H_2**	8.9	21.0	57.4	28.3	32.2	66.8
	CO_2	3.7	4.6	12.4	8.2	6.4	14.5
Selectivity		2.4	4.6	4.6	3.4	5.0	4.6

d) 33% ZIF-8-PBI/Matrimid

Sample name		PZM33-M A	PZM33-M B	PZM33-M C	PZM33-I A	PZM33-I B	PZM33-I C
Permeance [GPU]	**H_2**	36.0	248.9	497.6	22.7	34.9	32.0
	CO_2	21.5	77.5	152.4	7.6	8.7	5.8
Selectivity		1.7	3.2	3.3	3.0	4.0	5.5

[a)] 1 GPU = 10^{-6} cm^3 (STP) cm^{-2} s^{-1} $cmHg^{-1}$ =3.35 $\times 10^{-10}$ mol m^{-2} s^{-1} Pa^{-1}.

PBI-ZIF-8 hollow fibers spun from condition B and post-treated under protocol I show a higher H_2/CO_2 selectivity than pure PBI fibers when the ZIF-8 loading is low. A further increase in ZIF-8 loading, the H_2/CO_2 selectivity of the fibers becomes closer to the selectivity of pure ZIF-8. This trend is quite similar to the previous observation from flat ZIF-8/PBI dense membranes. Figure 7.9 shows a comparison of their H_2/CO_2 selectivity as a function of ZIF-8 loading. Interestingly, the starting point of the significantly decline in H_2/CO_2 selectivity of hollow fibers shifts towards a low ZIF-8 loading and these fibers generally have a lower H_2/CO_2 selectivity than those dense membranes. One of the possible reasons for these differences may arise from (1) the intercalation of ZIF nano-particles as schematically elucidated in Figure 7.10; (2) the defects induced during the spinning of highly concentrated solutions; and (3) the substructure resistance due to the formation of an interface between the inner and outer layers.

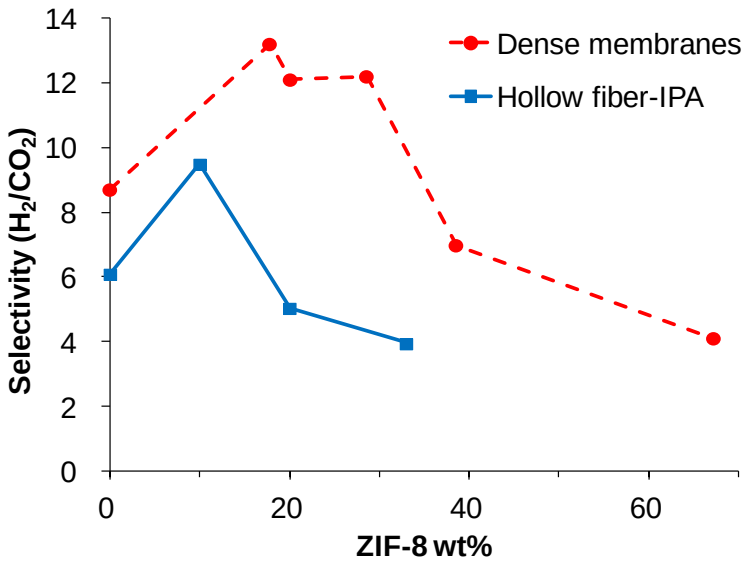

Figure 7.9 Comparison of selectivity vs. ZIF-8 loading patterns between symmetric dense membranes and asymmetric dual-layer hollow fiber membranes (Condition B, with IPA solvent-exchange)

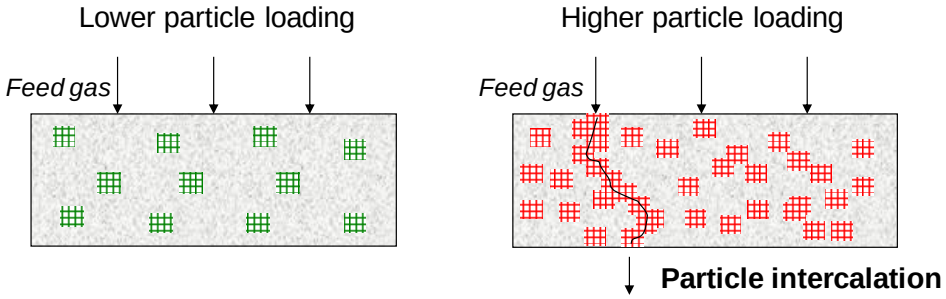

Figure 7.10 Proposed scheme for gas transportation paths through the nano-composite membranes comprising a lower and a higher particle loadings

Intercalation may occur when the local particle loading is high enough so that some of them bridge with one another across the entire membrane thickness. As a result, gas penetrants preferentially transport across the membranes via low selectivity ZIF-8 particles. Based on the H_2 permeability of ZIF-8/PBI symmetric flat membranes and the pure gas permeance of the PBI/ZIF-8 (i.e., PZM10-I B) hollow fibers, the calculated dense layer is about 1800nm, which is consistent with the values of about 2000 nm obtained from the R parameter (Figure 7.8) and of about 1600 nm from the

FESEM picture (Figure 7.7 top right). Therefore, the slightly low selectivity of hollow fiber membranes may be attributed to the effect of intercalation among ZIF-8 nano-particles.

On the other hand, hollow fibers with a high ZIF-8 loading (i.e., 33 wt%) do not result in a high H_2/CO_2 selectivity. Besides the intercalation effect, this is also due to the fact that spinning solutions with a high ZIF-8 loading are much more viscous than diluted solutions for the casting of flat dense membranes. Hence the dispersion of ZIF-8 nano-particles in hollow fibers is not as good as that in dense membranes. As a consequence, defects may be formed and then lower the H_2/CO_2 selectivity. In addition, based on FESEM pictures as shown in Figure 7.7 left bottom, an interface between inner and outer layers of the hollow fiber is formed due to good miscibility between PBI and Matrimid [38, 41, 70]. This may increase the substructure resistance, and lower the flux and selectivity [85]. Future research will try to eliminate this dense interface.

7.3.5 Mixed gas separation performances from ambient to high temperatures

To explore potential applications to separate hydrogen from steam reforming products or syngas, mixed gas tests from 25 °C to 180 °C were therefore conducted using hollow fibers spun from condition B and solvent exchanged by protocol I with different ZIF-8 nano-particle loadings. A 50/50 (v/v) H_2/CO_2 gas mixture of 7 atm was used as the feed and Figure 7.11 displays the gas separation performance. Compared with pure gas data, the mixed gas show decreased H_2 permeance and H_2/CO_2 separation factor at room temperature. This phenomenon is due to the effect of sorption competition

because there is a large amount of CO_2 adsorbed into the cavities of ZIF-8 nano-particles [79, 80]. As a consequence, H_2 transportation is blocked, leading to the reduction of H_2 permeance and separation factor. Interestingly, the H_2/CO_2 separation factor increases with an increase in testing temperature. This phenomenon is mainly attributed to the unique solution-diffusion characteristics of the PBI-ZIF-8 membranes; namely, a decline in CO_2/H_2 solubility selectivity and a big jump in H_2 diffusivity at high temperatures without losing H_2/CO_2 diffusivity selectivity [78]. Since ZIF-8 has a higher capacity for CO_2 sorption than ZIF-7, ZIF-8/PBI hollow fibers show a greater temperature enhancement on H_2/CO_2 separation factor than ZIF-7/PBI nano-composite membranes [64]. This indicates that the CO_2 solubility of ZIF-8 nano-particles plays an important role in determining the overall membrane performance at high temperatures.

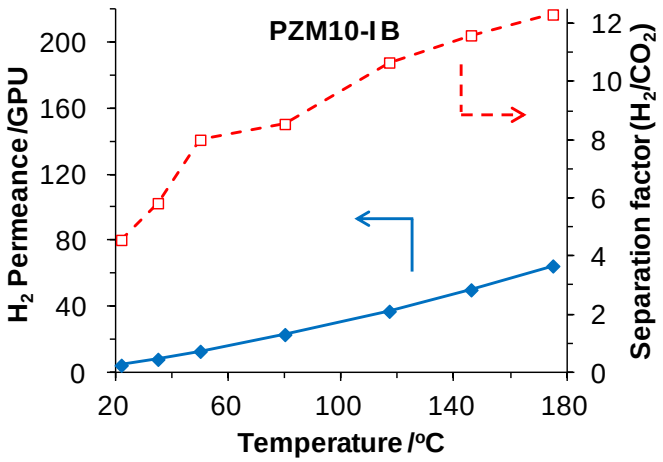

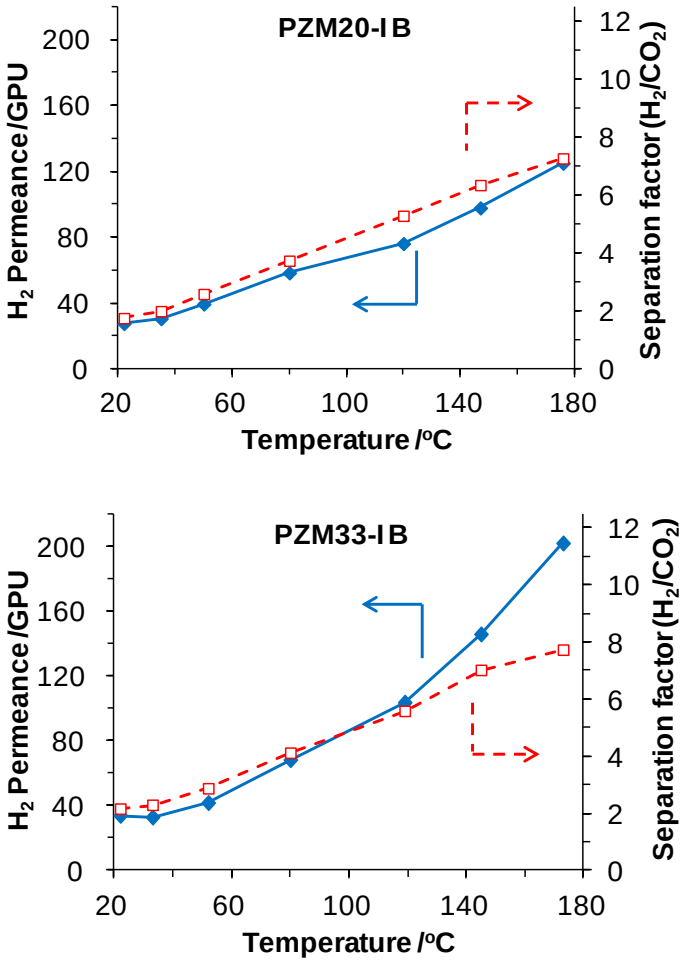

Figure 7.11 H_2/CO_2 (50/50) mixed gas permeation results of hollow fibers from ambient to high temperature

In addition, based on the mixed gas results, two types of hollow fibers may be developed for hydrogen purification at high temperatures: (1) PZM10-I B fibers which have a medium H_2 permeance (64.5 GPU at 180 °C) and a high selectivity (12.3), and (2) PZM33-I B fibers which have a high H_2 permeance (202 GPU at 180 °C) and a medium selectivity (7.7). These two membranes may be both useful for hydrogen production depending on the process design and the purity requirement in industrial applications.

7.4 Conclusions

For the first, we have synergistically combined the strengths of both ZIF-8 nano-particles and PBI polymer and designed their nano-composite membranes for hydrogen purification at high temperatures. Due to good compatibility between ZIF-8 and PBI, membranes with an extremely high ZIF loading of 58.7 wt% can be prepared. However, different from ZIF-7/PBI composite membranes, a decline in H_2/CO_2 selectivity at high ZIF-8 loading was found for the newly developed ZIF-8/PBI dense membranes due to the larger cavity size and much higher porosity of ZIF-8. Compared to PBI dense membranes, the 30/70 ZIF-8/PBI nano-composite material significantly enhances the H_2 permeability from 3.7 Barrer to 105.4 Barrer together with improved H_2/CO_2 selectivity from 8.7 to 12.3 at 35 ℃, far surpassing the Robeson upper bound and other polymeric materials in literatures.

We have also fabricated ZIF-8/PBI nano-composites in a useful form as dual-layer hollow fibers. Without post annealing and silicone rubber coating, the dual-layer fibers show impressive H_2/CO_2 separation performance. However, the intercalation phenomenon among ZIF-8 particles was observed when the nano-particle loading is high. In addition, interface resistance between inner and outer layers may affect the gas transport. Two types of hollow fibers targeted at either high H_2/CO_2 selectivity or high H_2 permeance have been developed; namely, (1) PZM10-I B fibers with a medium H_2 permeance of 64.5 GPU (2.16×10^{-8} mol m^{-2} s^{-1} Pa^{-1}) at 180 ℃ and a high selectivity of 12.3, and (2) PZM33-I B fibers with a high H_2 permeance of 202 GPU (6.77×10^{-8} mol m^{-2} s^{-1} Pa^{-1}) at 180 ℃ and a medium selectivity of 7.7. The newly

developed ZIF-8/PBI nano-composite material has great potential for harsh industrial applications such as syngas and hydrogen production.

7.5 References

[1] M. I. Hoffert, K. Caldeira, G. Benford, D. R. Criswell, C. Green, H. Herzog, A. K. Jain, H. S. Kheshgi, K. S. Lackner, J. S. Lewis, H. D. Lightfoot, W. Manheimer, J. C. Mankins, M. E. Mauel, L. J. Perkins, M. E. Schlesinger, T. Volk, T. M. L. Wigley, Engineering: Advanced technology paths to global climate stability: Energy for a greenhouse planet, Science, 298 (2002) 981-987.

[2] J. A. Turner, A realizable renewable energy future, Science, 285 (1999) 687-689.

[3] M. Momirlan, T. N. Veziroglu, Current status of hydrogen energy, Renewable and Sustainable Energy Reviews, 6 (2002) 141-179.

[4] M. Momirlan, T. N. Veziroglu, The properties of hydrogen as fuel tomorrow in sustainable energy system for a cleaner planet, International Journal of Hydrogen Energy, 30 (2005) 795-802.

[5] N. W. Ockwig, T. M. Nenoff, Membranes for hydrogen separation, Chemical Reviews, 107 (2007) 4078-4110.

[6] L. Shao, B. T. Low, T. S. Chung, A. R. Greenberg, Polymeric membranes for the hydrogen economy: Contemporary approaches and prospects for the future, Journal of Membrane Science, 327 (2009) 18-31.

[7] S. A. Stern, Polymers for gas separations: The next decade, Journal of Membrane Science, 94 (1994) 1-65.

[8] P. Bernardo, E. Drioli, G. Golemme, Membrane gas separation: A review/state of the art, Industrial and Engineering Chemistry Research, 48 (2009) 4638-4663.

[9] R. W. Baker, Future directions of membrane gas separation technology, Industrial and Engineering Chemistry Research, 41 (2002) 1393-1411.

[10] J. G. Wijmans, R. W. Baker, The solution-diffusion model: A review, Journal of Membrane Science, 107 (1995) 1-21.

[11] M. Kawakami, H. Iwanaga, Y. Hara, M. Iwamoto, S. Kagawa, Gas permeabilities of cellulose nitrate/poly(ethylene glycol) blend membranes, Journal of Applied Polymer Science, 27 (1982) 2387-2393.

[12] H. Lin, E. Van Wagner, B. D. Freeman, L. G. Toy, R. P. Gupta, Plasticization-enhanced hydrogen purification using polymeric membranes, Science, 311 (2006) 639-642.

[13] L. Shao, T. S. Chung, In situ fabrication of cross-linked PEO/silica reverse-selective membranes for hydrogen purification, International Journal of Hydrogen Energy, 34 (2009) 6492-6504.

[14] H. Chen, Y. Xiao, T. S. Chung, Synthesis and characterization of poly (ethylene oxide) containing copolyimides for hydrogen purification, Polymer, 51 (2010) 4077-4086.

[15] A. Car, C. Stropnik, W. Yave, K. -V. Peinemann, Pebax®/polyethylene glycol blend thin film composite membranes for CO_2 separation: Performance with mixed gases, Separation and Purification Technology, 62 (2008) 110-117.

[16] J. Xia, S. Liu, C. H. Lau, T. S. Chung, Liquidlike poly(ethylene glycol) supported in the organic-inorganic matrix for CO_2 removal, Macromolecules, 44 (2011) 5268-5280.

[17] C. H. Lau, S. Liu, D. R. Paul, J. Xia, Y. C. Jean, H. Chen, L. Shao, T. S. Chung, Silica nanohybrid membranes with high CO_2 affinity for green hydrogen purification, Advanced Energy Materials, 1 (2011) 634-642.

[18] L. Shao, J. Samseth, M. B. Hägg, Crosslinking and stabilization of nanoparticle filled PMP nanocomposite membranes for gas separations, Journal of Membrane Science, 326 (2009) 285-292.

[19] Y. Liu, R. Wang, T. S. Chung, Chemical cross-linking modification of polyimide membranes for gas separation, Journal of Membrane Science, 189 (2001) 231-239.

[20] J. D. Wind, C. Staudt-Bickel, D. R. Paul, W. J. Koros, Solid-state covalent cross-linking of polyimide membranes for carbon dioxide plasticization reduction, Macromolecules, 36 (2003) 1882-1888.

[21] C. H. Lau, B. T. Low, L. Shao, T. S. Chung, A vapor-phase surface modification method to enhance different types of hollow fiber membranes for industrial scale hydrogen separation, International Journal of Hydrogen Energy, 35 (2010) 8970-8982.

[22] B. T. Low, Y. Xiao, T. S. Chung, Y. Liu, Simultaneous occurrence of chemical grafting, cross-linking, and etching on the surface of polyimide membranes and their impact on H_2/CO_2 separation, Macromolecules, 41 (2008) 1297-1309.

[23] L. Shao, C. H. Lau, T. S. Chung, A novel strategy for surface modification of polyimide membranes by vapor-phase ethylenediamine (EDA) for hydrogen purification, International Journal of Hydrogen Energy, 34 (2009) 8716-8722.

[24] B. T. Low, T. S. Chung, H. Chen, Y. C. Jean, K. P. Pramoda, Tuning the free volume cavities of polyimide membranes via the construction of pseudo-interpenetrating networks for enhanced gas separation performance, Macromolecules, 42 (2009) 7042-7054.

[25] B. T. Low, Y. Xiao, T. S. Chung, Amplifying the molecular sieving capability of polyimide membranes via coupling of diamine networking and molecular architecture, Polymer, 50 (2009) 3250-3258.

[26] Q. Li, J. O. Jensen, R. F. Savinell, N. J. Bjerrum, High temperature proton exchange membranes based on polybenzimidazoles for fuel cells, Progress in Polymer Science (Oxford), 34 (2009) 449-477.

[27] D. R. Coffin, G. A. Serad, H. L. Hicks, R. T. Montgomery, Properties and applications of celanese PBI - polybenzimidazole fiber, Textile Research Journal, 52 (1982) 466-472.

[28] K. Y. Wang, Q. Yang, T. S. Chung, R. Rajagopalan, Enhanced forward osmosis from chemically modified polybenzimidazole (PBI) nanofiltration hollow fiber membranes with a thin wall, Chemical Engineering Science, 64 (2009) 1577-1584.

[29] L. C. Sawyer, R. S. Jones, Observations on the structure of first generation polybenzimidazole reverse osmosis membranes, Journal of Membrane Science, 20 (1984) 147-166.

[30] K. Y. Wang, T. S. Chung, J. J. Qin, Polybenzimidazole (PBI) nanofiltration hollow fiber membranes applied in forward osmosis process, Journal of Membrane Science, 300 (2007) 6-12.

[31] G. M. Shi, Y. Wang, T. S. Chung, Dual-layer PBI/P84 hollow fibers for pervaporation dehydration of acetone, AIChE Journal, 58 (2012) 1133-1145.

[32] Y. Wang, T. S. Chung, B. W. Neo, M. Gruender, Processing and engineering of pervaporation dehydration of ethylene glycol via dual-layer polybenzimidazole (PBI)/polyetherimide (PEI) membranes, Journal of Membrane Science, 378 (2011) 339-350.

[33] Q. Yang, K. Y. Wang, T. S. Chung, A novel dual-layer forward osmosis membrane for protein enrichment and concentration, Separation and Purification Technology, 69 (2009) 269-274.

[34] K. Y. Wang, M. M. Teoh, A. Nugroho, T. S. Chung, Integrated forward osmosis-membrane distillation (FO-MD) hybrid system for the concentration of protein solutions, Chemical Engineering Science, 66 (2011) 2421-2430.

[35] D. R. Pesiri, B. Jorgensen, R. C. Dye, Thermal optimization of polybenzimidazole meniscus membranes for the separation of hydrogen, methane, and carbon dioxide, Journal of Membrane Science, 218 (2003) 11-18.

[36] S. C. Kumbharkar, Y. Liu, K. Li, High performance polybenzimidazole based asymmetric hollow fibre membranes for H_2/CO_2 separation, Journal of Membrane Science, 375 (2011) 231-240.

[37] K. A. Berchtold, J. S. Young, K. W. Dudeck, J. Acquaviva, F. Onorato, S. D. Hopkins, A. R. Greenberg, S. Brahmandam, E. S. Peterson, J. R. Klaehn, Novel polymeric-metallic composite membranes for CO_2 separations at elevated temperatures, presented at Fifth Annual Conference on Carbon Capture & Sequestration, Alexandria (2006).

[38] S. S. Hosseini, N. Peng, T. S. Chung, Gas separation membranes developed through integration of polymer blending and dual-layer hollow fiber spinning process for hydrogen and natural gas enrichments, Journal of Membrane Science, 349 (2010) 156-166.

[39] T. S. Chung, Z. L. Xu, Asymmetric hollow fiber membranes prepared from miscible polybenzimidazole and polyetherimide blends, Journal of Membrane Science, 147 (1998) 35-47.

[40] S. C. Kumbharkar, P. B. Karadkar, U. K. Kharul, Enhancement of gas permeation properties of polybenzimidazoles by systematic structure architecture, Journal of Membrane Science, 286 (2006) 161-169.

[41] S. S. Hosseini, M. M. Teoh, T. S. Chung, Hydrogen separation and purification in membranes of miscible polymer blends with interpenetration networks, Polymer, 49 (2008) 1594-1603.

[42] S. H. Han, J. E. Lee, K. J. Lee, H. B. Park, Y. M. Lee, Highly gas permeable and microporous polybenzimidazole membrane by thermal rearrangement, Journal of Membrane Science, 357 (2010) 143-151.

[43] S. C. Kumbharkar, U. K. Kharul, Investigation of gas permeation properties of systematically modified polybenzimidazoles by N-substitution, Journal of Membrane Science, 357 (2010) 134-142.

[44] M. Sadeghi, M. A. Semsarzadeh, H. Moadel, Enhancement of the gas separation properties of polybenzimidazole (PBI) membrane by incorporation of silica nano particles, Journal of Membrane Science, 331 (2009) 21-30.

[45] O. M. Yaghi, M. O'Keeffe, N. W. Ockwig, H. K. Chae, M. Eddaoudi, J. Kim, Reticular synthesis and the design of new materials, Nature, 423 (2003) 705-714.

[46] S. Kitagawa, R. Kitaura, S. I. Noro, Functional porous coordination polymers, Angewandte Chemie - International Edition, 43 (2004) 2334-2375.

[47] J. Caro, Are MOF membranes better in gas separation than those made of zeolites, Current Opinion in Chemical Engineering, 1 (2011) 77-83.

[48] K. S. Park, Z. Ni, A. P. Côté, J. Y. Choi, R. Huang, F. J. Uribe-Romo, H. K. Chae, M. O'Keeffe, O. M. Yaghi, Exceptional chemical and thermal stability of zeolitic imidazolate frameworks, Proceedings of the National Academy of Sciences of the United States of America, 103 (2006) 10186-10191.

[49] Y. S. Li, F. Y. Liang, H. Bux, A. Feldhoff, W. S. Yang, J. Caro, Molecular sieve membrane: Supported metal-organic framework with high hydrogen selectivity, Angewandte Chemie - International Edition, 49 (2010) 548-551.

[50] S. R. Venna, M. A. Carreon, Highly permeable zeolite imidazolate framework-8 membranes for CO_2/CH_4 separation, Journal of the American Chemical Society, 132 (2010) 76-78.

[51] Y. Liu, E. Hu, E. A. Khan, Z. Lai, Synthesis and characterization of ZIF-69 membranes and separation for CO_2/CO mixture, Journal of Membrane Science, 353 (2010) 36-40.

[52] A. Huang, H. Bux, F. Steinbach, J. Caro, Molecular-sieve membrane with hydrogen permselectivity: ZIF-22 in LTA topology prepared with 3-aminopropyltriethoxysilane as covalent linker, Angewandte Chemie - International Edition, 49 (2010) 4958-4961.

[53] A. Huang, W. Dou, J. Caro, Steam-stable zeolitic imidazolate framework ZIF-90 membrane with hydrogen selectivity through covalent functionalization, Journal of the American Chemical Society, 132 (2010) 15562-15564.

[54] Y. Pan, Z. Lai, Sharp separation of C2/C3 hydrocarbon mixtures by zeolitic imidazolate framework-8 (ZIF-8) membranes synthesized in aqueous solutions, Chemical Communications, 47 (2011) 10275-10277.

[55] H. Bux, A. Feldhoff, J. Cravillon, M. Wiebcke, Y. S. Li, J. Caro, Oriented zeolitic imidazolate framework-8 membrane with sharp H_2/C_3H_8 molecular sieve separation, Chemistry of Materials, 23 (2011) 2262-2269.

[56] H. Bux, C. Chmelik, J. M. Van Baten, R. Krishna, J. Caro, Novel MOF-membrane for molecular sieving predicted by IR-diffusion studies and molecular modeling, Advanced Materials, 22 (2010) 4741-4743.

[57] J. Y. Z. Xie, J. Wang, J. Bai, H. Yin, B. Yuan, J. Lu, Y. Zhang, L. Zhou, C. Duan, Deposition of chemically modified α-Al_2O_3 particles for high performance ZIF-8 membrane on a macroporous tube, Chemical Communications, 48 (2012) 5977-5979.

[58] G. Xu, J. Yao, K. Wang, L. He, P. A. Webley, C. -S. Chen, H. Wang, Preparation of ZIF-8 membranes supported on ceramic hollow fibers from a concentrated synthesis gel, Journal of Membrane Science, 385–386 (2011) 187-193.

[59] S. Kulprathipanja, R. W. Neuzil, N. N. Li (Allied-Signal Inc.), Separation of fluids by means of mixed matrix membranes, US patent 4740219 (1988).

[60] T. S. Chung, L. Y. Jiang, Y. Li, S. Kulprathipanja, Mixed matrix membranes (MMMs) comprising organic polymers with dispersed inorganic fillers for gas separation, Progress in Polymer Science (Oxford), 32 (2007) 483-507.

[61] L. Y. Jiang, Y. Wang, T. S. Chung, X. Y. Qiao, J. Y. Lai, Polyimides membranes for pervaporation and biofuels separation, Progress in Polymer Science (Oxford), 34 (2009) 1135-1160.

[62] V. Abetz, T. Brinkmann, M. Dijkstra, K. Ebert, D. Fritsch, K. Ohlrogge, D. Paul, K. V. Peinemann, S. P. Nunes, N. Scharnagl, M. Schossig, Developments in membrane research: From material via process design to industrial application, Advanced Engineering Materials, 8 (2006) 328-358.

[63] D. Li, R. Wang, T. S. Chung, Fabrication of lab-scale hollow fiber membrane modules with high packing density, Separation and Purification Technology, 40 (2004) 15-30.

[64] T. Yang, Y. Xiao, T. S. Chung, Poly-/metal-benzimidazole nano-composite membranes for hydrogen purification, Energy and Environmental Science, 4 (2011) 4171-4180.

[65] J. C. Tan, T. D. Bennett, A. K. Cheetham, Chemical structure, network topology, and porosity effects on the mechanical properties of zeolitic imidazolate frameworks, Proceedings of the National Academy of Sciences of the United States of America, 107 (2010) 9938-9943.

[66] L. Y. Jiang, T. S. Chung, C. Cao, Z. Huang, S. Kulprathipanja, Fundamental understanding of nano-sized zeolite distribution in the formation of the mixed matrix single- and dual-layer asymmetric hollow fiber membranes, Journal of Membrane Science, 252 (2005) 89-100.

[67] S. Husain, W. J. Koros, Mixed matrix hollow fiber membranes made with modified HSSZ-13 zeolite in polyetherimide polymer matrix for gas separation, Journal of Membrane Science, 288 (2007) 195-207.

[68] L. Y. Jiang, T. S. Chung, S. Kulprathipanja, Fabrication of mixed matrix hollow fibers with intimate polymer-zeolite interface for gas separation, AIChE Journal, 52 (2006) 2898-2908.

[69] N. Widjojo, T. S. Chung, S. Kulprathipanja, The fabrication of hollow fiber membranes with double-layer mixed-matrix materials for gas separation, Journal of Membrane Science, 325 (2008) 326-335.

[70] T. S. Chung, W. F. Guo, Y. Liu, Enhanced Matrimid membranes for pervaporation by homogenous blends with polybenzimidazole (PBI), Journal of Membrane Science, 271 (2006) 221-231.

[71] D. F. Li, T. S. Chung, R. Wang, Y. Liu, Fabrication of fluoropolyimide/polyethersulfone (PES) dual-layer asymmetric hollow fiber

membranes for gas separation, Journal of Membrane Science, 198 (2002) 211-223.

[72] D. T. Clausi, W. J. Koros, Formation of defect-free polyimide hollow fiber membranes for gas separations, Journal of Membrane Science, 167 (2000) 79-89.

[73] L. Jiang, T. S. Chung, D. F. Li, C. Cao, S. Kulprathipanja, Fabrication of Matrimid/polyethersulfone dual-layer hollow fiber membranes for gas separation, Journal of Membrane Science, 240 (2004) 91-103.

[74] N. Peng, T. S. Chung, J. Y. Lai, The rheology of Torlon® solutions and its role in the formation of ultra-thin defect-free Torlon® hollow fiber membranes for gas separation, Journal of Membrane Science, 326 (2009) 608-617.

[75] L. M. Robeson, The upper bound revisited, Journal of Membrane Science, 320 (2008) 390-400.

[76] M. D. Guiver, H. N. Le Thi, G. P. Robertson (Seaby & Associates), Composite gas separation membranes, US patent 2002/0062737A1 (2002).

[77] T. S. Chung, L. Shao, P. S. Tin, Surface modification of polyimide membranes by diamines for H_2 and CO_2 separation, Macromolecular Rapid Communications, 27 (2006) 998-1003.

[78] H. Huang, W. Zhang, D. Liu, B. Liu, G. Chen, C. Zhong, Effect of temperature on gas adsorption and separation in ZIF-8: A combined experimental and molecular simulation study, Chemical Engineering Science, 66 (2011) 6297-6305.

[79] J. R. Li, Y. Ma, M. C. McCarthy, J. Sculley, J. Yu, H. K. Jeong, P. B. Balbuena, H. C. Zhou, Carbon dioxide capture-related gas adsorption and separation in metal-organic frameworks, Coordination Chemistry Reviews, 255 (2011) 1791-1823.

[80] S. K. Nune, P. K. Thallapally, A. Dohnalkova, C. Wang, J. Liu, G. J. Exarhos, Synthesis and properties of nano zeolitic imidazolate frameworks, Chemical Communications, 46 (2010) 4878-4880.

[81] W. Macdonald, C. Y. Pan (Alberta Helium Limited), Method for drying water-wet membranes, US patent 3842515 (1974).

[82] H. C. Park, Y. S. Moon, H. W. Rhee, J. Won, Y. S. Kang, U. Y. Kim, Effect of solvent exchange on the morphology of asymmetric membranes, in Membrane Formation and Modification, (Eds: I. Pinnau, B. D. Freeman), American Chemical Society, Washington, DC (1999) Ch.8.

[83] C. L. Yaws, Thermophysical properties of chemicals and hydrocarbons, William Andrew, Norwich (2008).

[84] C. Hansen, Hansen Solubility Parameters: A User's Handbook, Second Edition, CRC Press, Boca Raton, (2007).

[85] I. Pinnau, W. J. Koros, Relationship between substructure resistance and gas separation properties of defect-free integrally skinned asymmetric membranes, Industrial and Engineering Chemistry Research, 30 (1991) 1837-1840.

CHAPTER 8

CONCLUSIONS AND RECOMMENDATIONS

8.1 Conclusions

8.1.1 A review of the research objectives of this work

Membrane technology possesses evident potential for hydrogen purification with the advantages in the aspect of energy efficiency, cleanness, flexibility, footprint, environmental impact, and so on. Polymers are the dominant materials for gas separation membranes fabrication due to the good processability and relatively lower costs. For H_2/CO_2 separation, due to the undesirable coupling H_2-selective diffusivity and CO_2-selective solubility, majority of the polymeric membranes exhibit poor intrinsic H_2/CO_2 selectivity. PBI is a specific polymer with high intrinsic H_2/CO_2 selectivity but extremely low H_2 permeability. Comparing with polymeric materials, ZIFs crystalline materials show higher gas separation performance, but are much harder to be fabricated into membranes in a large scale and economical way.

In this work, we synergistically combined the strengths of both PBI polymer and ZIFs nano-particles and designed their nano-composite membranes for hydrogen purification at high temperatures. Detailed investigations were carried out in the aspects of material characterizations, gas permeation mechanism, as well as performance evolution using feed streams containing CO or water impurities. The practicability of ZIFs/PBI nano-composite material is demonstrated in a useful configuration as dual-layer hollow fibers which are of greater commercial importance.

8.1.2 ZIFs/PBI nano-composite materials design and fabrication

The particle synthesis method and the particle-polymer mixing procedure significantly affect the properties of the resultant MMMs. To overcome the common drawbacks of MMMs, three types of ZIFs nanoparticles were synthesized and incorporated into PBI solutions via the direct-mixing of as-synthesized wet-state nanoparticles. The membranes from this new developed method exhibit much better particle-polymer adhesion and more uniform particle dispersion than the traditional dry-state mixing method, thus display better gas separation performances and advantages in other physical properties.

ZIF-7 was firstly studied because of its small cavity size exactly between the kinetic diameters of H_2 and CO_2, which may render a higher H_2/CO_2 selectivity for the membrane. By mixing the as-synthesized ZIF-7 nano-particles without the traditional drying process with PBI, the resultant membranes not only achieve an unprecedented ZIF-7 loading as high as 50 wt %, but also overcome the low permeability nature of PBI. The membranes exhibit characteristics of high transparency and mechanical flexibility, together with enhanced H_2 permeability and ideal H_2/CO_2 permselectivity surpassing both neat PBI and ZIF-7 membranes. Advanced instrument analyses have confirmed the unique ZIF-polymer interface and elucidate mixed matrix structure that contributes to the high ZIF loading and enhanced gas separation performance superior to the prediction from the Maxwell model. The high thermal stability, good dispersion of ZIF nano particles with minimal agglomeration and the attractive gas separation performance at elevated temperatures indicate the bright prospects of this nano-composite membrane material design strategy.

ZIF-8 was studied because of its high gas permeability, acceptable intrinsic H_2/CO_2 selectivity and good stability. Due to the small particle sizes and good compatibility between ZIF-8 and PBI, membranes with an extremely high ZIF loading of 63.6 vol % can be prepared. However, different from ZIF-7/PBI composite membranes, a decline in H_2/CO_2 selectivity at high ZIF-8 loading was found for the newly developed ZIF-8/PBI dense membranes due to the larger cavity size and much higher porosity of ZIF-8. Compared to PBI dense membranes, the 30/70 (w/w) ZIF-8/PBI nano-composite material significantly enhances the H_2 permeability from 3.7 Barrer to 105.4 Barrer together with improved H_2/CO_2 selectivity from 8.7 to 12.3 at 35 ℃, far surpassing the Robeson upper bound and other polymeric materials in literatures. Because ZIF-8/PBI membrane material displays the best mixed gas separation performances, further evaluations of membrane performances were mainly focused on it.

ZIF-90 was also used for the PBI based nano-composite membrane fabrication because it offers more chemical versatility due to the extra aldehyde group on the imidazolate linkers, which may provide more flexibility of post modifications for further improvements and more applications. Since there is no literature available about nano-scale ZIF-90 particles synthesis, we developed a novel procedure to synthesize ZIF-90 nanocrystals at room temperature. The nanocrystals show identical morphology, crystalline and chemical structure while a significantly reduced particle size (around 100 nm) as compared with the ZIF-90 particles in previous studies. The derived ZIF-90/PBI nano-composite membranes exhibit homogeneous particle dispersion and fine particle-polymer adhesion, as well as excellent hydrogen purification performance at various testing conditions. The 45/55 (w/w) ZIF-90/PBI

membrane with the highest ZIF-90 volume loading up to 50.9 vol% possesses the best ideal H_2/CO_2 separation performance with a moderate H_2 permeability of 24.5 Barrer and a high H_2/CO_2 selectivity of 25.0 in pure gas permeation tests at 35 ℃. The membrane also shows promoted gas separation performance during mixed gas tests at 180 ℃ with a H_2 permeability of 226.9 Barrer and a H_2/CO_2 separation factor of 13.3.

8.1.3 Evaluation of membrane performances in industrially modeling conditions

Typically, PBI based H_2-selective membranes exhibit better H_2/CO_2 selectivity at high temperatures because of the great reduction of CO_2 solubility with temperatures, which makes our aim possible if the separation takes place at high temperatures. We examined the temperature-dependent separation performance of 30/70 (w/w) ZIF-8/PBI membrane and 60/40 (w/w) ZIF-8/PBI membrane from 35 ℃ to 230 ℃, both membranes show obviously increased H_2/CO_2 selectivity with increasing test temperature. The 30/70 (w/w) ZIF-8/PBI membrane has a remarkably high H_2/CO_2 selectivity of 26.3 among those polymeric membranes, together with good H_2 permeability of around 470 Barrer at 230 °C; while the 60/40 (w/w) ZIF-8/PBI membrane shows the highest ever reported H_2 permeability of 2015 Barrer in those polymer membranes with a H_2/CO_2 selectivity of around 12.3 at 230 °C. This unique performance arises from the synergistic combination of (1) a substantial increase in H_2/CO_2 solubility selectivity due to a significant drop in CO_2 sorption in ZIF-8 nano-particles at elevated temperatures and (2) a minor drop in H_2/CO_2 diffusivity selectivity due to the relatively rigid backbone and high thermal stability of the PBI polymer.

Conventional syngas is produced with many byproducts as impurities. They must be removed simultaneously with CO_2 at elevated temperatures. Mixed gas data show that the presence of CO or water vapor impurity in the feed gas stream does not significantly influence the membrane performance at 230 ℃. Thus, the newly developed H_2-selective membranes may have bright prospects for hydrogen purification and CO_2 capture in realistic industrial applications such as syngas processing, integrated gasification combined cycle (IGCC) power plant and hydrogen recovery.

8.1.4 Fabrication of ZIF-8-PBI/Matrimid hollow fibers

We have fabricated ZIF-8/PBI nano-composites in a useful form as dual-layer hollow fibers. Without post annealing and silicone rubber coating, the dual-layer fibers show impressive H_2/CO_2 separation performance. We found that the immersion in isopropanol helps maintaining the outer layer morphology without collapse comparing with the traditional solvent exchange procedure using methanol as the second exchange solvent. Nonetheless, the intercalation phenomenon among ZIF-8 particles was observed when the nano-particle loading is high. In addition, interface resistance between inner and outer layers may affect the gas transport. Two types of hollow fibers targeted at either high H_2/CO_2 selectivity or high H_2 permeance have been developed; namely, (1) PZM10-I B fibers with a medium H_2 permeance of 64.5 GPU (2.16×10^{-8} mol m^{-2} s^{-1} Pa^{-1}) at 180 ℃ and a high selectivity of 12.3, and (2) PZM33-I B fibers with a high H_2 permeance of 202 GPU (6.77×10^{-8} mol m^{-2} s^{-1} Pa^{-1}) at 180 ℃ and a medium selectivity of 7.7.

8.2 Recommendations and future work

8.2.1 Plasticization phenomenon in ZIFs/PBI membranes at high pressures

Plasticization induced by high partial pressure of high condensable gas penetrant increases the polymer chain mobility and penetrant diffusion coefficients, thus reduces the diffusivity selectivity. H_2-selective membranes based on diffusivity selectivity are far more sensitive to CO_2-induced membrane plasticization. Since the partial pressure of CO_2 in syngas can be as high as ~30 atm, the effect of plasticization is more or less present and should be taken into serious consideration. The onset of plasticization depends on pressure, time, temperature, and membrane thickness, thus it is necessary to study the plasticization phenomenon with different feed composition, operating parameters, and membrane configurations. For high temperature hydrogen purification, the plasticization behavior may be accelerated in ultra-thin films (such as the thin functional layers of hollow fibers) because of the severe swelling effects caused by CO_2. Fortunately, the plasticization phenomenon is less pronounced at higher temperatures due to the lower solubility coefficients at higher temperatures.

8.2.2 Optimization of hollow fiber spinning conditions

Commercialized membranes usually contain thin selective skin layers with the thickness of several hundred nanometers. Some fibers even possess ultra thin selective layers of less than 100 nm. In this study, because we only aim to demonstrate the processibility of ZIF-8/PBI nano-composite material, the thickness of the dense skin

is as thick as about 2000 nm. Further study may be focused on reducing the dense skin thickness to improve the H_2 permeance via spinning condition and post treatment optimization. On the other hand, due to the fact that spinning solutions with high ZIF-8 loadings are much more viscous than diluted solutions for the casting of flat dense membranes, the H_2/CO_2 selectivity starts to decline at relatively low ZIF-8 loading (i.e., 33 wt%) comparing with dense flat-sheet membranes. Improved doping preparing methods need to be developed in order to delay the occurrence of intercalation effect. Last but not least, it is also observed that a thick interface is formed between inner and outer layers of the hollow fiber, which may increase the substructure resistance, and lower the flux and selectivity. Future research may be carried on in the aspects of material combination design and spinning condition optimization to eliminate this dense interface.

8.2.3 Thin layer doping of ZIFs/PBI material on a porous substrate

Besides hollow fibers spinning, there may be other methods to make ZIFs/PBI nano-composite material into commercial attractive membrane configurations. One possible way is the thin layer doping of this material on a porous substrate. The substrates can be hollow fibers, porous tubes or asymmetric flat sheet membranes, making from either polymers or inorganics. The ZIFs/PBI layers can be doped by coating, in situ particle formation, or thin film composite membrane synthesis. A main challenge needs to be overcome might be to ensure the thin functional layer is defect-free, in order to keep the selectivity of the membrane. Despite the potential challenges, this method may offer much more flexibility to utilize the ZIFs/PBI nano-composites, and expand the application fields of this promising membrane material.

PUBLICATIONS

Journal Papers:

1. **Tingxu Yang,** Youchang Xiao, Tai Shung Chung, Poly-/metal-benzimidazole nano-composite membranes for hydrogen purification, Energy & Environmental Science, 4 (2011) 4171-4180.
2. **Tingxu Yang,** Gui Min Shi, Tai Shung Chung, Symmetric and asymmetric zeolitic imidazolate frameworks (ZIFs)/polybenzimidazole (PBI) nanocomposite membranes for hydrogen purification at high temperatures, Advanced Energy Materials, 2 (2012) 1358-1367.
3. **Tingxu Yang,** Tai Shung Chung, High performance ZIF-8/PBI nano-composite membranes for high temperature hydrogen separation consisting of carbon monoxide and water vapor, International Journal of Hydrogen Energy, 38 (2013) 229-239.
4. **Tingxu Yang,** Tai Shung Chung, Room-temperature synthesis of ZIF-90 nanocrystals and the derived nano-composite membranes for hydrogen purification, submitted to Journal of Materials Chemistry A.
5. Gui Min Shi, **Tingxu Yang**, Tai Shung Chung, Polybenzimidazole (PBI)/zeolitic imidazolate frameworks (ZIF-8) mixed matrix membranes for pervaporation dehydration of alcohols, Journal of Membrane Science, 415-416 (2012) 577-586.
6. Mohammad Askari, **Tingxu Yang**, Tai Shung Chung, Natural gas purification and olefin/paraffin separation using cross-linkable dual-layer hollow fiber membranes comprising β-Cyclodextrin, Journal of Membrane Science, 423-424 (2012) 392-403.

7. Lin Hao, Pei Li, **Tingxu Yang**, Tai Shung Chung, Room temperature ionic liquid/ZIF-8 mixed-matrix membranes for pre-combustion and post-combustion CO_2 capture, accepted by Journal of Membrane Science.

Conferences and Presentations:

1. Membrane Science and Technology (MST) Symposium 2011, Oral presentation, Singapore, 24-25 Aug, 2011.
2. Asian Research Network (ARN) Summer Camp 2011, Poster presentation, Wakoshi and Hakone, Japan, 26-29 Aug 2011.
3. American Institute of Chemical Engineers (AIChE) Annual Meeting 2011, Oral presentation, Minneapolis, United States, 16-21 Oct, 2011.
4. Singapore International Energy Week 2012, poster presentation, Singapore, 22-25 Oct, 2012.
5. American Institute of Chemical Engineers (AIChE) Annual Meeting 2012, Oral presentation, Pittsburgh, United States, 28 Oct-02 Nov, 2012.

Patent:

1. **Tingxu Yang**, Youchang Xiao, Tai Shung Chung, Preparation of zeolitic imidazolate frameworks-polybenzimidazole mixed-matrix composite and the applications for gas and vapor separation, International patent, WO 2012/112122.